CR-119889

REPORT NO. GDC-DCF70-002
CONTRACT NAS 8-21036

TELEVISION BROADCAST SATELLITE STUDY

VOLUME IV ✦ APPENDICES

GENERAL DYNAMICS
Convair Aerospace Division

REPORT NO. GDC-DCF70-002

TELEVISION BROADCAST SATELLITE STUDY

TVBS SYSTEM

APPENDICES

VOLUME IV

CONTRACT NAS 8-21036

31 December 1970

Prepared for
E. C. Hamilton, COR
National Aeronautics and Space Administration
George C. Marshall Space Flight Center
Huntsville, Alabama

Prepared by
CONVAIR AEROSPACE DIVISION OF GENERAL DYNAMICS
San Diego, California

PRECEDING PAGE BLANK NOT FILMED

FOREWORD

This report was prepared by the San Diego operation of the Convair Aerospace Division of General Dynamics under Contract NAS8-21036, Television Broadcast Satellite Study, for the George C. Marshall Space Flight Center of the National Aeronautics and Space Administration. The work was administered under the technical direction of the Astrionics Laboratory of the George C. Marshall Space Flight Center.

TABLE OF CONTENTS

Report GDC-DCF 70-002

TELEVISION BROADCAST SATELLITE STUDY

FINAL REPORT - VOLUME IV

TECHNICAL APPENDICES

Contract NAS8-21036

31 December 1970

APPENDIX A

PARAMETRIC ANALYSIS

Convair Aerospace Division

GENERAL DYNAMICS

A

PARAMETRIC ANALYSIS

The following sections were prepared by the Hughes Aircraft Company in support of the TV Broadcast Satellite Study contract.

INDEX

1.0 POWER CONDITIONING

1.1 Power Conditioning Efficiency

Table A-1 is a summary of data from various sources on power conditioning efficiency. The first four entries reflect Hughes designs intended for high voltage and high power, at a regulation of ± 1.0 percent. The efficiencies associated with these designs range from 81 to 96 percent, with the actual efficiency depending on the approach.

The first entry is an SCR Morgan-type pre-regulator followed by a DC-DC converter. This approach involves more complexity and less efficiency than any other. The second is a transformer-rectifier circuit followed by a vacuum-tube high-efficiency switching regulator. This approach offers the highest efficiency, however, it suffers from heavier weight and poorer transient response.

The third approach is a hybrid combining an SCR DC-DC converter with a vacuum-tube switching regulator. It produces a reasonable 88 percent efficiency with less weight penalty.

The fourth Hughes entry is an all-solid-state inverter with pulse-width-modulated regulation. This offers the ultimate in low weight and volume. It is also an example of high efficiency coupled with the modular approach. This type of approach is quite attractive and can be adapted to higher powers.

Table A-2 compares representative high-voltage vacuum-tube and solid-state switching devices.

The final two entries in Table A-1 were taken from data contained in the GE Multikilowatt Transmitter Study, (Vol. II. FTK Phase I, Document No. 68SD4268, 10 June 1968, Contract NAS 8-21886). Although many pertinent

Table A-1.

POWER CONDITIONING EFFICIENCY DATA SUMMARY

DESIGN APPROACH	EFFICIENCY (PERCENT)	DATA SOURCE	COMMENTS
SCR Morgan type Pre-reg. (90) followed by DC-DC converter (90)	81	Hughes Air-borne/missile electronics technology	13 KV $\pm$1% at 1.65 amps
Transformer-Rectifier(98) followed by Vacuum-Tube switching regulator (98)	96	Hughes air-borne/missile electronics technology	13 KV $\pm$ 1% at 1.65 amps
SCR DC-DC Converter (90) followed by vacuum-tube switching	88	Hughes/air-borne/missile electronics technology	13 KV $\pm$ 1% at 1.65 amps
Transistor Inverters with pulse width modulated regulation	93	Hughes Ion Engine Technology	2 KV $\pm$ 1% at 1.0 amps, 8 inverters in series. (Efficiency applicable up to 2 KW/module)
Unknown	85 to 90	G. E.	Up to 5 KW total power
Unknown	80 to 83	G. E.	Above 5 KW total power

Numbers in parenthesis are efficiencies of devices in tandem.

Table A-2.

COMPARISON OF SWITCHING DEVICES

DEVICE TYPE	VOLTAGE RATING, VOLTS	CURRENT RATING, AMPERES	RELATIVE SWITCHING SPEED
Eimac 4 PR 250 High-Vacuum Tetrode	50,000	0.35 (Continuous)	Fast
Solitron SDT 8955 Transistor	300	60	Fast
Westinghouse 2N3888 SCR	500	275	Slow
General Electric C154 E SCR	500	110	Slow
General Electric C54 E SCR	500	55	Slow

design details are not reported, the GE efficiencies correlate well with similar Hughes experience. The GE efficiencies appear to be biased slightly lower than the Hughes efficiencies. However, on the basis of all the Hughes and GE data, it seems reasonable to expect efficiencies in the 90-percent range, or at least in the high 80's.

1.2 Protection Circuitry

High-power traveling-wave tubes, like other high-voltage devices, may be expected to arc from time to time. The TWT can stand a moderate amount of energy from the arc, and if properly protected, will remain operational. The energy storage capacitor used in the output of the modulator power supply often has sufficient stored energy to permanently damage the TWT if all of this energy enters into the arc. One means of protection against this is an electronic crowbar circuit.

Crowbar Action

The electronic crowbar circuit protects the TWT by sensing when an arc or other fault occurs. It then places an electronic short circuit across the power supply output. Within microseconds, it discharges the stored energy of the output capacitor and removes the voltage from the TWT to prevent damage to the tube. The short circuit path might consist of an SCR and is designed to carry large currents during the initial crowbar action. The modulator power supply should be designed to de-energize upon the initiation of a crowbar, and be capable of withstanding the short-circuit load until then.

Crowbar Sensing

Proper operation of an electronic crowbar requires sensing of TWT currents at a point which will properly discern the arc currents. Since the arc forms from the gun to the anode (usually connected to the body of the TWT), the crowbar sensing should either be total current or anode current. Collector current alone should not be used. If the anode is connected to the slow-wave structure (body) of the TWT, sensing of the body current may be used to give a more sensitive indication of arcs. This also may be used to sense excessive interception of the electron beam caused by excessive RF input, insufficient magnetic field or other reasons.

Crowbar Circuits

Some of the basic crowbar circuits that have been used in the past are shown in Figure A-1; the crowbar acts as a high-current shunt across the HV power supply. Figure A-2 shows an application of an SCR used as the operating element of the crowbar.

Protection of Gridded Traveling-Wave Tubes

The need for protection of the grids in TWTs has been demonstrated by the failure of grids which were not properly protected. The desire for high-mu, low-interception grids in TWTs requires the use of fine wires close to the cathode surface. The resulting grids, while structurally sound, may easily be damaged by arcing.

The mechanism of such a damaging arc is believed to be as follows:

1. For any of several reasons, an arc may develop between the anode and the grid support structure, which can withstand the moderate energy of the arc.
2. The grid is rapidly carried positive with respect to the cathode.

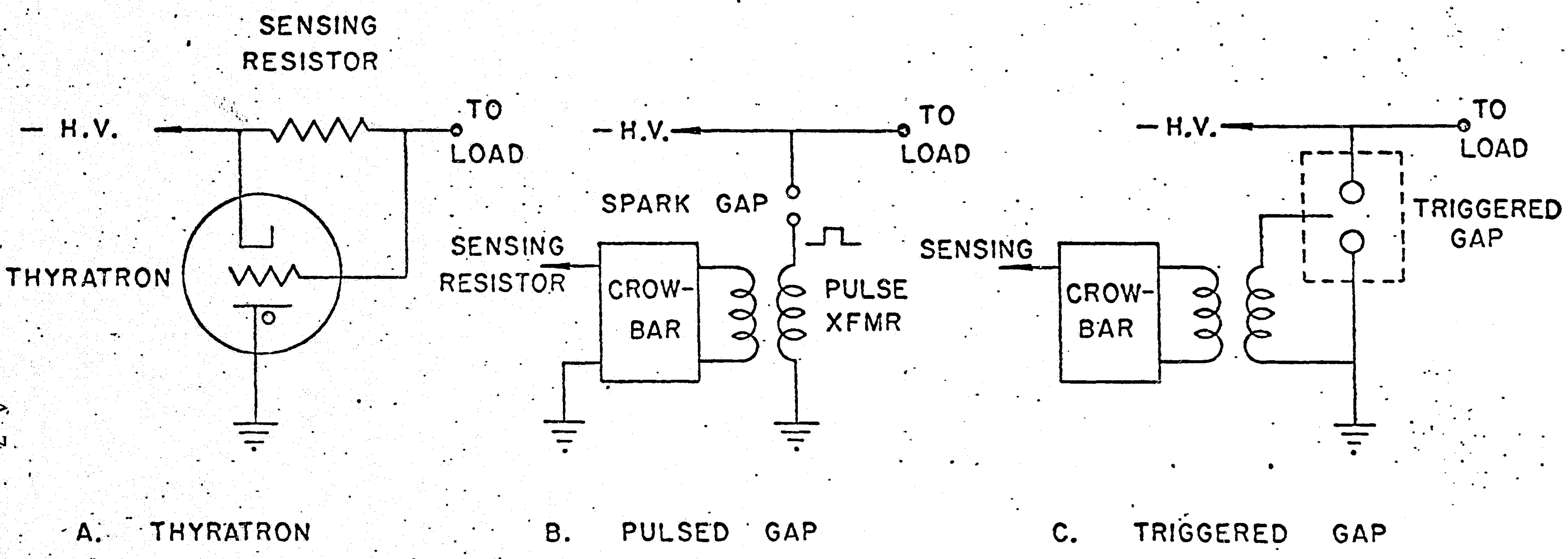

Figure A-1. Basic Crowbar Circuits

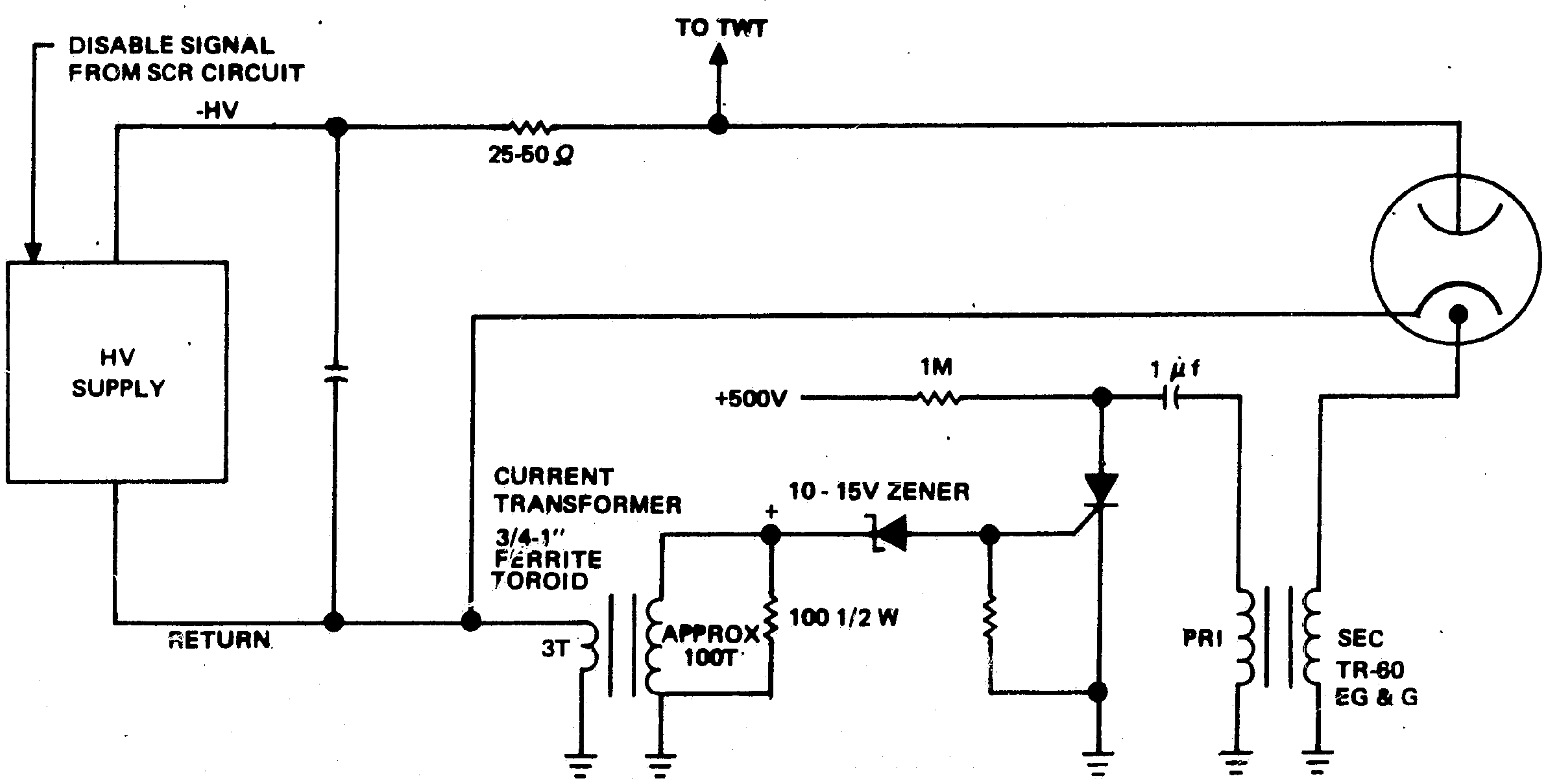

Figure A-2. SCR Crowbar Circuit

NOTES: (1) Current transformer has approximately 1 V/A output and load resistor is selected for that ratio.

(2) Arc tube is typically EG and G type GP-14. Pick proper tube for voltage range desired.

(3) A voltage can be picked off the SCR circuit to shut down the main HV supply.

3. A point is reached where the grid-to-cathode voltage is sufficient to initiate an arc between the grid wires and the cathode surface.

4. The two arcs in series, between the cathode and anode, permit a high current to flow between the cathode and grid wires, which can result in severe damage to the grid wires.

The most direct method of avoiding damage to the grid wires is to introduce a spark-gap, or other means external to the TWT, which will prevent the grid-to-cathode voltage from rising to a damaging level. The breakdown rating on such a device should be roughly 50 percent greater than the maximum negative grid bias or positive grid-to-cathode voltage. It also appears desirable to introduce an arc-current-limiting resistor of from 10 to 100 ohms in series with the high-voltage supply. A spark-gap should typically be connected directly between the grid and cathode of the tube with the shortest possible leads. This device should break down within 1 μsec under a 1,500-volt pulse.

Figure A-3 is a block diagram incorporating both a crowbar and a spark-gap to protect the grid of the TWT.

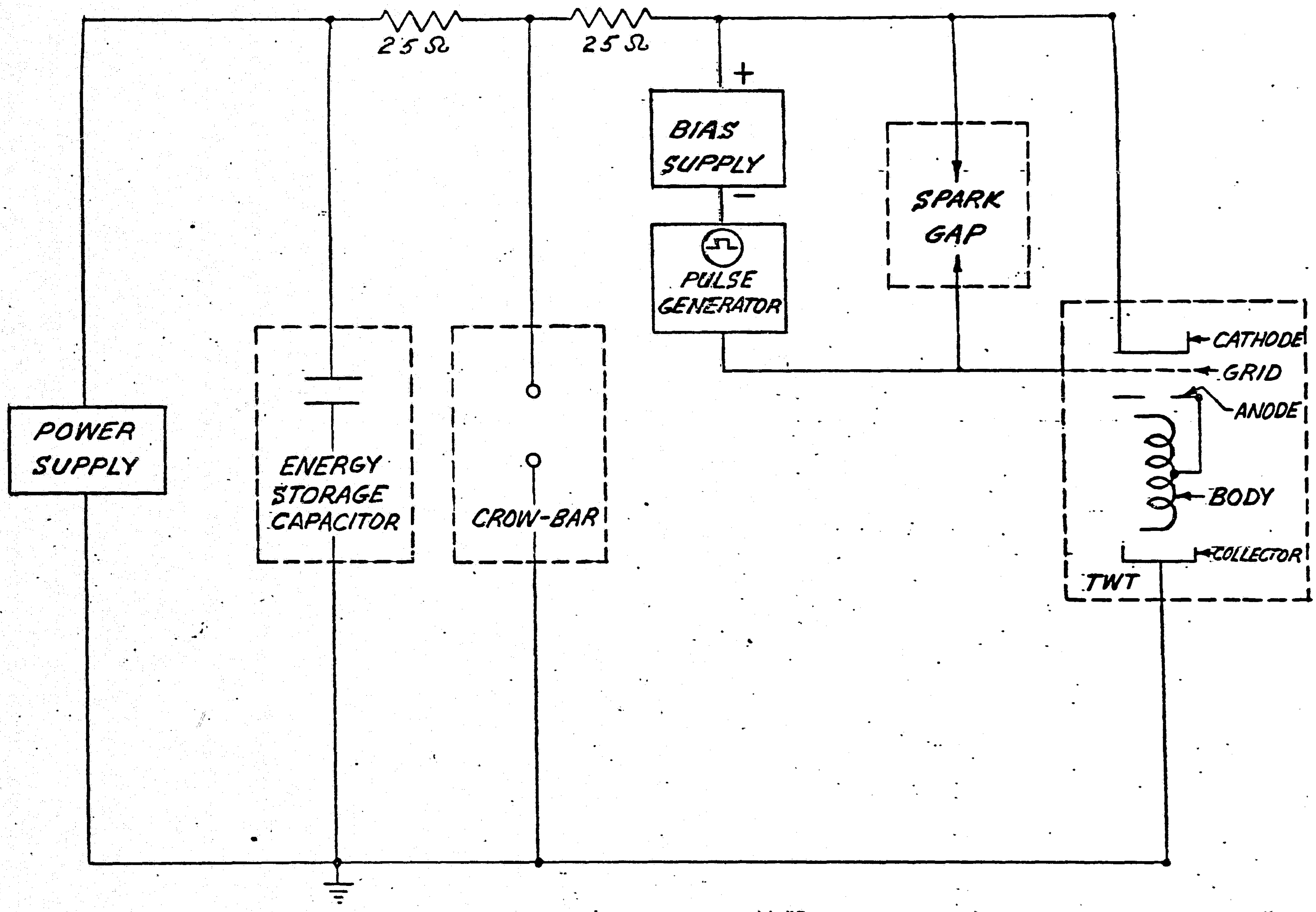

Figure A-3. Circuit Diagram forProtective Circuitry

2. TELEMETRY AND COMMAND

2.1 Background

The T and C system suitable for the housekeeping functions for a TV Broadcast Satellite can be roughly sized on the basis of the following baseline description of the spacecraft and its mission.

1. The spacecraft is 3-axis attitude stabilized. (That is, no spinning/despun interface exists for the T and C system, as is the case for gyrostat-type spacecraft.)
2. The spacecraft is intended to be operational (rather than experimental), which tends to reduce the T and C data load.
3. A fully redundant system is needed to meet spacecraft reliability objectives.
4. The signal format need to allow only for non-real-time T and C. (That is, no exotic real-time transients need to be transmitted either up or down.)
5. Compatibility with an appropriate ground complex must be decided on. Specifically, the existing Intelsat ground complex is dominantly shaped by the real-time control requirement that is characteristic of a spin-stabilized spacecraft, i.e., it is not appropriate here. For the purpose of a first cut, a ground complex similar to the NASA/STADAN/ATS facilities was assumed. It seemed reasonably appropriate, and it was a convenient assumption since there exists spacecraft hardware of known performance and weight that is compatible with that ground complex.

6. The spacecraft is large and complex, which tends to increase the data load. For this reason, a central/remote concept is convenient, i.e., a central unit provides signals to a series of decoders, or accepts signals from a series of multiplexers located at the using function. This approach distributes the data collection and distribution tasks, which results in a flexible and versatile system and reduces overall weight and cost. Specifically, the remote multiplexer can accept varying ratios of analog and digital channels. The remote decoder provides command flexibility in groups of 64 pulse and 4 magnitude commands. A sizable weight reduction is achieved, since each remote unit is connected to the central unit by only three wires, as opposed to 60-70 wires for the conventional approach.

2.2 Command Subsystem

A representative command group consists of redundant command receivers, redundant demodulator/decoders, and eight sets of redundant remote decoders. The subsystem is capable of accepting a standard NASA Pulse Code Modulation (PCM) Instruction Command. The subsystem is completely redundant and capable of executing 512 pulse commands and 32 8-bit magnitude commands via redundant paths. Figure A-3 is a block diagram of the command subsystem showing the interconnection between units. Table A-3 summarizes performance.

The command receivers accept the PCM/FSK/AM amplitude-modulated onto an RF carrier in the 148 to 155-MHz band. The receivers demodulate the PCM/FSK/AM

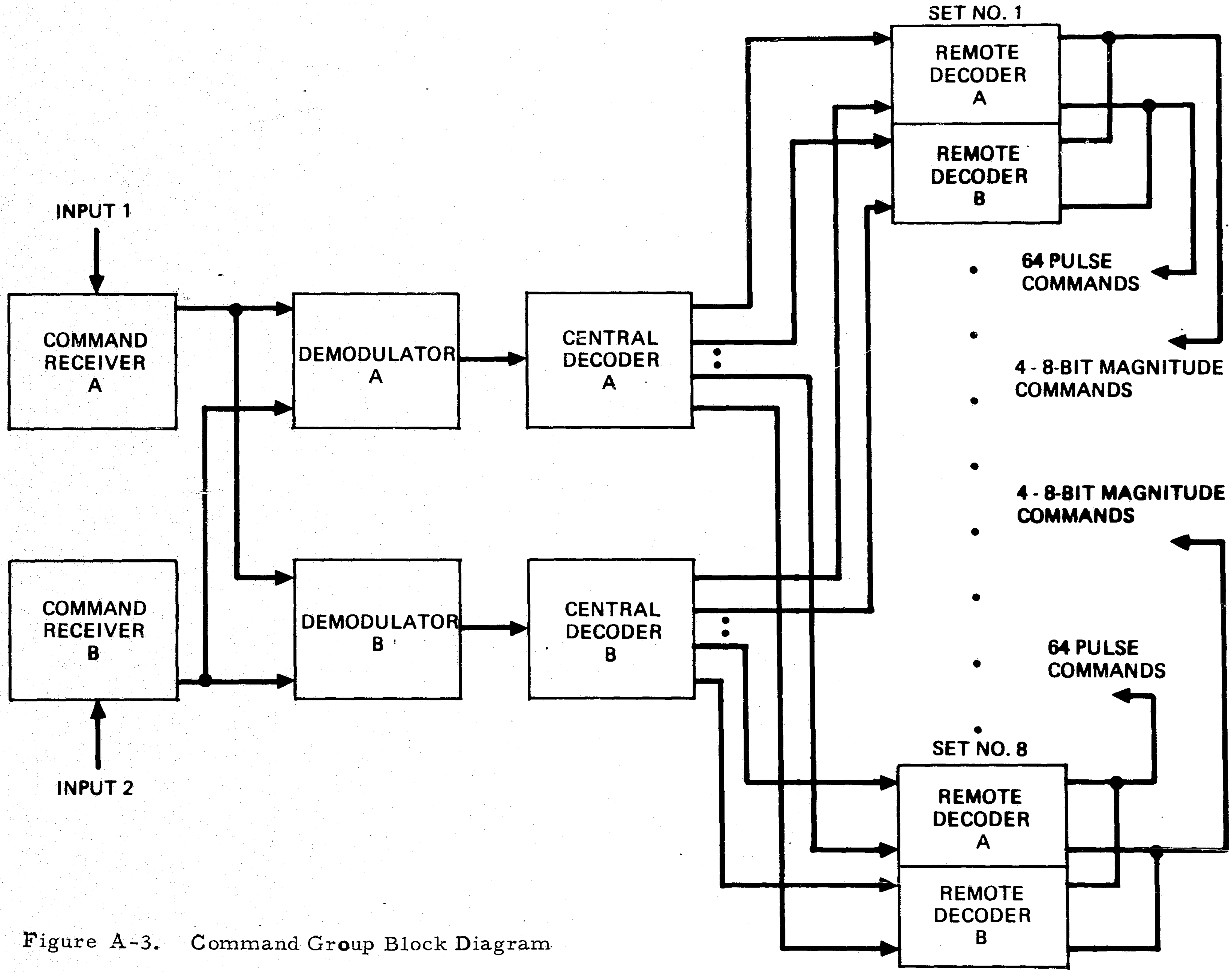

Figure A-3. Command Group Block Diagram

Table A-3. Summary of Command Group Characteristics

Command Receiver		
Carrier Frequency	148 to 154 MHz	
Noise Figure	8 db	
Sensitivity	-105 dbm	
Modulation Type	AM/FSK	
Command Demodulator/Decoder		
Circuit Type	Integrated Circuit	
Bit Rate	128 bps	
Word Length	64 bits	
Preamble	14 bits	
Spacecraft Address	7 bits	
Remote Decoder Address	5 bits	
Command	5 bits	
Complement of Spacecraft Address, Remote Address, and Command	23 bits	
Conclusion	1 bits	
Code Type	PCM 1 and 0 plus clock	
Number of outputs		
Pulse	512	
and		
Magnitude	32	
Number of Units for Full Redundancy		
Receiver	2	
Demodulator/Decoder	2	
Remote Decoder (assumes 64 pulse and 4 magnitude commands per unit)	16	
Unit Volume (per unit; non-redundant)		
Receiver	35 cu. in.	
Demodulator/Decoder	160 cu. in.	
Remote Decoder	28 cu. in.	
Unit Weight (per unit; non-redundant)		
Receiver	0.8 lbs.	
Demodulator/Decoder	2.8 lbs.	
Remote Decoder	0.7 lbs.	
Unit Power (per unit; non-redundant	Standby	Operate
Receiver	N/A	0.5W
Demodulator/Decoder	N/A	2.5W
Remote Decoder	0.2W	1.0W

signal and pass it to the demodulator/decoder. The pulse code modulation consists of two subcarrier frequencies in the 7 to 12-KHz band modulated by a sinusoidal bit-synchronization signal of 128 Hz. The bit-synchronization signal is 50 percent amplitude modulated onto the data subcarriers.

The PCM command demodulators receive the FSK/AM signal from both command receivers. The demodulator asynchronously samples the command receiver output, at a rate which guarantees a complete sample of each receiver output during any command introduction time. A receiver lock circuitry causes the demodulator to lock onto the first receiver to provide a valid output when sampled. In the event of a command receiver failure, the receiver lock circuitry will lock onto the operational receiver. The signal from the receiver not being sampled is shunted to ground.

The input signal to the demodulator consists of two frequency-shift-keyed subcarriers in the 7 to 12-KHz range; both amplitude modulated at 128 Hz. The AM/FSK audio input is passed through an input amplifier and bandpass filter. The bandpass filter output is amplified and fed to the FSK and AM demodulator and subcarrier level detector. The subcarrier level detector provides a logical one when it detects signal strengths at the audio input greater than 1.0 volt rms and a logical zero for signal strengths less than 0.5 volt rms. Hence, the subcarrier level detector rejects broadband noise from the receiver, and data is valid only when the detector is in the logical one state.

The AM demodulator detects the 128-Hz sine-wave amplitude modulation and provides a properly phased 128-Hz square wave for clock information. The FSK detector consists of bandpass filters followed by limiters and discriminators. From this the digital data is detected. The zero's, one's, clock, and subcarrier-present signal is fed to the central decoder section.

The central decoder performs message checks on incoming digital data and decodes the remote decoder address to select the destination of the command message for further processing. The data format will consist of a sixty-four bit word shown in Figure A-4 Each command message word will contain the following information.

13 zero bits	one bit	7 bit spacecraft address	5 bit remote decoder	11 bit command	complement of spacecraft address remote address and command	4 zero bits

Figure A-4. Command Word Format

The decoder will start processing digital data from its associated demodulator once a subcarrier-level signal is received. The decoder must receive at least 8 consecutive zeros followed by a message synchronization "one", followed immediately by the specified spacecraft address. The spacecraft address is externally selected by a program plug. If the specified address is not found, or the message synchronization "one" is not detected after sixteen zeros are received, the decoder will reject commands until a break in subcarrier returns it to a standby state. The decoder will return to a standby state if a break in data subcarrier is detected during receipt of a command message. Further processing of the command will be inhibited until reciept of a synchronization pattern.

The decoder will process the command if an initial decoder address check passes. At the end of the 23 bits of command, a bit-by-bit-check of the command message is made against the received complement bits. The command will be rejected if any bit fails to check.

Once a bit-by-bit check passes, the remote decoder address is decoded. The 11 bits of command information is reformatted into the following command frame shown in Figure A-5 and sent to the addressed remote decoder.

4 bit sync	1 bit mode	2 bit magnitude address	8 bit command	1 bit parity

Figure A-5. Remote Decoder Command Word Format

A synchronization pattern will be generated by the central decoder prior to sending the 11 bits of received data. A parity bit will be inserted on the 11 bits of received data. The data to the remote will be transmitted in bilevel manchester code and a third level executive state. The execute state will follow the command word for automatic execution of the received data if all checks pass in the central decoder. Each redundant demodulator/decoder has the capability to address 16 remote decoders, thereby providing complete redundancy for the execution of 512 pulse commands and 32 8-bit magnitude commands. Each demodulator/decoder contains its own regulator which provides several regulated voltages. In the event of an internal failure, current limiting will be provided to minimize power drain on the spacecraft bus.

2.3 Telemetry Subsystem

A representative telemetry group consists of a redundant pair of central encoders and a number (approximately 70) of redundant remote multiplexers (Figure A-6). The central encoder addresses each of the remote multiplexers in sequence and processes the telemetry data returning from them. The remote multiplexers are located near the TM data sources, thereby reducing the system harness weight. Performance of the telemetry group is summarized in Table A-4.

Each remote multiplexer is capable of accepting high-level analog and bilevel digital data in various mixes as a function of pin programming at the remote. The allowable data mixes or modes are: 1) 32 analog; 2) 14 analog, 16 digital; 3) 5 analog, 24 digital; 4) 32 digital. The remote multiplexer time-multiplexes the data and provides a PAM output data line to the central encoder. The central encoder interrogates the remote multiplexer via a single Manchester-coded (bi-phase) control line. Thus, the remote multiplexer/central encoder interface consists of two wires, control and PAM data.

The PAM analog and digital data from the remote multiplexers is processed and synchronized by the central encoder which then generates a Manchester-coded PCM output bit stream to the telemetry transmitters. Analog-to-digital conversion of analog data is provided by the central encoder.

Signal conditioning of temperature and pressure tranducers is provided by means of a constant-current generator which is located in the central encoder and is switched out to those remote multiplexers requiring signal

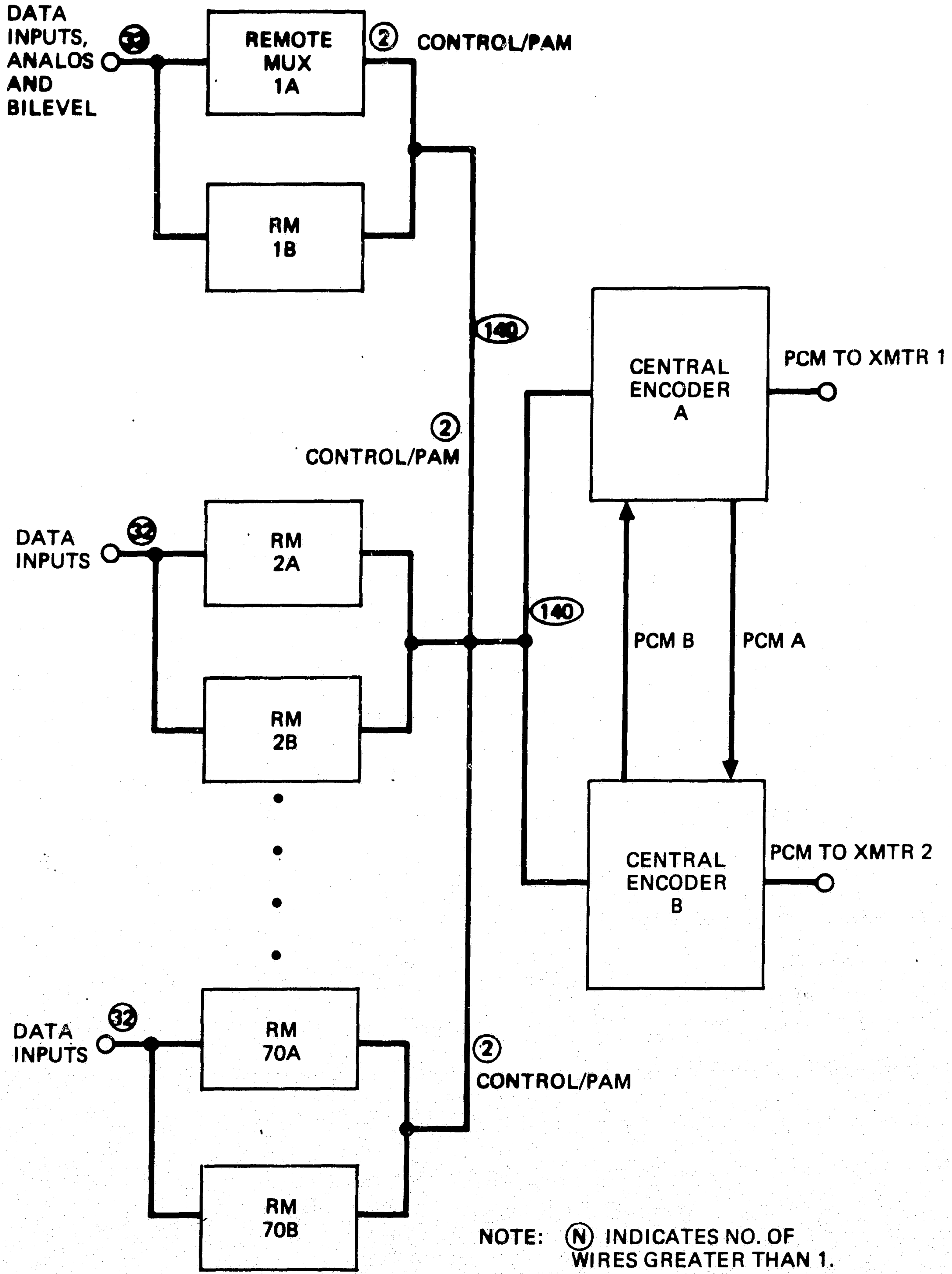

Figure A-6. Telemetry Group Block Diagram

Table A-4. Summary of Telemetry Group Characteristics

Telemetry Transmitter		
Carrier Frequency	136 to 138 MHz	
Power Output	2 w	
Telemetry Encoder		
Circuit Type	Integrated Circuits	
Word Length	8 bits	
Frame Synchronization	32 bits	
Bit Rate	400 bits per second	
Code Type	PCM Code (NRZ-L)	
Number of Words	500	
Number of inputs		
Analog	250	
and		
Digital	2000 bits	
Number of units for full redundancy		
Transmitter	2	
Encoder	2	
Remote multiplexer (assumes either 32 analog inputs or 32 digital bits per unit)	140	
Unit Volume (per unit; non-redundant)		
Transmitter	38 cu. in.	
Encoder	156 cu. in.	
Remote Multiplexer	15 cu. in.	
Unit Power Consumption (per unit; non-redundant)	Standby	Operate
Transmitter	0.4 W	6.0W
Encoder	0.2 W	1.0W
Remote Multiplexer	0.11W	1.0W
Unit Weight (per unit; non-redundant)		
Transmitter	1.0 lbs.	
Encoder	4 lbs.	
Remote Multiplexer	0.3 lbs.	

conditioning.

As in the command group equipment, current-limiting power supplies are used to condition internal power for the telemetry group equipment. The units described in the above configuration of a representative telemetry and command subsystem for the TV Broadcast Satellite have either been qualified for use on such spacecraft as ATS-A through E and MIL-COMSAT I or are currently being developed for ongoing space programs, particularly ATS-F and -G. As a result, the data and performance summarized above are quite firm.

2.4 Cost of Satellite-Borne T & C Equipment

A budgetary cost estimate for a T and C system as described would be $850 K recurring/spacecraft, plus $170 K non-recurring (for system integration, tests, software, etc.).

2.5 Cost of T & C Ground Equipment

Items Excluded:

- Site Cost
- Site Preparation
- Access Road
- Utilities Access
- Standby Power
- Building
- Air Conditioning
- Crew Quarters
- Transportation to Site(s)
- Equipment Installation (other than antenna)

Basic Capability of Station: Antenna is semi-fixed, equatorial mount, push-button control over ± 10 degrees Az-El. No tracking capability. Station is limited purpose, intended only for TV Broadcast Satellite house-keeping. (It is NOT intended to be a flexible multi-purpose station.) Real time T & C capability (as is needed for spinner type spacecraft) is not called for, nor is it provided. Pre-programmed computer control for uplink or down-link data (as needed for multiple-mission, multiple-satellite capability) is not called for, nor is it provided.

Equipment List (NOTE -- Costs are budgetary estimates only):	for one	for two
Antenna, crossed-yagi type, similar to TACO D-1365A, including site work and cables to building, at a U.S. location (supervised by manufacturer of antenna).	60K	105K
Command Transmitter, similar to Collins 242-C and Exciter 242-F, with self-contained Power Supplies	47K	94K
(*) Telemetry Recovery and Display, including telemetry receivers (2), in polarization diversity, similar to DEI/Nems-Clark/Vitro, including tracking filters, diversity combiner, discriminator; PCM signal conditioner, data simulator and comparator, tape and graphic recorders, displays, TTY readout. (*) Command Generator Console	330K	480K

(*) NOTE that these items may be common to those used for satellite ground checkout, in which case part of their cost may be included in the satellite procurement.

3. COST OF UP-LINK GROUND TERMINAL

To provide a basis for cost estimates for the uplink transmitting equipment, cost data were collected based on recent experience with the earth station at Itaboraí, Brazil, and various other ground terminals.

Table A-5 gives the initial and annual operating costs for the uplink transmitter. The initial transmitter cost includes power amplifier, power supply, and power conditioning equipment, display and control equipment (allows for monitoring transmitter r-f outputs only, i.e., excluding baseband) heat exchanger, and exciter. The power tubes are either traveling wave tubes (TWT) or klystrons as indicated in the table. TWT transmitters are capable of much larger instantaneous bandwidths than klystron transmitters, but TWT's are about one half as efficient as klystrons. The annual operating cost includes tube replacement based on continuous operation, 4,000-hour tube life, and an electric power rate of 10¢ per kilowatt-hour (this rate will be less for a U. S. station using commercial utilities). Other operating and maintenance costs are not included since they are highly dependent upon the nature of the labor used, the location of the ground station, and any peculiar logistics problems that might be encountered.

The cost data presented for the uplink antennas in Table A-6 assumes average soil conditions and reasonable wind specifications (i.e., survival in 120-mph winds). All antennas are limited to approximately $\pm 5^{\circ}$ motion on both axes. The antenna cost includes

Table A-5. Transmitter

Estimated installed cost and annual operating cost (replacement tubes and prime power only).

TUBE TYPE AND POWER OUT	INITIAL COST	ANNUAL OPERATING COST
5-KW TWT or 10-KW Klystron *	$100 K	$100 K
1-KW TWT or Klystron	$ 50 K	$ 45 K
300-W TWT	$ 31 K	$ 22 K
20-W TWT	$ 7 K	$ 5 K

*Because of a 2:1 ratio of efficiencies, these transmitters have identical initial and operating costs.

Table A-6. Antenna

Estimated cost for complete, installed, limited-motion equatorial-mount parabolic reflector, subreflector and feed.

DIAMETER (Feet)	COST ($)
8'	$ 10 K
10'	15 K
18'	40 K
25'	55 K
30'	70 K
42'	120 K
60'	400 K
85'	800 K
98'	875 K

feed, drive motors, and mechanisms, but does not include servo electronics.

Table A-7 lists costs for an uplink transmitter using a 5-kw TWT or 10-kw klystron, and associated ground station equipment without redundancy. Items (a) through (e) constitute a breakdown of the 5-kw TWT or 10-kw klystron transmitter cost presented in Table A-5. The remaining entries in Table A-7 are not included in the transmitter costs of Table A-5 since these costs do not vary significantly with output power of the transmitter. Thus, the total cost of items (f) through (k) is a fixed cost that must be added on to any of the transmitter costs in Table A-5. In order to arrive at the total hardware cost (not including building and facilities), the cost for an antenna (from Table A-6) must also be included, of course.

The cost of the building and associated facilities is highly dependent upon location, terrain, weather conditions, and many other factors. The cost of construction labor, for instance, varies greatly with the location of the ground station. However, some general cost estimates may be given. In the case of the Brazil ground station, the total cost for site access, site preparation, buildings, kitchen and office equipment, fuel tanks, wiring, plumbing, and air conditioning was in the range $850 K to $1 M. Some of this cost, however, arose from the need for wells, water puification, dormitories, street lights, and roads at that particular site. Such costs would not be incurred for a U. S. site with access to roads and commercial utilities. Costs for comparable buildings and associated facilities for a ground station in the U. S. might run to about $200 K to $300 K in an area where minimum site preparation is needed and where utilities are more accessible than at the Brazilian site.

Table A-7. Ground Station Equipment (No Redundancy)

a.	Cooling System This includes heat exchangers, but not air-conditioning for the building.	$ 5K
b.	Power Supply Power conditioning equipments costs are included.	33K
c.	Power Amplifier Applies for 5-kw TWT or 10-kw klystron.	35K
d.	Exciter	7K
e.	Transmitter, R-F Display and Control Equipment	20K
f.	Transmitter Display and Control Equipment Baseband, including monitoring, patching and display of audio, synch and color video.	20K
g.	Transmission line - 100' at $10/foot Includes labor, materials, and all fittings.	1K
h.	Synch Generator Includes four-output distribution system.	5K
i.	FM Modulators	5K
j.	Up-Converters (double conversion)	15K
k.	Hardware for minimum orderwire capability	7K

4. UPLINK RECEIVER

4.1 Noise Density at the Satellite Due to the Earth

The main beam of a high-gain satellite receiving antenna will normally be contained by the earth. From the point of view of the receiver, the earth may be considered a radio noise source. It is important that the noise density at the satellite due to the earth be known, so that its impact on the design of the uplink can be ascertained.

The radio noise temperature of the earth as a whole has been given as $254^{\circ}K$[18]. An earth temperature of approximately $280^{\circ}K$ is ordinarily used for gross system calculations. Its importance depends on its relative contribution to the overall system temperature. Heretofore, the noise temperature of spacecraft receivers has been high enough so that the effect of the earth contribution has been small. It may be expected that by 1975 and beyond, satellite receiver noise temperatures will be sufficiently low so that the earth temperature will be significant. In addition, as uplink antenna beams become narrower (to accommodate ground transmitters having low ERP), the fine structure of the earth noise sources may become increasingly important.

Indications are that the effective earth temperature varies only very slightly between daytime and nighttime. However, no hard data have been reported to confirm this.

A preliminary literature search revealed no significant information on the fine structure of earth radio noise sources as received by satellites. No scheduled experiments for this purpose[16] were discovered. A mapping of the sea surface thermal temperature by Nimbus I for some parts of the world has been done[4] and indicates the kind of information that might be required with respect to radio noise. A study has also been done[20] on the apparent radio temperature of the sea at 19.4 GHz and 35. GHz at an altitude of 1.KM. For a vertical angle less than 10^{o}, the apparent temperature at 19.4 GHz was approximately $140^{o}K$ and at 35 GHz was approximately $150^{o}K$. A preliminary study at Hughes Aircraft Company suggests a temperature of approximately $50^{o}K$ in the 2. to 10. GHz range for sea water.

Radio noise mapping at UHF by means of aircraft[7] has been done over some U. S. cities. Fine structure noise temperatures more than $50,000^{o}K$ at the frequencies of 226. MHz, 305. MHz and 369.MHz were measured. It is of interest to note that the radio noise temperature over Miami increases during the tourist season. Some limited measurements by aircraft[19] were also made at higher frequencies.

Extrapolating radio noise measurements made by aircraft to the noise seen by a satellite is a somewhat uncertain exercise. Practical results must ultimately be obtained by means of direct measurement. Some of the factors to be considered are the effect of the heaviside layer,[1,3,6,8,9,10,13] planet reflected extra-terrestrial noise, the earth's magnetic field, and natural terrestrial sources such as lightning in addition to man-made noise.

An analytical radio noise model based on the ideas of radio astronomy[2,3,5,11,12,14,15,17,21] was developed for possible use in radio noise measurements and their application. In Figure A-7 is shown the satellite antenna with a beam of Ω sterads. D is the distance between the satellite and the earth and it is assumed large compared to all other dimensions. Noise radiation from the earth is assumed to take place from a hypothetical hemispherical bump* on the

*Mathematical equivalent of a diffuse noise source.

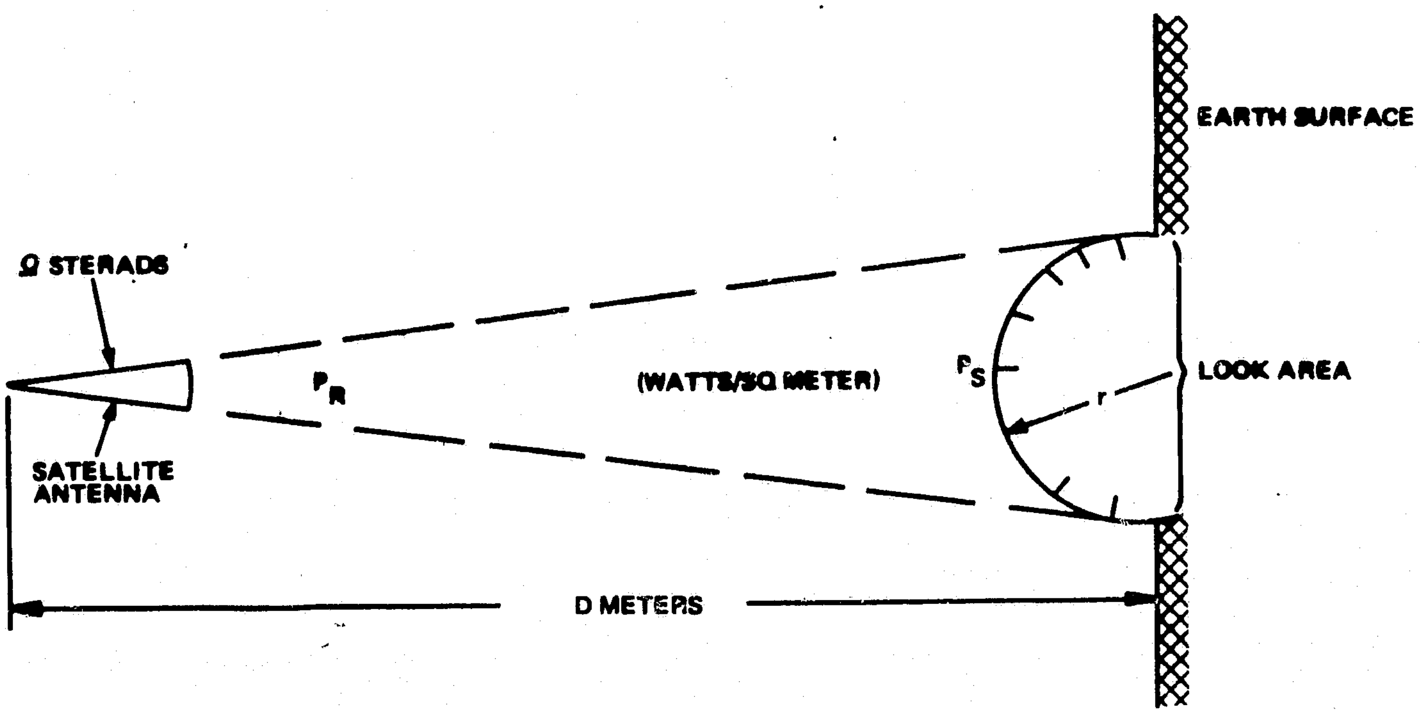

Figure A-7. Satellite-Earth Configuration earth's surface. The bump has a diameter equal to the beamwidth intercepted on the earth's surface.

The noise density at the satellite is

$$P_R = P_S \frac{r^2}{D^2} \quad \text{for } r << D \tag{1}$$

where

P_R = satellite noise density (watts/sq. meter)

P_S = earth noise density (watts/sq. meter)

r = bump radius (meters)

D = distance (meters)

The area on the earth intercepted by the beam is

$$\pi r^2 = D^2 \Omega \tag{2}$$

Substituting (2) in (1) results in

$$P_R = \frac{P_S \Omega}{\pi} \tag{3}$$

The extremely simple expression of Equation (3) relates the earth noise density to the received noise density in terms only of the receiver antenna beam width.

A useful form of Equation (3) is

$$B = \frac{P_S}{\pi} \text{ watts/sq. meter/sterad} \tag{4}$$

where B is called the source brightness.

The analysis above is independent of the means whereby the noise at the source is produced. A noise source could be a city where the noise is electrically generated or the sun in which thermal effects cause the noise. It is sometimes convenient to assume that all observed noise sources are thermally generated regardless of the real mechanism, and thereby derive an equivalent temperature.

This temperature, called the brightness temperature, is defined as the temperature of a black body source that matches the noise density of the observed data.

The Raleigh-Jeans formula is usually used at radio frequencies to relate noise to temperature. It is

$$P_S = \frac{2\pi\ k\ T}{\lambda^2} \text{ watts/square meter/H}_Z \tag{5}$$

where

k = Boltzmans constant (1.38×10^{-23} Joules/degree)

T = Temperature ^oK

λ = Wavelengths (meters)

When Equation (5) is substituted in (4) there results for the brightness temperature

$$T_B = \frac{B\lambda^2}{2k} \ {}^oK \tag{6}$$

It must be remembered of course that the brightness temperature is fictitious and is usually determined by measurement at a particular frequency. It can be used as an equivalent temperature in noise calculations but only at the frequencies substantiated by measurement.

The implications of the above relations become more evident when the satellite antenna is described in terms of an isotropic antenna.

The capture area of an antenna is

$$A_C = \frac{G\lambda^2}{4\pi} \tag{7}$$

where G = antenna gain compared to an isotropic antenna.

The total noise power captured by the satellite antenna is therefore, from Equations (3) and (7), using the relation $\Omega G = 4\pi$,

$$P_T = P_R A_C = \frac{P_S \lambda^2}{\pi} \tag{8}$$

Substituting the Raleigh-Jeans formula (Equation 5) in (8) results in

$$P_T = 2\ kT \quad \text{watts}/H_Z \tag{9}$$

The total received power may contain random polarizations and it is sometimes assumed that they are equi-likely. With this assumption, the total noise power given in Equation (9) should be halved when the receiving antenna is circularly polarized.

With the assumptions of Equations (1), (5) and (7), it is evident that the total noise power captured by the antenna when exposed to a thermal noise source is independent of the antenna beamwidth and the distance. It is a function of the source temperature only. This relation is convenient to use for astronomical purposes but should be used with caution when scanning the earth.

Large earth areas or the earth as a whole may contain a major source of noise of thermal origin but noise generated by inhabited areas is of a composite nature that should be determined by direct measurement.

4.3 BIBLIOGRAPHY

1. Herbert H. Reed, "Noise Curves for High-Gain Antennas", Microwaves, April 1967, p. 46

2. Donald B. Harris, "Microwave Radiometry", Part 1, Microwave Journal, April 1960, pp. 41-46. Ibid., Part 2, May 1960, pp. 47-54.

3. George G. Haroules, "Radiometric Techniques Applicable to the Measurement of Solar Activity and Atmospheric Attenuation at Millimeter Wavelengths", NASA TR R-306, April 1969

4. Lewis J. Allison and James S. Kennedy, "An Evaluation of Sea Surface Temperature as Measured by the Nimbus I High Resolution Infrared Radiometer", NASA TN D-4078, November 1967

5. Alex G. Smith and Thomas D. Carr, "Radio Exploration of the Planetary System", D. Van Nostrand Company, Inc., 1964, pp. 33-38

6. Leonard C. Humphrey, "Planet Reflected Extraterrestrial Noise", IEEE Transactions on Radio Frequency Interference, March 1963, pp. 83-85.

7. George Ploussios, "City Noise and its Effects Upon Airborne Antenna Noise Temperatures at UHF", IEEE Trans. Aerospace and Electronic Systems, Vol. AES, No. 1, January 1968, pp. 41-51

8. George H. Millman, "Cosmic Noise Limits Long Range Radar", Space/Aeronautics, January 1961, pp. 124-129

9. E. N. Skomal, "Man-Made Noise, Sources and Characteristics", Frequency, January-February 1967, pp. 14-19

10. James F. Lee, "Natural Interference in Space Systems", Electronic Design, August 3, 1960, pp. 90-93

11. Wilbur L. Pritchard, "Microwave Aspects of Space Communications", Microwave Journal, August 1963, pp. 52-64

12. Hugh P. Taylor, "The Radiometer Equation", Microwave Journal, May 1967, pp. 39-42

13. F. Horner, "Radio Noise in Space Originating in Natural Terrestrial Sources", Planet Space Sci., 1965, Vol. 13, pp. 1137-1150

14. W. L. Weeks, "Antenna Engineering", McGraw-Hill Book Company, 1968, pp. 301-307

15. J. A. Roberts, "Radio Emission from the Planets", Planet Space Sci., 1963, Vol. II, pp. 221-259

16. Jean R. Oliver and Harry L. Wolbers, "A Program Plan for Earth Orbital Space Astronomy", IEEE Transactions on Aerospace and Electronic Systems, Vol. AES-5, No. 2, March 1969, pp. 242-252

17. Klaus Kuenzi and Erwin Schanda, "A Microwave Scanning Radiometer", Correspondence IEEE Transactions on Microwave Theory and Techniques, September 1968, pp. 789-791

18. "Reference Data for Engineers", 1968, Howard W. Sams and Company, Inc., Chapters 27, 34

19. A. H. Mills, "Final Report, Measurement and Analysis of Radio Frequency Noise in Urban, Suburban, and Rural Areas", (General Dynamics, Convair Division,) 1969, NASA CR-72490.

20. A. Stogryn, "The Apparent Temperature of the Sea at Microwave Frequencies," IEEE Transactions on Antennas and Propagation, Vol. AP-15, No. 2, March 1967, pp. 278-286.

21. Cornell H. Mayer, "Thermal Radio Radiation from the Moon and Planets," IEEE Transactions on Antennas and Propagation, Vol. AP-12, No. 7, December 1964, pp. 902-913.

Report GDC-DCF 70-002

TELEVISION BROADCAST SATELLITE STUDY

FINAL REPORT - VOLUME IV

TECHNICAL APPENDICES

Contract NAS8-21036

31 December 1970

APPENDIX B

NOISE AND TELEVISION SIGNAL QUALITY

Convair Aerospace Division

GENERAL DYNAMICS

B

NOISE AND TELEVISION SIGNAL QUALITY

1.1 QUALITY AND GRADING OF TELEVISION PICTURES

The effect of random noise is familiar to most viewers of broadcast television because of the appearance of 'snow' in monochrome pictures. In a satellite broadcast system noise is added to the signal at various stages in the path from the uplink transmitter through the satellite transponder and ground receiving system.

Data on the subjective effects caused by various levels of noise upon television pictures are essential in order to establish a reliable basis for the specification of signal to noise ratio in connection with a satellite broadcast system.

The effect of random noise on color TV is similar to the variations of luminance which occur on a monochrome picture, but with the addition of variations in chromaticity (Ref. 1 and 2). Because of the smaller bandwidth occupied by the chrominance signal the chromaticity variations have a coarser structure than the luminance variations. The luminance signal is mostly affected by low-frequency noise and the chrominance signal mostly by noise around the chrominance subcarrier. The proportion of chromaticity variations to luminance variations is thus greater for triangular noise than for flat noise.

The output-noise-amplitude spectrum of an FM receiver is triangular because of FM discriminator characteristics, i.e., the higher the frequency of noise energy the greater the corresponding discriminator noise output. In an ideal AM system the detected noise response is essentially flat. In practice a signal may be transmitted through multiple networks with differing response characteristics, thus the overall noise response encountered in actual practice is generally somewhere between flat and triangular.

In order to account for variations in noise spectra and also to allow for the fact that the visibility of noise is a function of frequency, it has become a standard practice in the television field to measure noise with the aid of a weighting network, (Ref. 3). It has been observed that equal amplitudes of noise at different frequencies have different degradation effects due to the distribution in the picture and the reaction of the eye. Generally, noise in the higher frequency region is more tolerable to the human observer than that in the low end of the video baseband.

Frequency weighting from experiments and studies conducted at Bell Telephone Labs in 1953 and 1961 are illustrated in Figure B-1 and listed in Table B-1. The purpose of using these weightings for monochrome and color TV is to make the subjective evaluation of various types of viewing material independent of the shape and bandwidth of the noise. CCIR random-noise weightings taken from CCIR recommendation 421-1 (Ref. 4) are listed in Table B-2.

"Subjective tests of pictures impaired by distortion and noise provide basic data for the design of television broadcasting systems but their complex nature is a source of difficulty. The results are affected by the many arbitrary factors involved in choosing such features as the type of psychometric test, the class of observers, the test picture and viewing conditions. . ." (Ref. 7.).

The simplest form of quality-grading impairment testing is that in which only a single intentional impairment is present and the principal variable is the magnitude of the distortion or noise which is applied to degrade an otherwise near-perfect picture.

In order to control the viewing environment and conditions most subjective tests have been made under laboratory conditions. A program of this nature which used a large and carefully selected sample of observers was the Television Allocations Study Organization, (TASO) which assembled a selected group of observers from colleges and community organizations, (Ref. 8).

The results of the TASO studies; which analyzed, measured and evaluated the effects of random noise and other types of interference upon viewer satisfaction with television pictures, have been widely used in the United States to define performance requirements for video transmission systems. The estimated signal/noise ratio desired as a function of the percentage of viewers rating a picture as being of a certain quality or better is shown in Figures B-2 and B-3.

Tables B-3 through B-7 illustrate picture grading scales which list quality and degree of impairment in various ways, (Ref. 7).

There appears to be doubt about the validity of using the data obtained by means of utilizing the nomenclature listed in several of the scales included in these Tables. There is suspicion that several of the scales would not be suitable since doubt is raised in the observers mind about what the scale is attempting to define.

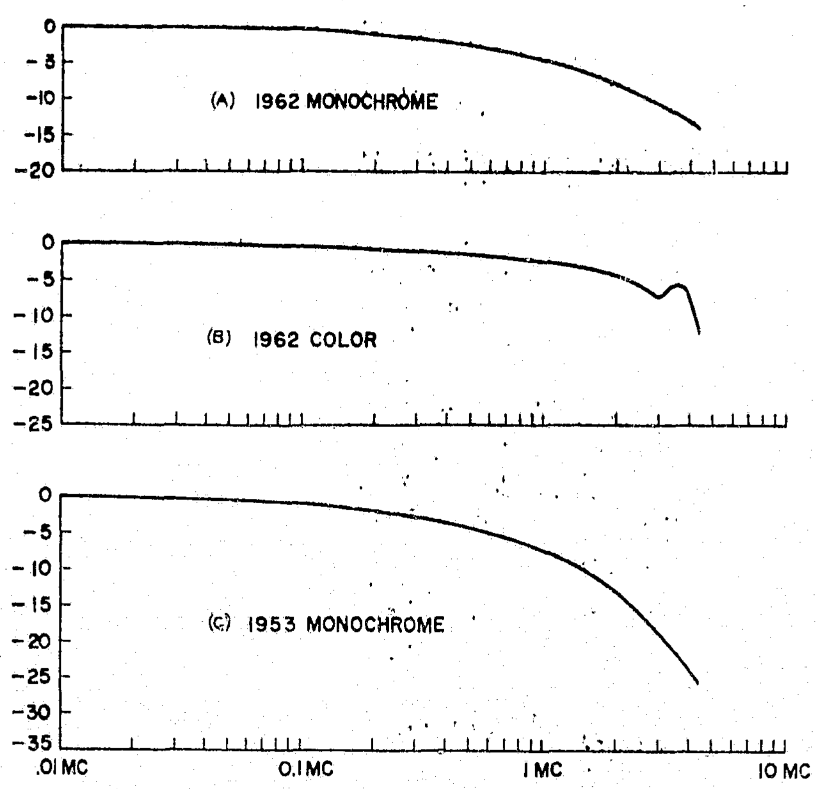

Figure B-1 Random Interference Weightings (Ref. 5)

Table B-1 Monochrome and Color Weightings
(Ref. 5)

Frequency, Mc	1962 Monochrome, Db	1962 Color	1953 Monochrome, Db
0.1	-0.3	-0.4	-1.0
0.3	-1.7	-1.0	-3.0
0.5	-2.8	-1.4	-4.5
0.7	-3.6	-1.9	-5.8
0.9	-4.4	-2.3	-7.0
1.0	-4.7	-2.5	-7.6
1.1	-5.1	-2.7	-8.2
1.3	-5.8	-3,1	-9.2
1.5	-6.5	-3.5	-10.3
1.7	-7.1	-3.8	-11.3
1.9	-7.8	-4.4	-12.4
2.0	-8.1	-4.7	-13.0
2.1	-8.4	-5.0	-13.7
2.3	-8.9	-5.5	-14.9
2.5	-9.5	-6.1	-16.0
2.7	-10.0	-6.6	-17.2
2.9	-10.5	-7.3	-18.3
3.0	-10.8	-7.4	-18.8
3.1	-11.0	-7.2	-19.4
3.3	-11.5	-6.0	-20.5
3.5	-11.9	-5.5	-21.5
3.7	-12.4	-5.6	-22.4
3.9	-12.8	-6.5	-23.4
4.0	-13.0	-7.5	-23.8
4.1	-13.2	-8.6	(-24.2)
4.3	-13.7	-10.7	(-25.0)
4.5	-14.3	-13.2	(-25.8)

Table B-2. Random Noise Weightings
(Ref. 6)

Number of Lines	f_c [1] (MHz)	Theoretical Weighting (dB), for	
		"White" noise	"Triangular" Nose
525 M(Canada and U. S. A)		6•1	10•2
525 M (Japan)	4	8•5	16•3
625 B, C, G, H	5	8•5	16•3
625 D, K, L	6	9•3	17•8
819 F	5	8•5	16•3
819 E	10	8•5	16•3

[1] f_c is the nominal upper video-frequency limit of the system (MHz).

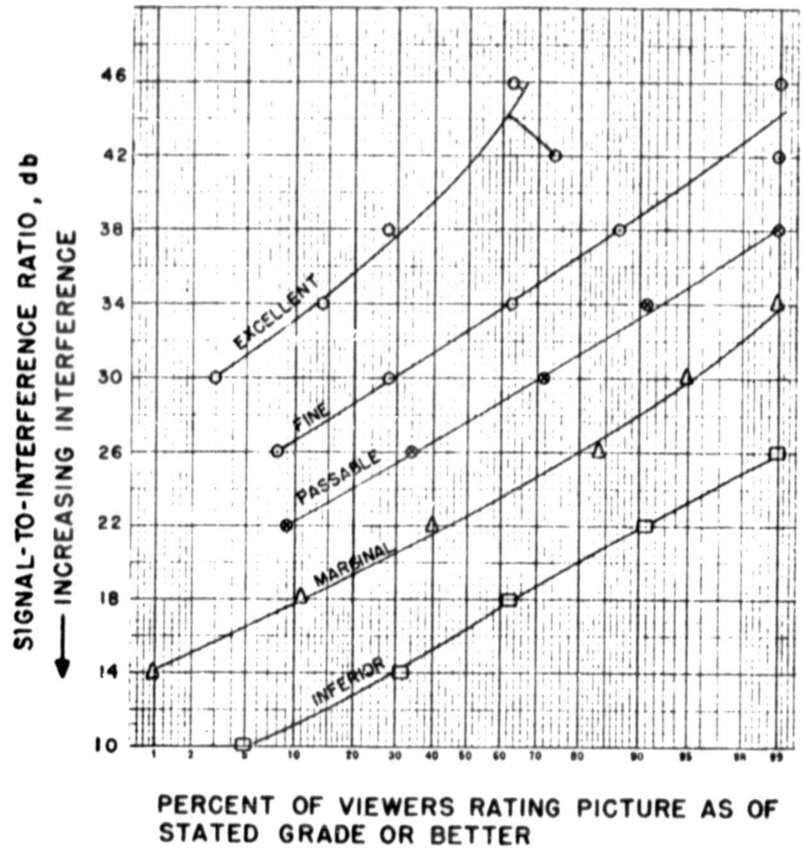

Fig. 8—Random-noise interference with Miss TASO picture. Test 9 (19M and 34J), using 38 male and 38 female observers.

Figure B-2. Results of TASO Studies (Ref. 8)

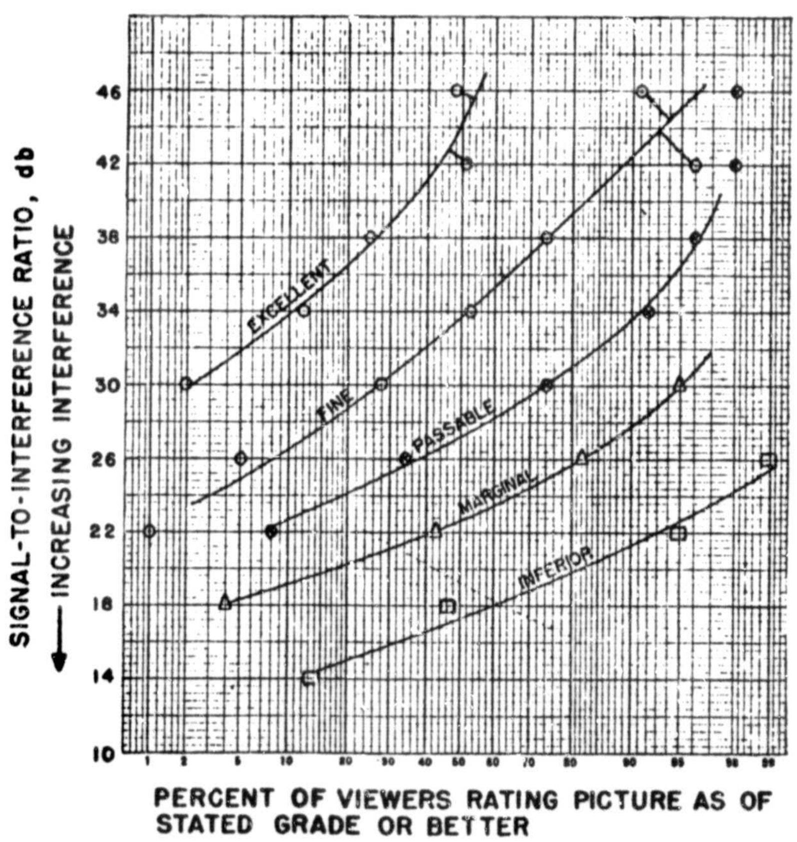

Fig. 9—Random-noise interference, averaging the results from seven scenes not including Miss TASO. Observers were 16 women who participated in all seven tests.

Figure B-3. Results of TASO Studies (Ref. 8)

Table B-3 Bell Laboratories 'Impairment' Scale
(Ref. 7)

Comment Number	
1	Not perceptible
2	Just perceptible
3	Definitely perceptible, but only slight impairment to picture
4	Impairment to picture but not objectionable
5	Somewhat objectionable
6	Definitely objectionable
7	Extremely objectionable

Table B-4 BBC 'Impairment' Scale
(Ref. 7)

Score	
1	Imperceptible
2	Just perceptible
3	Definitely perceptible but not disturbing
4	Somewhat objectionable
5	Definitely objectionable
6	Unusable

Table B-5 BBC 'Quality' Scale
(Ref. 7)

Score	
1.	Excellent
2	Good
3	Fairly good
4	Rather poor
5	Poor
6	Very poor

Table B-6 TASO 'Mixed' Scale
(Ref. 7)

Number	Name	Description
1	Excellent	The picture is of extremely high quality; as good as you could desire
2	Fine	The picture is of high quality providing enjoyable viewing. Interference is perceptible
3	Passable	The picture is of acceptable quality. Interference is not objectionable
4	Marginal	The picture is poor in quality and you wish you could improve it. Interference is somewhat objectionable
5	Inferior	The picture is very poor but you could watch it. Definitely objectionable interference is present
6	Unusable	The picture is so bad that you could not watch it.

Table B-7 Referred 5 Grade 'Quality' Scale
(Ref. 7)

Grade	
A	(Excellent)
B	(Good)
C	(Fair)
D	(Poor)
E	(Bad)

The 'preferred' 5 grade quality scale has been used in England, (Ref. 7). The adjectives in that scale are placed inside parantheses to emphasize the alphabetical scale and to suggest that words were intended as hints rather than rigid definitions.

In the English test results shown in Figures B-4 and B-5 the mean score (P5 in Table B-9) is obtained by assigning scores of 1.0, 0.75, 0.5 and 0.25, and 0 to the quality grader A to E respectively. The condition where P5 = .5 is designated as the mid-opinion mark point. "The stepped curves represent the opinion of a hypothetical median observer in the sense that each vertical transition between two grades occurs at a level of impairment such that half the observers are expected to place themselves in the higher grade(s) and half in the lower". (Ref.7) .

Three general methods have been used in the reduction of data characterized by: (1) numerous observations and observers, (2) a number of reasonably close spaced signal/interference ratios, (3) a choice of several merit ratings which have been intended to constitute equal steps of subjective picture quality. The cumulative frequency distributions was used to plot the data obtained during the TASO studies. This method plots the data as the percent of observations which rated the signal/noise ratio as the stated grade or better. This type of presentation may be used to estimate the signal/noise ratio required to provide a given picture quality to a specified percentage of the receivers.

The second method used averages the data of all quality ratings obtained, assuming equally spaced ratings. According to Dean (Ref. 8) this method has two disadvantages in that it is necessary to assume equally spaced quality ratings and secondly that the original distribution of grades cannot be recovered. The mean observer presentation has the advantage that the plots are more easily understood since the curves show poor grades correlated with low signal/interference ratios and high grades correlated with high signal/interference ratios.

The third method was not used in the TASO studies though this method has been used recently in the English studies. The English method considers specific grades of service and uses a mathematical model to describe the relationship between opinion distribution and mean score. The results of several test programs conducted in England are shown in Figure B-4 and B-5.

Table B-8 Signal/Noise Ratios, as Measured (Unweighted) and After Allowance for the UK 625-Line Monchrome Weighting

Mark Point	Unweighted		Weighted		
	Flat	Triangular	Flat	Triangular	Average
Midopinion	28.7	23.6	35.2	35.9	35.6
B/C Transition	30.8	25.1	37.3	37.4	37.4
5% Unfavourable	32.6	26.3	39.1	38.6	38.8
A/B Transition	36.9	29.1	43.4	41.4	42.4

Table B-9. Signal/Weighted-Noise Ratio for Noise in the Luminance Channel Alone

ps	Mark Point	dB
0.500	Midopinion	34.1
0.620	B/C Transition	35.8
0.780	95% Favourable	38.6
0.859	A/B Transition	40.6

Signal/Weighted-Noise Ratios for Noise in the Chrominance Channel Alone

0.500	Midopinion	28.2
0.620	B/C Transition	29.7
0.780	95% Favourable	32.1
0.859	A/B Transition	33.8

p_s = mean score

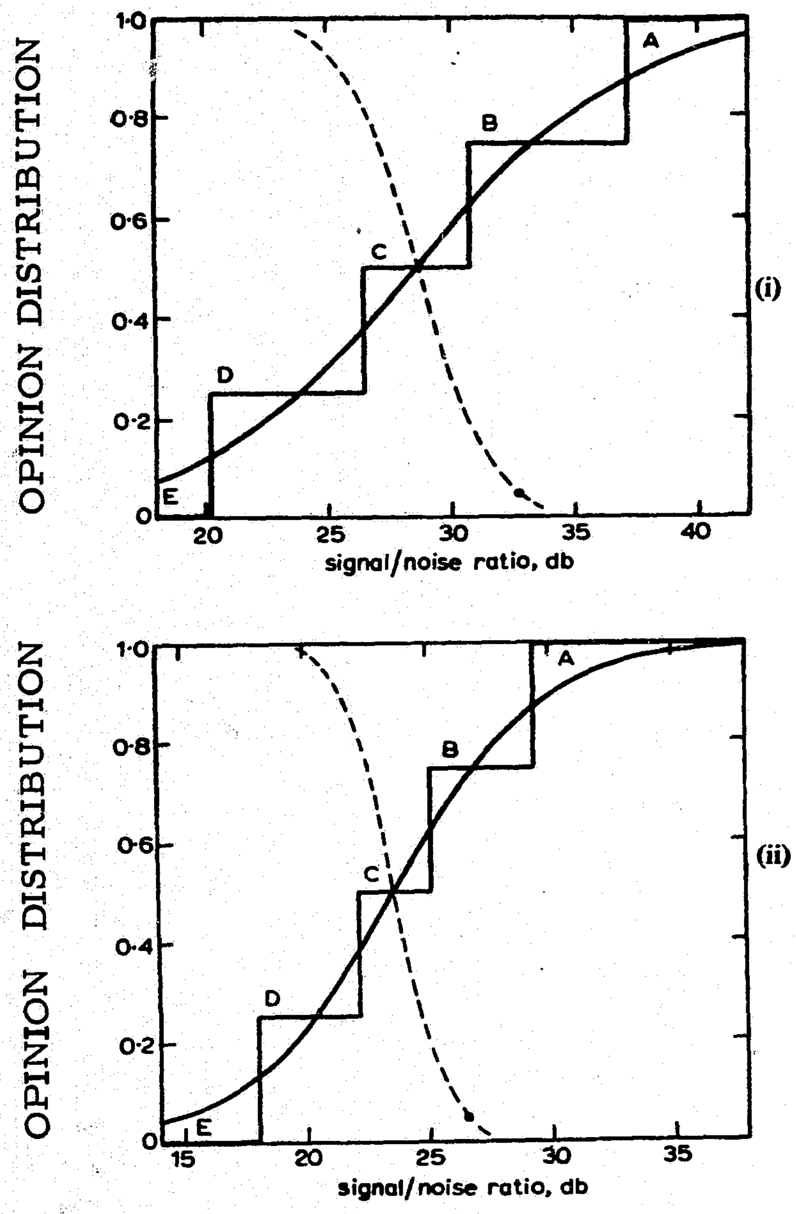

Figure B-4 Average Result After Correction for Residual Impairment (Monochrome)

(i) Flat noise
(ii) Triangular noise
____ mean score
---- proportion of unfavorable opinions

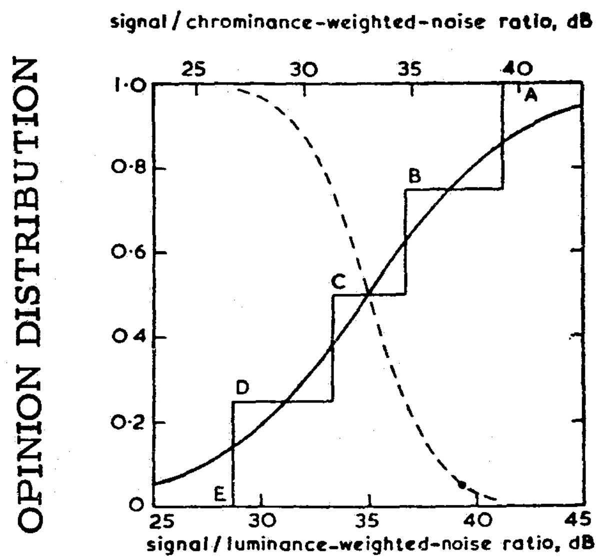

Figure B-5 Flat Noise, Result After Correction for Residual Impairment

——— mean score; stepped curve refers to median observer
------ proportion of unfavourable opinions

Laboratory performed picture quality tests are made in the absence of certain powerful influences, such as program interest and the associated sound, which normally tend to divert a viewer's attention from any technical imperfections that may exist in a picture. Also, still pictures have been used extensively in a majority of these grading tests and it has been observed (Ref. 7) that grading by the viewing of still pictures results in the establishment of more stringent requirements than those obtained in conjunction with motion pictures.

During the random noise tests used to establish the TASO grading results, noise was combined with a high level RF carrier at the receiver RF input terminals. The noise spectrum of the noise generator was flat within $\pm$ 3 db over the TV channel which was used during the tests. Furthermore, the noise spectrum was flat within $\pm$ 1 db over the frequency band extending from the picture carrier to the color subcarrier. (No noise weighting was used).

Signal/interference ratios for various presentations were produced by maintaining the desired signal at a constant level and varying the noise level. The signal/interference ratio used in the random noise tests was the ratio of RF rms signal during sync peak divided by the rms noise voltage over a 6MHz channel.

No instruments were used during the TASO grading tests to simulate the interference generated by automobile ignition systems, vibrators, shavers and similar sparking devices.

Since automotive ignition noise appears to be the predominant constituent of urban and suburban noise in the VHF and UHF bands, (Ref. 9), the combined effects of impulse noise and random noise on picture quality must be considered in order to obtain a realistic appraisal of the effects of quasi-impulsive noise upon television picture viewing (Ref. 10).

Quasi-impulsive noise is an interference of an intermediate type between two extreme types of noise, i.e., thermal or white noise of irregular amplitude and shape with impulses following one another in such a manner that their effects overlap. The second type is impulsive noise, which consists of successive impulses shorter in duration than the time constant of the receiver separated by intervals so long that their effects do not overlap. The two main types of quasi-impulsive interference are atmospheric noise and man-made noise. Man-made noise may, for certain periods of time, occur quasi-periodically, with fairly constant shape and amplitude. Such interference requires special methods of measurement, (Ref. 11) and the prediction of its effects on receivers is difficult.

An AMVSB monochrome television picture is transmitted over the modulation range, between 12.5% and 75% of the maximum carrier voltage, with 12.5% representing full white in the picture, and a level of 67.5% representing black. The synchronizing signal is transmitted by increasing the power of the transmitter to 100% during part of the blanking interval between picture lines and frames.

Any impulsive noise such as that caused by ignition or lightning, added to the signal arriving at the detector of a TV receiver causes, in general, an increase in the instantaneous voltage at the detector (Ref. 12). Some cancellation of the signal may occur, but, provided that the radio and intermediate frequency amplifiers have been designed so that no blocking occurs, reductions in the instantaneous value caused by noise of the signal is negligible compared with increases. As a result, impulse noise produces mainly black dots of very low visibility in the picture and spikes exceeding the normal level of the sync pulse in the sync signal.

If a noise spike is higher than the sync pulse, it can be removed completely from the sync signal by using noise gating and/or noise inverting circuitry.

The variation of the video signal caused by variation of the received RF signal may be reduced to a few percent of the total signal by using pulsed AGC which operates over the working range of the AGC circuit.

1.2 FCC DEFINITIONS OF GRADE A AND B SERVICE CONTOURS (Ref. 13)

Grade A represents a specific value of ambient median field strength existing 30 feet above ground which is deemed to be sufficiently strong, in the absence of interference from other stations, but with due consideration given to man-made noise typical of urban areas, to provide a picture which the median observer would classify as of "acceptable" quality, assuming a receiving installation (antenna, transmission line, and receiver) considered to be typical of suburban or not too distant areas. This signal level is sufficiently strong to provide such a picture at least 90% of the time, at the best 70% of receiving locations. The grade A contour represents the outer geographic limits within which the median field strength equals or exceeds the Grade A value. The specific values for Grade A are 68 dbu (2.5mV/m) for Channels 2 to 6, 71 dbu (3.5 mV/m) for Channels 7 to 13, and 74 dbu (5.0 v/m) for Channels 14 to 83.

Grade B represents a specific value of ambient median field strength existing 30 feet above ground which is deemed to be sufficiently strong, in the absence of man-made noise or interference from other stations, to provide a picture which the median observer would classify as of "acceptable" quality, assuming a receiving installation (Antenna, transmission line, and receiver) considered to be typical of outlying or near-fringe areas. This signal level is sufficiently strong to provide such a picture at least 90% of the time, at the best 50% of receiving locations. The Grade B contour represents the outer geographic limits within which the median field strength equals or exceeds the Grade B value. The specific values for Grade B are 47 dbu (0.22mV/M) for Channels 2 to 6, 56 dbu (0.63mV/m) for Channels 7 to 13, and 64 dbu (1.6 mV/M for Channels 14 to 83).

Although "acceptable" quality is not further defined in the background material leading to these standards, the assumed signal-to-noise ratio (S_{nr}) of 30 db would indicate a quality similar to that described by the Television Allocation Study Organization (TASO) as Grade 3 or "passable" which is described as follows: "The picture is of acceptable quality. Interference is not objectionable."

With respect to "city grade service," no comparable statistics are included in the aforementioned reference,(14) but presumably this would entail the same quality of picture, which would be available to a higher percentage of locations and/or a higher percentage of the time, in the face of an even poorer receiving antenna and/or more severe man-made noise limitation.

Thus it appears that the present picture quality which is generally available in the U.S., assuming nominal receiving equipment, is equivalent to the TASO grade 3 which is rated as being passable and described as a picture of acceptable quality with perceptible interference which is not objectionable.

1.3 MAN-MADE NOISE

Figure B-6 summarizes indigenous noise data which was obtained from several recent study program final reports and other technical publications. Line (1) in Figure B-6 is a plot of the maximum urban indigenous noise level used in the Jansky Bailey Report. The Jansky Bailey data was taken from the ITT Radio Engineers Handbook. The other data shown in the figure was obtained from the Jansky Bailey Report and other data compiled during feasibility studies of satellite voice broadcasting which were conducted by G.E. and RCA and directed by NASA. The noise levels shown in Figure B-6 are given in terms of equivalent brightness temperature as seen by a half-wave matched dipole.

Conclusions which may be drawn from this survey are:

1. Automotive ignition noise is the probable predominant constituent of urban and suburban noise in the VHF and UHF bands.
2. The indigenous noise level varies with time. (Noise levels have been observed to vary 16 db between peak traffic flow periods and quiet periods during the evening)
3, Noise measurements obtained exhibit very high peak-to-rms ratios.
4. Average man-made noise levels may be reduced by 10 db or more if automotive ignition noise is eliminated.
5. The results of antenna noise discrimination measurements conducted by G.E. during the voice broadcast study indicate that a high antenna ($>$3 db) elevated 45^{o} from the horizon provides a reduction in man-made noise of approximately one-half the antenna power gain.
6. Polarization effects upon noise levels observed appear to be insignificant.
7. For low noise locations the reception of man-made noise should tend to increase .
8. The effects of antenna height, location, orientation and shielding have not been measured or analyzed to any significant extent with respect to reception from synchronous orbit by small ground stations. (Ref. 15)
9. The division of noise levels into urban, suburban, and rural areas is arbitrary. The noise level, in general, appears to increase with population density through this relationship has not been proven and appears to be a poor description of the actual situation. The manmade noise level appears to be more closely associated with the proximity of automotive throughfares than to the number of people living in a given area.

10. Man-made noise other than that due to automotive ignition is caused primarily by rotating electrical machinery, electrical appliances, power transmission lines and power stations. The noise levels observed to emanate from high voltage transmission lines and power stations increase during periods of high humidity or rainy weather.

When low noise amplifiers are used, noise from external sources becomes a predominant factor in the determination of the system signal to noise ratio. When this is the case it is desirable to consider antenna designs that reduce the reception of noise relative to the desired signal. Thus one of the main objectives to be accomplished in the design of a ground station antenna is to reduce the side and back lobe levels as much as possible within the specified cost constraints.

Assuming an optimally designed antenna the second objective which should be considered is that of obtaining a low noise installation. The use of shielding provided by surrounding terrain and structures should be considered in selecting a location for a receiving antenna installation. If suitable shielding terrain or structures are not available the use of pits, construction of walls or fences and the use of suitable RF absorbent material should be considered for installations where a high level ambient noise environment exists.

The amount of attenuation afforded by structures is shown in Figure B-7. The data in Figure B-7 was taken from the RCA voice broadcast study final report and represents the comparative signal loss between locations on the roof-top and inside a building for a signal from a terrestrial transmitter. The values were not corrected for the change in height and thus can only be used as a gross estimate of noise shielding which might be obtained from various structures.

The use of natural terrain, earth walls, and excavated pits for the shielding of communication satellite antenna from radio interference propagating at low angles has been considered by several authors, (Ref. 16). Care is taken to install large communication antennas in low noise locations which utilize the natural terrain for shielding. (The 210 foot Goldstone installation is a good example of this type of installation). The use of this type of shielding to obtain isolation from man-made noise sources and interfering signals may also be considered with respect to small receiving stations operating in conjunction with a synchronous orbit TV broadcast satellite. Isolation magnitudes on the order of 40 db should be obtainable

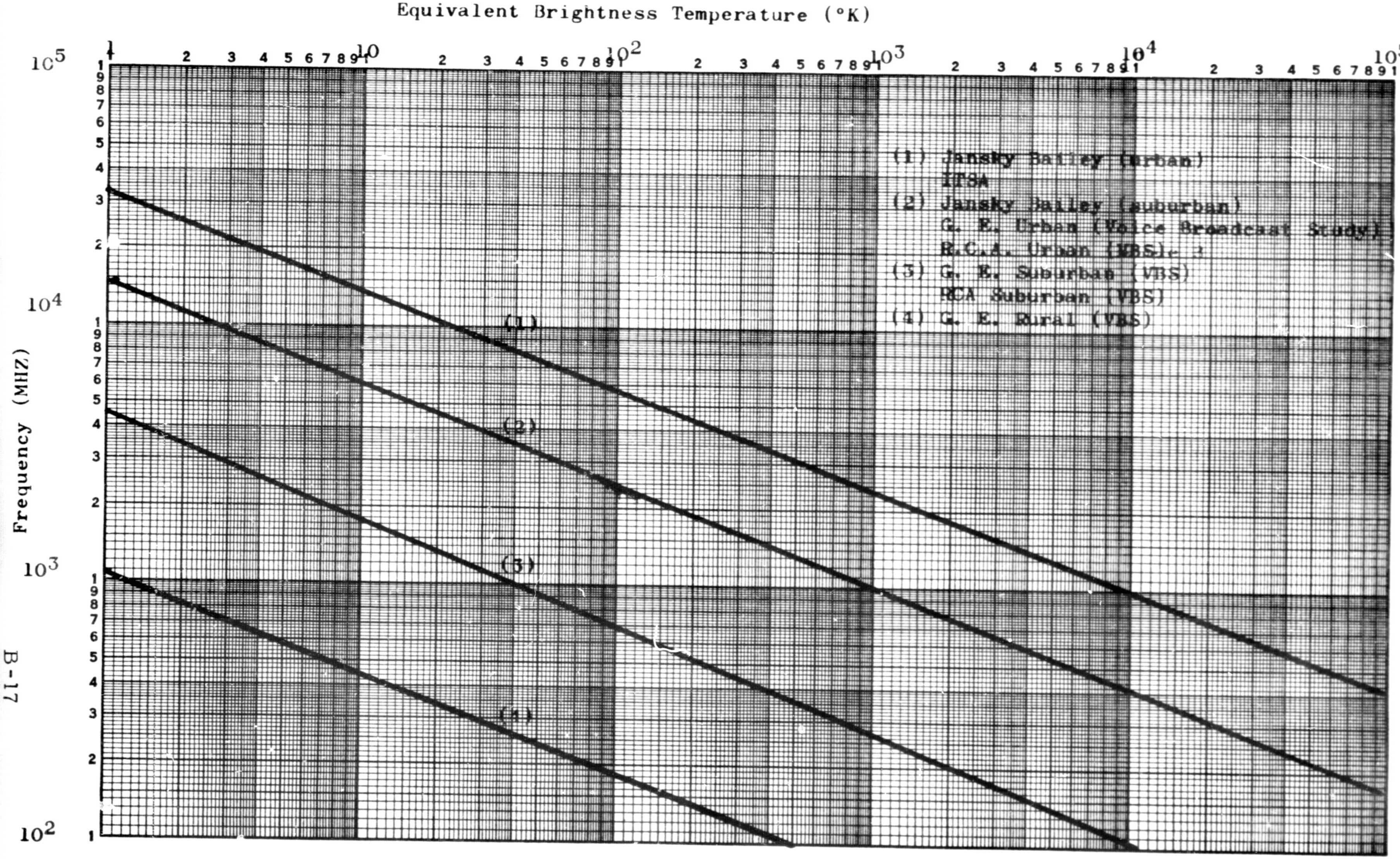

Figure B-6 Indigenous Noise Data Summary by using pits. For a given pit the magnitude of shielding will increase slightly with frequency in the upper UHF and microwave frequency bands, (Ref. 16).

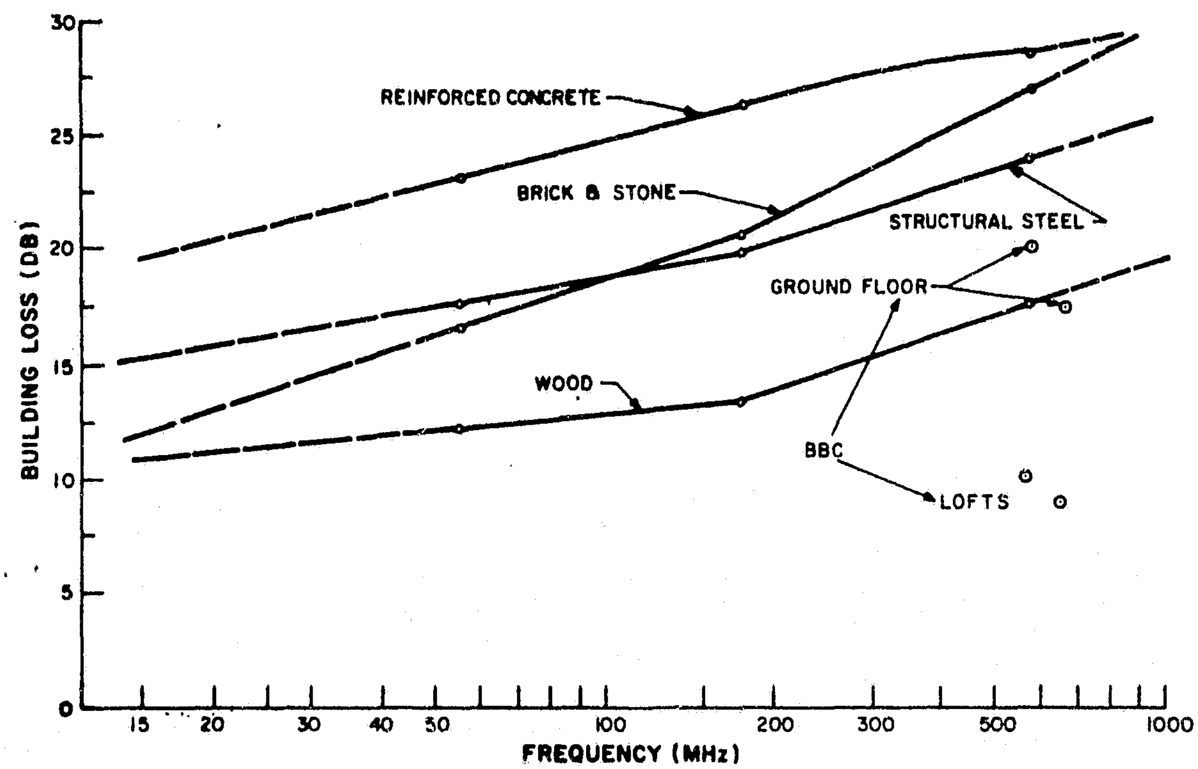

Figure B-7. Attenuation Caused by Various Structures (from RCA VBS)

1-4 MAN-MADE NOISE LITERATURE SURVEY

1. Measurement and Analysis of Radio Frequency Noise in Urban, Suburban and Rural Areas. Final Report, By A. H. Mills, General Dynamics/Convair Technical Management P. Kuhns, NASA LeRC, Contract NAS 3-9714, NASA CR-72490, GD/C-AWV 68-001.

   Abstract:

   Radio frequency noise was measured from the air and on the ground in urban, suburban, and rural areas. The primary objectives were to determine the characteristics of man-made as a function of frequency, time of day and location and also determine the correlation between the air and ground measurement results. (Test data has not been evaluated)

2. G. E. Voice Broadcast Mission Study, Volume II. Final Report NASA Contract No. NASw-1475, July 14, 1967, Document No. 67SD4330.

Abstract:

G. E. conducted a limited program to measure man-made noise. The data obtained by G. E. agreed closely with other data which had been obtained earlier. It was noted in the G. E. report that the ITT and Hammar data was significantly higher than any other data. (The ITT data agrees closely to data which was obtained in downtown Washington, D. C. amidst traffic by W. Q. Criehlow of the Institute for Telecommunication Sciences and Aeronomy)

The results of the G. E. Antenna noise discrimination measurements indicate that a high gain ($>$3 db) antenna elevated 45^{o} from the horizon provides a reduction in man-made noise level of approximately half the antenna power gain.

3. RCA Voice Broadcast Study, Final Report, Contract No. NASw-1476-Prepared for NASA headquarters, May 1967.

RCA undertook a limited man-made noise measurement program in support of the Voice Broadcast Study. The primary purpose of the test program was to determine expected levels of unintentionally generated man-made noise in urban areas. The survey was conducted at sites located in the New York City - New Jersey metropolitan areas. Measurements were performed at three frequencies: 20 MHZ, 109 MHZ and 800 MHZ. Both dipole and directive antennas were used in the VHF and UHF measurements. The directive antennas were used to determine if signal-noise discrimination could be obtained by virtue of directivity.

The results of the directive antenna noise discrimination measurements indicated on a gross basis that a directive antenna pointed 45^{o} above the horizon will have a noise gain on the order of that of a dipole, possibly less.

20

4. <u>Technical and Cost Factors that Affect Television Reception from a Synchronous Satellite.</u> Final Report, Contract NASw-1305, June 30 1966, Atlantic Research, Jansky and Bailey Systems Engineering Dept.

ITT Radio Engineer Handbook man-made noise data is presented and converted to an equivalent brightness temperature. The study considers a satellite in synchronous orbit and ERP's ranging from 30 dbw to 90 dbw. The look angle is assumed to be 43^{o} from the receiving site. In order to minimize the effect of a limited knowledge of values of indigenous noise a 40 db range of noise level values was considered.

In order to determine the relative effects on man-made noise suppression of directive antennas,the solid angle over which this source of noise was effective was defined to be the solid angle extending from the horizon to 10^{o} and 360^{o} about the receiving antenna. The effect of an antenna on the reception or suppression of man-made noise was determined by calculating the average gain of the antenna in the directions bounded by the solid angle defined.

5. E. N. Skomal, "Distribution and Frequency Dependence of Unintentionally Generated Man-Made VHF/UHF noise in Metropolitan Areas", IEEE transactions on EMC, Part I, September 1965, Vol. EMC-7 NV-3 Page 263 - 278. Part II , December 1965, Vol. EMC-7 No. 4, Page 42 - 427.

An analysis and evaluation of previously published metropolitan area man-made noise data over the 200 to 500 MHZ frequency range was performed. The conclusion was made that unintentionally generated man-made noise in urban and suburban areas is impulsive in form and random in occurrence. No reliable evidence of any existing correlation between ambient noise level and population density was determined. Skomal concludes that automotive ignition noise is the probable predominant constituent of urban and suburban radio noise in the VHF/UHF frequency bands.

REFERENCES

1. Charles E. Dean, "Measurements of the Subjective Effects of Interference in Television Reception" Proceedings of the IRE, Page 1035 - 1049, June 1960. "In all tests, the observers were divided into four groups of about five subjects each, two of the groups observing color receivers while the other two observed monochrome receivers. Equal quantities of data were therefore obtained for color and monochrome reception. Comparisons of the data for the two cases have been made in a few instances and revealed little difference, with a suggestion of a slightly greater tolerance for interference when receiving a color picture. The data for color and monochrome reception are therefore pooled in most of the plots giving the panel findings".

2. J. W. Allnatt, and R. D. Prosser, "Subjective Quality of Color-Television Pictures Impaired by Random Noise", Proc. IEE (British) Vol. 113, No. 4, April 1966, Page 55-1557. "... over an appreciable range of the noise spectra occurring in practice, the signal/noise ratios for monochrome television are up to 1.5 db greater than the corresponding values for the luminance channel in color television".

3. J. M. Barstow, and H. N. Christopher, "The Measurement of Random Video Interference to Monochrome and Color Television Pictures", Communication and Electronics, 1962, Page 313.

4. "Requirements for the Transmission of Monochrome Television Signals over Long Distances", CCIR Recommendation 421-1, Geneva 1965.

5. 3 Ibid.

6. 4 Ibid.

7. R. D. Prosser, et. al., "Quality Grading of Impaired Television Picture", Proc. IEE. Vol. 111, No. 3, March 1964, Page 491-502, (British)

8. Dean, op. cit.,

9. E. N. Skomal, "Distribution and Frequency Dependence of Unintenionally Generated Man-Made VHF/UHF Noise in Metropolitan Areas," IEEE Trans. On EMC, Part II December 1965, Vol. EMC-7 No. 4, Page 420-427.

10. CCIR Documents of the XIth Plenary Assembly, Oslo, 1966, Vol. V, Sound Broadcasting and Television, (Assessment of the quality of Television Pictures, Page 239).

11. G. E. Voice Broadcast Study.

12. Kenneth James, "A Simple Noise Eliminator for Television Receiver Synchronizing Circuits.", IEEE Trans. on Broadcast and Television Receivers, Vol. BTR-12 No. 1, April 1966.

13. Robert A. O'Connor, "Understanding Television's Grade A and Grade B Service Contours", IEEE Transactions on Broadcasting, Vol. BC-14 No. 4 December 1968, Page 137-143.

14. Section 73 of the FCC Rules and Regulations

15. Space Applications Summer Study, Vol. 3 Part II Broadcast 1967 Interim Report. "Particular attention should be given to exploiting the discrimination achievable by virtue of the high incidence angles typical for synchronous satellites. Local shielding of terrestial stations may be possible using a knowledge of the (constant) angular direction of the satellite.

16. George H. Hagn, et. al., "Pit Shielding For Communication Satellite Ground-Terminal Antennas". IEEE Transactions Electromagnetic Compatibility, June 1965, Vol. EMC 7, No. 2, Page 93-103.

Report GDC-DCF 70-002

TELEVISION BROADCAST SATELLITE STUDY

FINAL REPORT - VOLUME IV

TECHNICAL APPENDICES

Contract NAS8-21036

31 December 1970

APPENDIX C

FM/FM MULTIPLE VOICE CHANNEL TV TRANSMISSION

Convair Aerospace Division

GENERAL DYNAMICS

APPENDIX C

ANALYSIS OF FM/FM MULTIPLE VOICE CHANNEL TV TRANSMISSION

1. SUMMARY

The discussion on the following pages develops the equations necessary for the analysis of FM/FM techniques of transmitting multiple voice channel TV signals. The result of this analysis is summarized in one equation for input carrier-to-noise ratio as a function of RF bandwidth in terms of all of the various parameters of the modulation process. This equation can be represented in the form of trade-off curves of predetection carrier-to-noise ratio vs required RF bandwidth. From such curves we can quantitatively determine the cost of including multiple sound channels in terms of required bandwidth and carrier power. The curves also give us a means of comparing the FM/FM single carrier technique with other modulation schemes such as AM-VSB and FM/FM with multiple carriers.

2. GENERAL DISCUSSION

The purpose of this memo is to give the appropriate equations for one particular method of transmitting a TV picture with multiple sound channels. While a number of methods for providing multiple audio channels with the video channel for TV transmission are presently under consideration for satellite TV links, the method described in this memo seems most promising.[6] It is assumed that the reader is familiar with frequency modulation concepts and therefore basic FM equations such as those derived in References [1], [2], [3], [4], and [5] will be used in this memo.

The method under consideration requires multiple sound subcarriers (one for each audio channel) placed at frequencies above the highest video frequency. The composite baseband is then frequency modulated onto the main carrier for transmission. The following diagram illustrates the baseband signal:

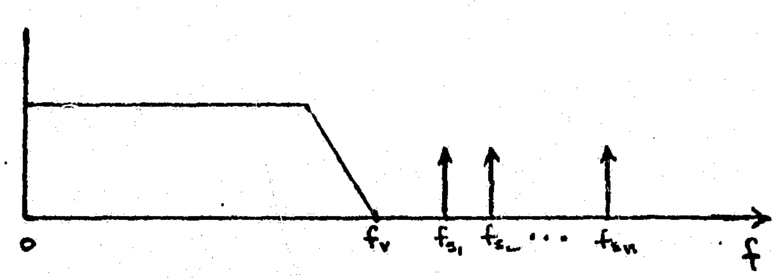

where

f_v = maximum video frequency

fs_i = frequency (no modulation) of the i^{th} subcarrier

$i = 1, 2, \ldots, n$

The n subcarriers are spaced with a guard band b_{gi} between them and a guard band b_v between the lowest frequency in the audio band and the upper video frequency f_v. Therefore, the total audio baseband bandwidth is

$$B_a = nb_a + \sum_{i=1}^{n-1} b_{gi} \tag{1}$$

where

b_a = the audio bandwidth

b_{gi} = guard band bandwidth between the i^{th} and $(i+1)^{th}$ channels.

The total baseband bandwidth is

B = video bandwidth + audio bandwidth

thus

$$B = (b_v + f_v) + (nb_a + \sum_{i=1}^{n-1} b_{gi}) \qquad (2)$$

Since the sound channels should all be of the same quality, it is reasonable to take the audio bandwidth, b_a, of each channel to be a constant.

The following diagram illustrates the baseband frequency allocation according to Equation 2.

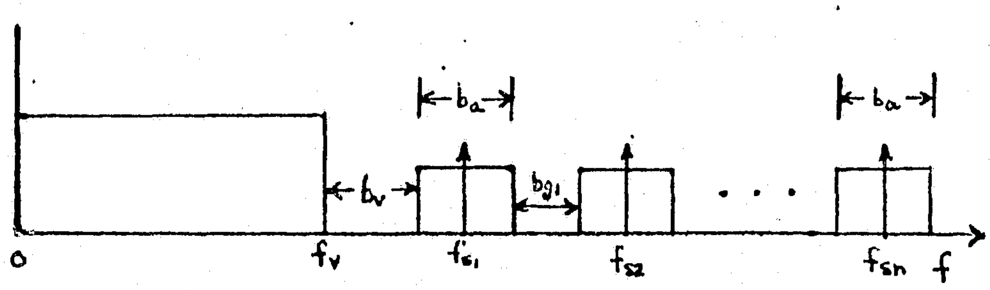

This baseband is then frequency modulated onto the main carrier (at frequency f_c) for transmission via the satellite link. The problem that remains is to determine the video signal-to-noise ratio and the audio signal-to-noise ratio in terms of the carrier-to-noise ratio as a function of the various modulation parameters.

3. DETERMINATION OF VIDEO SIGNAL-TO-NOISE RATIO

The signal-to-unweighted noise ratio at the output of the carrier demodulator can be written in terms of the predetection carrier-to-noise ratio by using the standard FM relation

$$\left(\frac{S}{N}\right)_v = 3\left(\frac{\Delta f_v}{f_v}\right)^2 \frac{B_{RF}}{2f_v} \left(\frac{C}{N}\right)_{IN} \tag{3}$$

where

B_{RF} = the RF carrier predetection noise bandwidth

Δf_v = the peak carrier deviation due to the video signal

Where it is assumed that $\left(\frac{C}{N}\right)_{IN}$ is above threshold. This can be written in terms of the carrier-to-noise density ratio as

$$\left(\frac{S}{N}\right)_v = \frac{3}{2} \frac{\Delta f_v^{\,2}}{f_v^{\,3}} \left(\frac{C}{\eta}\right)_{IN} \tag{4}$$

The ratio $\Delta f_v/f_v$ is often referred to as a video deviation ratio, D_v, or video modulation index. Equation 4 gives the average signal power to average noise power ratio. We will, however, be interested in the peak-to-peak "picture" power which is related to the average video signal power by

$$S_{picture} = \frac{1}{2} S_{p-p} = \frac{1}{2} (8S_{rms})$$

as is shown in Appendix A. Therefore,

$$\left(\frac{S}{N}\right)_{picture} = 4 \left(\frac{S}{N}\right)_v$$

and Equation 4 gives

$$\left(\frac{S}{N}\right)_{picture} = 6 \frac{(\Delta f_v)^2}{(f_v)^2} \left(\frac{C}{\eta}\right)_{IN} \tag{5}$$

as the p-p picture power-to-rms noise power ratio. It should be noted that Δf_v is the peak deviation of the carrier due to the video portion only and that no noise weighting factors or preemphasis improvement factors are included.

4. DETERMINATION OF AUDIO SIGNAL-TO-NOISE RATIO

At the output of the subcarrier demodulator, the signal (test-tone)-to-noise ratio is given by [3], [6], [7], [9]

$$\left(\frac{S}{N}\right)_a = \frac{3}{2} D_{ci}^{\,2} D_{si}^{\,2} \frac{B_{RF}}{2f_a} \left(\frac{C}{N}\right)_{IN} \tag{6}$$

where

D_{ci} = deviation ratio of the carrier due to the i^{th} audio subcarrier

D_{si} = deviation ratio of the i^{th} subcarrier due to its audio signal

f_a = highest audio baseband frequency

B_{RF} = total RF bandwidth

Since for our system, the peak subcarrier deviation Δf_{si} will be small compared to the subcarrier center frequency f_{si} for each of the audio channels, then [3], [6], [7]

$$D_{ci} = \frac{\Delta f_{ci}}{f_{si}}$$

and

$$D_{si} = \frac{\Delta f_{si}}{f_a}$$

where Δf_{ci} is the peak frequency deviation of the carrier due to the i^{th} subcarrier. Equation 6 can then be written

$$\left(\frac{S}{N}\right)_a = \frac{3}{4} \frac{(\Delta f_{ci})^2}{(f_{si})^2} \frac{(\Delta f_{si})^2}{(f_a)^3} \left(\frac{C}{\eta}\right)_{IN} \tag{7}$$

The overall peak carrier deviation, Δf_a, due to all of the audio subcarriers, is in general a complicated function of the individual Δf_{ci}. For multiple voice channels, Δf_a is usually taken to be the sum of the individual Δf_{ci} for a conservative analysis of the system.[6] This is probably the most correct approach for the particular system under consideration since the frequency deviations in the n channels will be highly correlated (with a high probability, the deviations due to the individual subcarriers will be at their peak values at the same times). This is also true since any music and special sound effects will most likely be the same in all voice channels. Furthermore, for some applications the voices on the n channels will be different dialects of the same language. For some types of channels, however, an rms addition of the individual frequency deviations is appropriate [8] and would probably provide a lower bound on Δf_a for our system with a large number of relatively uncorrelated voice channels.

We will require that the deviation ratio $D_{ci} = \frac{\Delta f_{ci}}{f_{si}}$ be a constant for all i to ensure that the individual voice channels will be of the same quality. Assuming that

$$\Delta f_a = \sum_{i=1}^{n} \Delta f_{ci} \tag{8}$$

and since

$$D_{ci} = \frac{\Delta f_{ci}}{f_{si}} = \frac{\sum_{i=1}^{n} \Delta f_{ci}}{\sum_{i=1}^{n} f_{si}} = \text{constant, all } i \tag{9}$$

then Equation 7 may be written

$$\left(\frac{S}{N}\right)_a = \frac{3}{4} \cdot \frac{(\Delta f_{si})^2}{(f_a)^3} \left(\frac{\Delta f_a}{\sum_{i=1}^{n} f_{si}}\right)^2 \left(\frac{C}{\eta}\right)_{IN} \tag{10}$$

The next step is to determine the subcarrier-to-noise ratio in the i^{th} channel in terms of the carrier-to-noise ratio. This may be expressed as [7]

$$\left(\frac{SC}{N}\right)_i = \frac{B_{RF}}{4\Delta f_{si}} \left(\frac{\Delta f_{ci}}{f_{si}}\right)^2 \left(\frac{C}{N}\right)_{IN} \tag{11}$$

and therefore

$$\left(\frac{SC}{N}\right)_i = \left(\frac{1}{4\Delta f_{si}}\right) D_{ci}^{\ 2} \left(\frac{C}{\eta}\right)_{IN} \tag{12}$$

If we now take the bandwidth of the i^{th} audio subcarrier channel to be

$$b_a = 2\Delta f_{si}$$

then Equation 12 becomes

$$\left(\frac{SC}{N}\right)_i = \frac{1}{2b_a} D_{ci}^{\ 2} \left(\frac{C}{\eta}\right)_{IN} \tag{13}$$

which agrees with [6]. For these relations to be valid, the peak subcarrier deviation must be small compared with its center frequency.

5. DETERMINATION OF REQUIRED RF BANDWIDTH

The RF bandwidth required by the main carrier is

$$B_{RF} = 2(\Delta f + B) \tag{14}$$

by Carson's rule. Here Δf is the peak frequency deviation of the carrier due to the video signal and all of the audio subcarriers and B is the total baseband bandwidth as in Equation 2. Again we have the problem of determining the peak frequency deviation of a carrier when it is being modulated by several signals. For a conservative design, we can let $\Delta f = \Delta f_v + \Delta f_a$ which is used in Reference [6], and will give an upper bound on the RF bandwidth. If we are willing to tolerate overmodulation for a small fraction of the time, then the RF bandwidth can be reduced. The expense of allowing overmodulation, however, is increased nonlinear distortion and therefore increased crosstalk. References [3] and [4] discuss this problem in further detail. For our analysis, we can use Equation 14 keeping in mind that we are being somewhat pessimistic and will require a higher carrier-to-noise ratio as a result.

6. SUMMARY OF ANALYTICAL RESULTS

The results of the previous discussion can be summarized in the following equations

(1) From Equation 5

$$\left(\frac{S}{N}\right)_{picture} = 6\,\frac{(\Delta f_v)^2}{(f_v)^3}\left(\frac{C}{\eta}\right)_{IN} \qquad \text{(S-1)}$$

or, in terms of the carrier RF bandwidth

$$\left(\frac{S}{N}\right)_{picture} = 6\,\frac{(\Delta f_v)^2}{(f_v)^3}\,B_{RF}\left(\frac{C}{N}\right)_{IN} \qquad \text{(S-2)}$$

(2) From Equation 7

$$\left(\frac{S}{N}\right)_{ai} = \frac{3}{4}\,\frac{(\Delta f_{ci})^2}{(f_{si})^2}\,\frac{(\Delta f_{si})^2}{(f_a)^3}\left(\frac{C}{\eta}\right)_{IN} \qquad \text{(S-3)}$$

or in terms of B_{RF}

$$\left(\frac{S}{N}\right)_{ai} = \frac{3}{4}\,\frac{(\Delta f_{ci})^2}{(f_{si})^2}\,\frac{(\Delta f_{si})^2}{(f_a)^3}\,B_{RF}\left(\frac{C}{N}\right)_{IN} \qquad \text{(S-4)}$$

which can be written

$$\left(\frac{S}{N}\right)_{ai} = \frac{3}{4}\,\frac{(\Delta f_a)^2}{\left(\sum_{i=1}^{n} f_{si}\right)^2}\,\frac{(\Delta f_{si})^2}{(f_a)^3}\,B_{RF}\left(\frac{C}{N}\right)_{IN} \qquad \text{(S-5)}$$

if

$$\frac{\Delta f_a}{\left(\sum_{i=1}^{n} f_{si}\right)} = D_{ci} = \frac{\Delta f_{ci}}{f_{si}} = \text{constant, all } i$$

(3) From Equation 13

$$\left(\frac{SC}{N}\right)_i = \frac{1}{4\Delta f_{si}} \frac{(\Delta f_{ci})^2}{(f_{si})^2} \left(\frac{C}{\eta}\right)_{IN} \tag{S-6}$$

which can be written in terms of B_{RF} and b_a*,

$$\left(\frac{SC}{N}\right)_i = \frac{1}{2b_a} D_{ci}^{\,2} \; B_{RF} \left(\frac{C}{N}\right)_{IN} \tag{S-7}$$

where

$$D_{ci} = \frac{\Delta f_a}{\sum_{i=1}^{n} f_{si}} = \frac{\Delta f_{ci}}{f_{si}} = \text{constant all } i$$

as in Equation S-5. In the remaining work, $f_s \triangleq \sum_{i=1}^{n} f_{si}$ will be used for convenience.

(4) Finally the maximum RF bandwidth can be written as

$$B_{RF} \leq 2(\Delta f_a + \Delta f_v + B)$$

by Carson's rule.

*Actually (S-7) is the more general expression in that (S-6) is a special case of (S-7) for $b_a = 2\Delta f_{si}$. Some authors [6][7] use $b_a > 2\Delta f_{si}$ which would alter equation (S-6).

7. APPLICATION OF RESULTS

In order to determine the important parameters for a given signal format, we can specify the signal-to-noise requirements $\left(\frac{S}{N}\right)_a$, $\left(\frac{S}{N}\right)_v$, and $\left(\frac{SC}{N}\right)$ and the signal format parameters (f_a, f_v, B, and $f_s = \sum_{i=1}^{n} f_{si}$) to give the desired system performance. The following sequence of equations may then be used to determine the necessary modulation parameters

(1) Dividing equation (S-7) by (S-4)

$$\frac{\left(\frac{SC}{N}\right)}{\left(\frac{S}{N}\right)_a} = \frac{2(f_a)^3}{3b_a(\Delta f_s)^2}$$

$$\therefore (\Delta f_s)^2 \, b_a = \frac{2}{3} f_a^{\,3} \frac{\left(S/N\right)_a}{\left(SC/N\right)}$$

where it is assumed that $\left(\frac{SC}{N}\right)$ and $\left(\frac{S}{N}\right)_a$ are constant for all channels (independent of i). If we let $b_a = 1.1\ (2^a \Delta f_s)$ where $2\ \Delta f_s$ is the maximum subcarrier peak-to-peak frequency deviation, then

$$\Delta f_s = f_a \left[\frac{\left(S/N_a\right)}{3.3\ (SC/N)}\right]^{\frac{1}{3}} \qquad \text{(I)}$$

This allows us to determine Δf_s for a given $\left(\frac{S}{N}\right)_a$ and $\left(\frac{SC}{N}\right)$ requirement.

(2) From equation (S-7)

$$\left(\frac{SC}{N}\right) = \frac{1}{2b_a} \left(\frac{\Delta f_a}{f_s}\right)^2 B_{RF} \left(\frac{C}{N}\right)_{IN}$$

where

$$f_s = \sum_{i=1}^{n} f_{si}$$

which gives the solution for Δf_a as

$$\Delta f_a = f_s \left[\frac{2b_a \left(\frac{SC}{N}\right)}{B_{RF} \left(\frac{C}{N}\right)_{IN}} \right]^{\frac{1}{2}} \tag{II}$$

(3) Solving equation (S-2) for Δf_v we have

$$\Delta f_v = f_v^{\frac{3}{2}} \left[\frac{(S/N)_{picture}}{6\ B_{RF} \left(\frac{C}{N}\right)_{IN}} \right]^{\frac{1}{2}} \tag{III}$$

(4) Finally, the bandwidth (worst case) is

$$B_{RF} = 2(\Delta f_a + \Delta f_v + B) \tag{IV}$$

For a given system, we can obtain trade-off curves of $\left(\frac{C}{N}\right)_{IN}$ versus B_{RF} from these four equations. Substituting for Δf_v and Δf_a from (II) and (III) into (IV) and solving for $\left(\frac{C}{N}\right)_{IN}$, we get

$$\left(\frac{C}{N}\right)_{IN} = \frac{4 \left\{ f_s \sqrt{2b_a \left(\frac{SC}{N}\right)} + f_v^{3/2} \sqrt{\frac{1}{6} \left(\frac{S}{N}\right)_{picture}} \right\}^2}{B_{RF} (B_{RF} - 2B)^2}$$

from which a curve of $\left(\frac{C}{N}\right)_{IN}$ versus B_{RF} may be obtained. Note that b_a may be expressed in terms of f_a, $\left(\frac{S}{N}\right)_a$, and $\left(\frac{SC}{N}\right)$ from equation I and the assumed relation between b_a and Δf_s.

If some other means of obtaining total peak frequency deviation on the main carrier is desired (such as rms addition), these equations and the resulting expression for $\left(\frac{C}{N}\right)_{IN}$ may easily be modified.

8. EXTENSION OF PREVIOUS RESULTS

In the derivation of equation (I), it was tacitly assumed that the audio deviation ratio $\Delta f_s/f_a$ is large enough to guarantee

$$2.0\ \Delta f_s < b_a \leq 2.2\ \Delta f_s \tag{A}$$

which is a fairly good approximation for audio deviation ratios larger than 10. This is based on the bandwidth required to pass all sidebands greater in magnitude than 10% of the unmodulated carrier amplitude without attenuation. For this same bandwidth criterion, Carson's rule is more accurate and can be used for deviation ratios down to about 0.5. For our problem, Carson's rule gives

$$b_a = 2(\Delta f_s + f_a) \tag{B}$$

A more strict condition used in [5] is

$$b_a = 2(\Delta f_s + 2f_a) \tag{C}$$

which gives the bandwidth required to pass all sidebands greater in magnitude than 5% of the unmodulated carrier amplitude.

Although any such relationship can easily be incorporated into the previous results, it is assumed that the Carson rule bandwidth is adequate for our purposes in the following derivation.

Equation (I) was obtained by dividing the equation

$$\left(\frac{SC}{N}\right) = \frac{1}{2b_a}\left(\frac{\Delta f_a}{f_s}\right)^2 B_{RF}\left(\frac{C}{N}\right)_{IN}$$

by the relation

$$\left(\frac{S}{N}\right)_a = \frac{3}{4}\left(\frac{\Delta f_a}{f_s}\right)^2 \frac{\Delta f_s^{\,2}}{f_a^{\,3}} B_{RF}\left(\frac{C}{N}\right)_{IN}$$

which gives

$$(\Delta f_s)^2\, b_a = \frac{2}{3} f_a^{\,3} \frac{\left(\frac{S}{N}\right)_a}{\left(\frac{SC}{N}\right)} \tag{D}$$

By setting $b_a = 2.2\Delta f_s$ from (1) and solving for Δf_s, we get (I) as the real root. Similarly, we can let $b_a = 2(\Delta f_s + f_a)$ from (2) and get a cubic equation in Δf_s.

$$(\Delta f_s)^3 + f_a(\Delta f_s)^2 - \frac{f_a^{\,3}}{3} R = 0 \tag{E}$$

where the ratio $\dfrac{\left(\frac{S}{N}\right)_a}{\left(\frac{SC}{N}\right)}$ is denoted by R.

This can be solved for Δf_s by substituting $(x - \frac{f_a}{3})$ for Δf_s and thereby reducing the equation to

$$x^3 - \frac{f_a^{\,2}}{2} x - \frac{f_a^{\,3}}{3}\left(R - \frac{2}{9}\right) = 0 \tag{F}$$

which has one real root and two complex conjugate roots. We are interested in only the real root of (F) which is given by

$$x = \frac{f_a}{\sqrt[3]{6}} \left\{ \left[R - \frac{2}{9} + \sqrt{R^2 - \frac{4}{9}R}\right]^{\frac{1}{3}} + \left[R - \frac{2}{9} - \sqrt{R^2 - \frac{4}{9}R}\right]^{\frac{1}{3}} \right\} \tag{G}$$

from which

$$\Delta f_s = x - \frac{f_a}{3} = f_a \left\{ \frac{\left[R - \frac{2}{9} + \sqrt{R^2 - \frac{4}{9}R}\right]^{\frac{1}{3}} + \left[R - \frac{2}{9} - \sqrt{R^2 - \frac{4}{9}R}\right]^{\frac{1}{3}}}{(6)^{\frac{1}{3}}} - \frac{1}{3} \right\}$$

For our modulation scheme R will usually be on the order of 10^2 so that

$$\Delta f_s \approx f_a \left\{ \left[\frac{2R}{6}\right]^{\frac{1}{3}} - \frac{1}{3} \right\} \tag{H}$$

Thus, if the deviation ratio is not large, we must use equation (G) or (H) rather than (I) to determine the audio subcarrier peak frequency deviation. If R is large ($R \gg \frac{4}{9}$), then (H) may be used as a good approximation.

This result does not affect equation (V), however, since this relation was left in terms of b_a to allow use of any bandwidth criterion such as (A), (B), or (C).

As an example, suppose we impose the following requirements for a four audio channel system (cf. reference [6])

$$\left(\frac{S}{N}\right)_{picture} = 30 \text{ db}$$

$$\left(\frac{S}{N}\right)_{a} = 40 \text{ db}$$

$$\left(\frac{SC}{N}\right) = 20 \text{ db}$$

$$f_a = 13 \text{ kHz}$$

$$f_v = 4.2 \text{ MHz}$$

$$f_s = 20.4 \text{ MHz}$$

$$B = 11.0 \text{ MHz}$$

We can solve for the audio subcarrier peak deviation from (H) which gives

$$\Delta f_s = 37 \text{ kHz}$$

and from (B)

$$b_a = 2(\Delta f_s + f_a) = 100 \text{ kHz}$$

This result is then substituted in (V) to get a relation for input predetection carrier-to-noise ratio as a function of predetection RF bandwidth (in MHz).

$$\left(\frac{C}{N}\right)_{IN} = \frac{16.2 \times 10^4}{B_{RF}(B_{RF}-11)^2}$$

This relation is shown in figure C-1 for the given system parameters.

Once a carrier-to-noise ratio and RF bandwidth are determined from the curve, the modulation parameters Δf_a and Δf_v can be computed from equations (II) and (III).

Figure C-1. Input Carrier-to-Noise Ratio
Versus RF Predetection Bandwidth

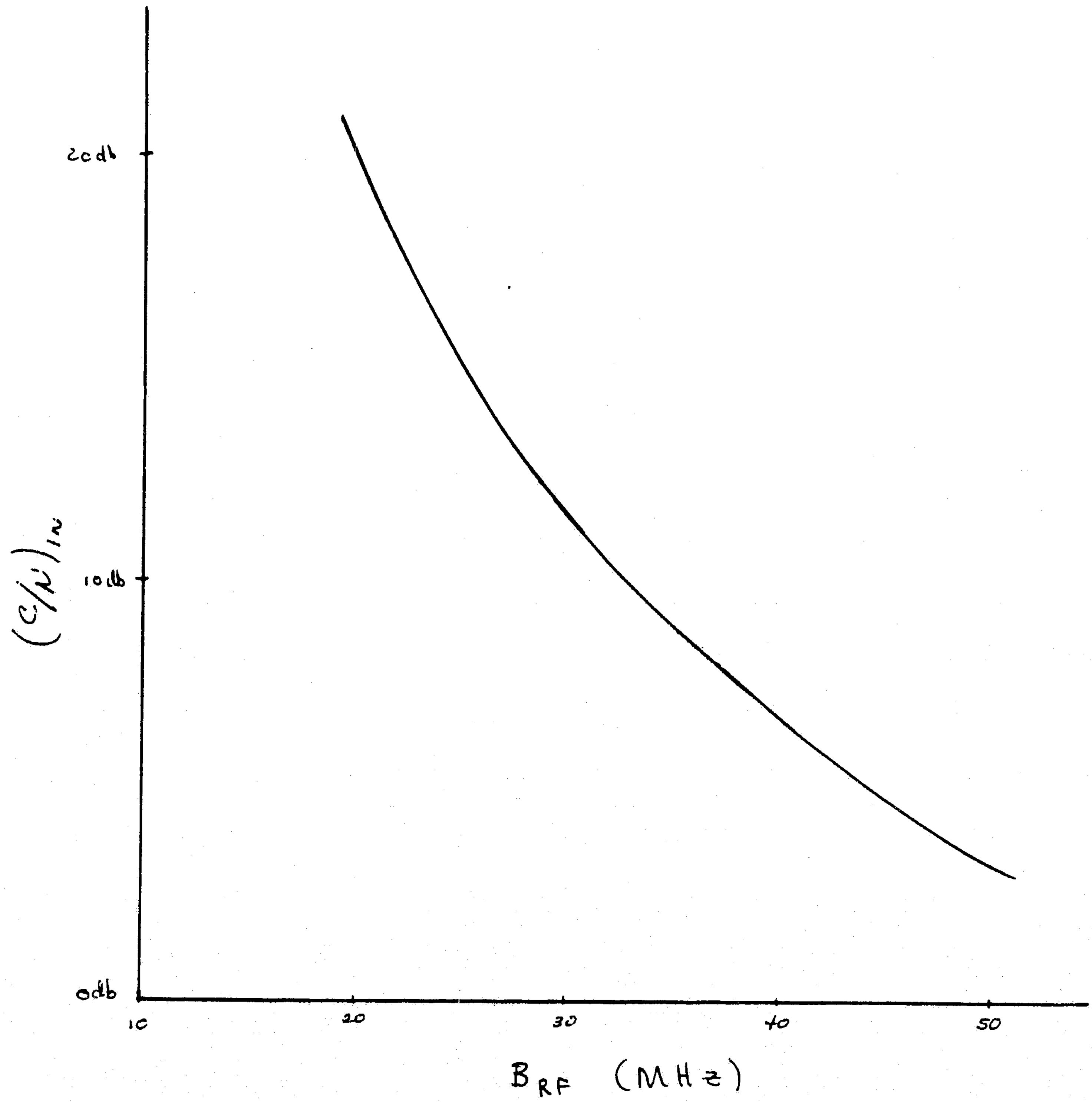

For $\left(\frac{S}{N}\right)_a = 40$ db

$\left(\frac{S}{N}\right)_{picture} = 30$ db

$\left(\frac{SC}{N}\right) = 20$ db

$f_a = 13$ kHz

$f_v = 4.2$ MHz

$f_s = 20.4$ MHz

9. REFERENCES

[1] Schwartz, M., Information Transmission, Modulation, and Noise, McGraw-Hill, 1959.

[2] Hancock, J.C., An Introduction to the Principles of Communication Theory, McGraw-Hill, 1961.

[3] Downing, J.J., Modulation Systems and Noise, Prentice-Hall, 1964.

[4] Nichols and Rauch, Radio Telemetry, John Wiley, 1954.

[5] Wozencraft and Jacobs, Principles of Communication Engineering, John Wiley, 1965.

[6] "Satellite Communications Systems Technolgical Studies and Investigations", Report No. 403301, Communications and Systems, Inc., 3 January 1969.

[7] Derivation and Summation of FM/FM and FM Signal-to-Noise Ratio Improvement and Pre-Emphasis Formulae," Hughes IDC 2292/201, from R.J. Rechter, 24 January 1967.

[8] "Required C/T for FDM/FM Communication Systems, Hughes IDC 2292/659, from J.H. Kagel, 24 April 1969.

[9] Cohen, W., "Signal-to-Noise Ratio in Modulated Systems", Electro-Technology, Part 1 - October 1965, Part 2 - January 1966.

[10] Bedford, L.H., "Television by Satellite", The Radio and Electronic Engineer, November 1968, Presented at the Meeting of the Comitato Internazionale de Televisione, Milan, April 1968.

Report GDC-DCF 70-002

TELEVISION BROADCAST SATELLITE STUDY

FINAL REPORT - VOLUME IV

TECHNICAL APPENDICES

Contract NAS8-21036

31 December 1970

APPENDIX D

LONG LIFE SUBSYSTEM ASSURANCE

Convair Aerospace Division

GENERAL DYNAMICS

APPENDIX D

LONG LIFE SUBSYSTEM ASSURANCE

1. RELIABILITY IMPROVEMENT MODEL

Generally three types of redundancy are assumed to be applicable to the TVBS: standby (e.g., electrical and electronic black boxes with means of inactivating or activating and switching out or in), active (e.g., attitude control or station keeping propulsion components with extra thrusters and valving to prevent failure in an uncontrollable thrusting mode) and voting (e.g., control logic). Obviously, some components are not feasible candidates for any type of redundancy, such as solar arrays or large antennas. These components would have lower level redundancy not being considered during this study phase, such as solar cell over-capacity as required for satellite lifetime or redundant antenna feeds.

It is assumed that infant failures have been eliminated through thorough check-out and component burn-in, end of life failures eliminated by adequate design life or provisioning of replacements, and that component failures occur independently. Therefore, system reliability is a function of a number of Poisson processes, that is, component failure rates are constant and independent, thus, for standby redundancy

$$R_s = e^{-\lambda t} \sum_{i=o}^{n+1} \frac{\left(P\lambda t\right)^i}{i!}, \text{ where}$$

e is the base of natural logarithms,

λ is component failure rate

t is required satellite lifetime

n is the number of standby components

P is the probability of successful switchover and activation

R_s is the reliability of the redundant combination.

Backup capability utilizing components of unequal failure rates is not considered, because such possibilities have not been identified. For the active parallel case:

$$R_s = \sum_{j=0}^{m-\ell} \binom{m}{j} e^{-(m-j)\lambda t} \left(1 - e^{-\lambda t}\right)^j \text{, where}$$

m is the total number in parallel

ℓ is the minimum number required.

It is assumed that failure of parallel units has no significant effect on failure rate of surviving units. Voting redundancy is similar to the active parallel case but the majority of an odd number of units is required.

In previous applications of the reliability improvement model, where reliability was increased as a function of added weight, the weight increments considered were those due only to the redundant elements themselves. Since the synthesis model will result in a minimum cost baseline system addition of redundant elements has cost implications beyond the mere cost of the added element. The added weight and power requirements changes the sizing of the attitude control and station keeping systems and prime power system. These changes result in satellite cost changes beyond that due only to the added element. Changes in weight, volume and power are interrelated, requiring solution of three simultaneous equations. These equations are readily obtained, by using the relationships derived for the synthesis model . However, all candidate redundancies must be considered to determine the one that provides the greatest reliability gain per unit cost. Another complication is that some TVBS configurations would start reliability improvement from a weight or volume boundary, requiring reduction in power capability to accommodate redundancy. This would affect ground system cost, bringing in additional terms influencing costs.

The model complexity will be increased by at least an order of magnitude by attempting to optimize redundancy. In order not to limit the number of performance possibilities studied during the parametric phase it was decided to use the reliability improvement model later, when the number of concepts would be limited. Otherwise, machine processing times would become prohibitive. At that time the cost of added redundancy will be balanced against the expected cost saving due to increased reliability. This will be calculated by multiplying the expected number of satellite launches over the system lifetime by launch cost. Expected satellite lifetime is

$$E\left(t_c\right) = \int_o^{t_r} R_c \, dt, \text{ where}$$

t_c is satellite lifetime,

R_c is satellite reliability as a function of time,

t_r is scheduled satellite lifetime.

Therefore, the expected total launch cost is

$$E\left(C_s\right) = \frac{C_c \, t_s}{E(t_c)}$$

where C_s is total launch costs during system lifetime,

C_c is the cost of a single launch

t_s is the required system lifetime.

2. RELIABILITY STUDIES

During the first half of this study it appears profitable to perform some of the typical reliability trade-off studies for the TVBS. In particular high-power elements are an important area of consideration. A typical example is the high-power output for the downlink. To begin with, the system life requirement can possibly be met by:

1. Launching a new satellite at the end of life of the output tube(s) of the previous satellite.
2. Operating multiple outputs in parallel at greatly reduced power levels per output device.
3. Developing high-power long-life solid state output devices.
4. Switching out the output tube(s) at end of life and switching in fresh tubes.

Alternative 1, may have to be used, at least in conjunction with one of the other alternatives. It is not attractive, because the high-power satellite will be in the larger size range, requiring greater launch costs. Alternative 3, is unlikely to be achieved in the time span of interest, except perhaps with a great deal of risk and large expenditures of funds. Alternative 4, may introduce problems in switching at high power levels, unless a means can be found to use the switches in lower power circuits to switch the devices. So far, alternative 2, looks the most promising, perhaps in conjunction with 4. This study will be completed during the next reporting period, along with studies of other reliability and life improvement candidates considered typical.

Table D-1 contains preliminary TVBS component failure rates for various alternative components. These will be refined by obtaining communication satellite experience data, particularly for power and communications subsystems. The failure rates are being used in the selected trade-off studies for reliability and life. The rates shown are based on component failure rates given in the Tri-Service and NASA Failure Rate Data Handbook SP63-470, adjusted for satellite environment. Rates at the low end of the given ranges were used, because of the practices of parts screening and other extensive testing usually associated with production of space systems. Also no maintenance will be performed on the satellite components during most of the system lifetime, so that the higher reported failure rates of maintained systems do not apply.

Table D-1. TVBS Component Failure Rates

SYSTEM Alternative Configuration	λ per 10^{-6} hrs.
ELECTRICAL POWER	
Solar Array	4.8
Nuclear Reactor	2.4
ATTITUDE CONTROL (NO REDUNDANCY ASSUMED)	
Ammonia Resisto-Jet	7.6
Ion Propulsion	12.1
Water Electrolysis	8.1
STATION KEEPING (NO REDUNDANCY ASSUMED)	
NH_3 Resisto-Jet	7.6
Ion Propulsion	12.1
H_2O Electrolysis	8.1
Nitrogen Cold Gas	15.9
Peroxide	15.9
THERMAL CONTROL	
Passive	≈ 0.0
Fluid Pipe	0.1
UPLINK ANTENNA	
Antenna	0.9
MULTIPLEXER	
Multiplexer (2)	3.6
TRANSPONDER	
Linear Translator	25.4
Frequency Multiplier	25.4
Modulation Converter	43.1
Demodulator-Modulator	39.4
OUTPUT STAGE	
Low Power	(Included Under Transponder)
High Power	3.1
DOWNLINK ANTENNA	
Rigid Dish	0.9
PETA	0.9
Phased Array	0.0
TELECOMMUNICATION ANTENNA	
Receiving Antenna	0.0
TELECOMMUNICATIONS RECEIVER	
Receiver	41.6
COMMAND AND CONTROL UNIT	
Unit	2.0
STRUCTURE	
Spacecraft	0.0

3. LONG LIFE SUBSYSTEM ASSURANCE

A major area which tends to limit the lifetime of a communication satellite in the kilowatt power output range is the output stage. If satellite useful life is to be extended up to ten years, it is necessary to provide output circuits that would be switched in as each previous circuit reaches its end of life or otherwise fails. Twenty-five thousand hours is projected to be the maximum guaranteed life achievable for microwave output tubes in the kilowatt range in the early 1970's. To achieve power outputs greater than 5 kw it is certainly desirable, if not absolutely required, to operate outputs simultaneously in parallel. In this manner both output overcapacity and derating of tubes will contribute to significantly improve reliability.

The effects of various ways of configuring outputs on output lifetimes were examined for two required power levels. The first level is 5 kw, to be provided by a minimum of one tube, with a conservatively assumed average life at that level output of 15,000 hours. The second level is 25 kw minimum, using at least five tubes operating in parallel to provide the required levels. These tubes also have an average assumed life of 15,000 hours under these conditions. In both cases, to provide for extended satellite life, it is assumed that the entire operating bank of output tubes is replaced by means of switching at 15,000-hour intervals. Actual design would provide for switching of individual tubes as the output of each degrades to less than the allowable threshold. But the difficulty of determining valid tube life distributions is avoided by the assumption of an arbitrary replacement interval. The satellite is assumed to transmit 24 hours a day. Tubes are switched in individually to replace tube failures at times other than end-of-life. As a simplifying assumption replacements of failures are replaced at the next scheduled bank replacement time, regardless of the number of hours that they operate, except, of course, when the replacement of the failure also fails. Although an order of replacement will probably be specified in design, it is assumed that any previously unused tube can replace any tube in use.

Each tube has a failure rate of 3.1 per 10^6 hours. The power supply that operates only in conjunction with its tube has a failure rate of 1.8 per 10^6 hours. The switching of a given tube, whether initiated via the command link or automatically on board the satellite, has a probability of 0.996 of proper occurrence. These parameters are based on sommunication satellite experience and are assumed to remain constant during satellite lifetime.

In the case of the 5 kw output, operating one tube at a time without redundancy, six tubes are required to achieve the possibility of a ten-year life. The probability of output survival for ten years is 0.636. By operating two tubes in parallel at a time in an active redundant configuration, the probability of survival to ten years is 0.994. However, twelve tubes are required. The probabilities of survival for these two configurations, with only enough banks to make survival to the given time possible, for any time to 90,000 hours are plotted in Figure D-1. Corresponding probabilities of survival of outputs designed for 90,000 hours of life as functions of operating time are shown in Figure D-2. More active tubes could be added, but it seems evident that further reliability gained in this manner is not worth the additional cost and weight.

Another possibility for the 5 kw case is to add extra tubes to be used only in the event of failure of a tube operating singly. One standby tube added to the six required for ten-year life results in a ten-year output reliability of 0.922. Three standbys raise reliability over 0.997. Thus nine tubes can be used to produce a reliability that exceeds that of twelve tubes in the active redundancy case. Figure D-3 shows the probabilities of survival of outputs designed for a given time plotted for times up to 90,000 hours for zero to three standby tubes. Probability of survival of outputs designed for 90,000 hours of life as a function of time is plotted in Figure D-4 for zero to three standbys.

Similarly, either active or standby redundancy can be used for the 25 kw case. Without redundancy the probability of output survival for ten years is 0.10. To achieve this possibility of 10-year life six banks of five tubes each or a total of 30 tubes, are required. One more tube operating in each bank improves reliability for any given mission length as shown in Figure D-5. At ten years the reliability becomes 0.89. However, a 25 kw output designed for six replacement cycles has a better chance of surviving four or five cycles than the 5 kw output, as seen by comparing Figure D-6 with D-2. Corresponding effects of using zero to six standby tubes on output reliability are shown in Figures D-7 and D-8. It is noted that four standbys produce more reliability improvement than a sixth active tube per bank. This means that for a ten-year lifetime the standby configuration using a total of 34 tubes has slightly greater reliability than the active redundant design with 36 tubes.

In general the standby redundant configurations require fewer tubes than those with active redundancy. This conclusion is always true where effects of switching can be ignored, because in standby redundancy the redendant elements are not stressed until used. In the calculations of survival probabilities switching reliabilities were taken into account. However, because each tube that operates must go through a switching cycle, the switching does not work peculiarly to the disadvantage of standby units. The actual unit switched is the tube power supply, which in turn energizes or de-energizes the tube, which begins or ceases operation, respectively.

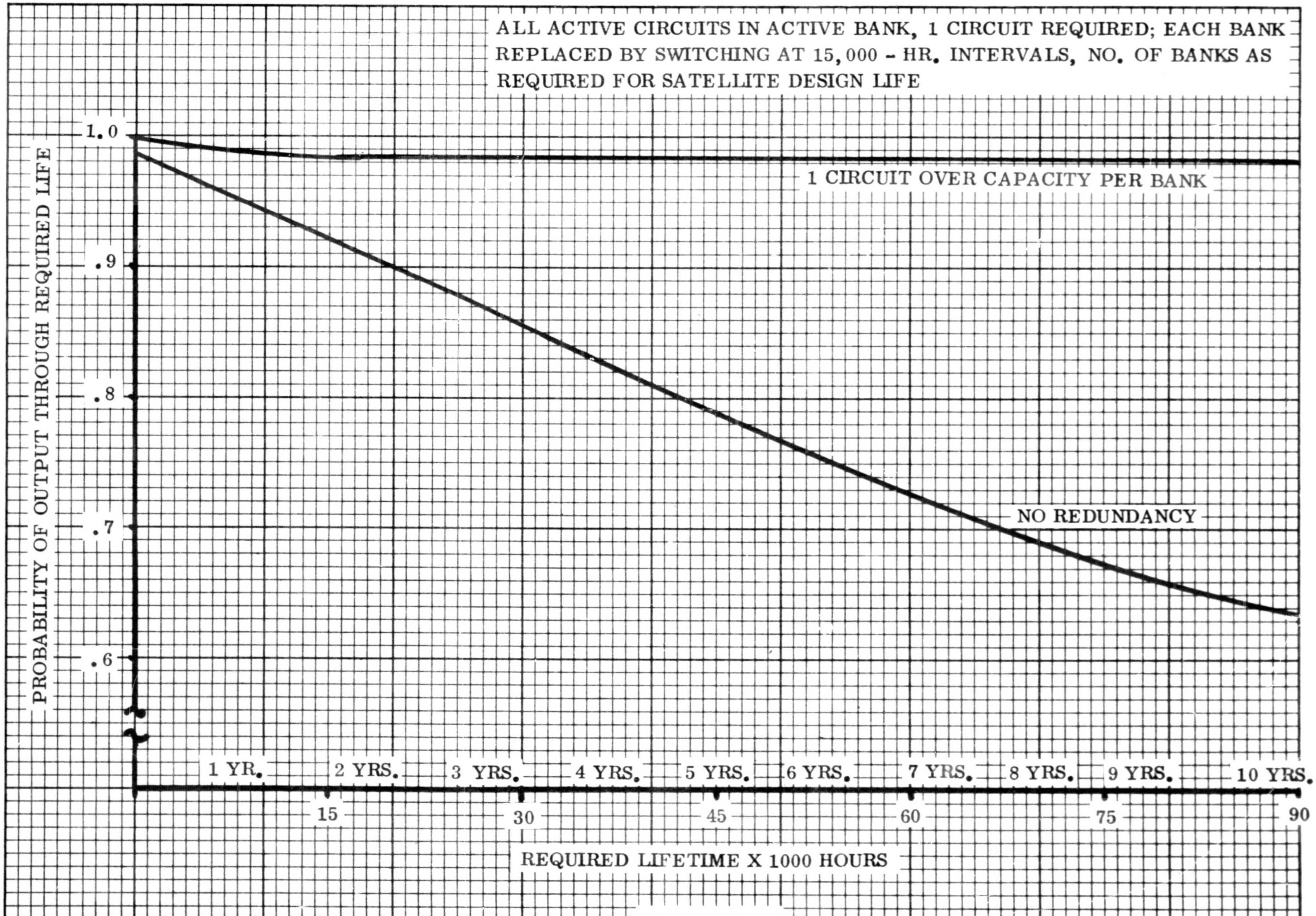
ALL ACTIVE CIRCUITS IN ACTIVE BANK, 1 CIRCUIT REQUIRED; EACH BANK REPLACED BY SWITCHING AT 15,000 - HR. INTERVALS, NO. OF BANKS AS REQUIRED FOR SATELLITE DESIGN LIFE
PROBABILITY OF OUTPUT THROUGH REQUIRED LIFE
1.0
.9
.8
.7
.6
1 CIRCUIT OVER CAPACITY PER BANK
NO REDUNDANCY
1 YR.
2 YRS.
3 YRS.
4 YRS.
5 YRS.
6 YRS.
7 YRS.
8 YRS.
9 YRS.
10 YRS.
15
30
45
60
75
90
REQUIRED LIFETIME X 1000 HOURS

Figure D-1.

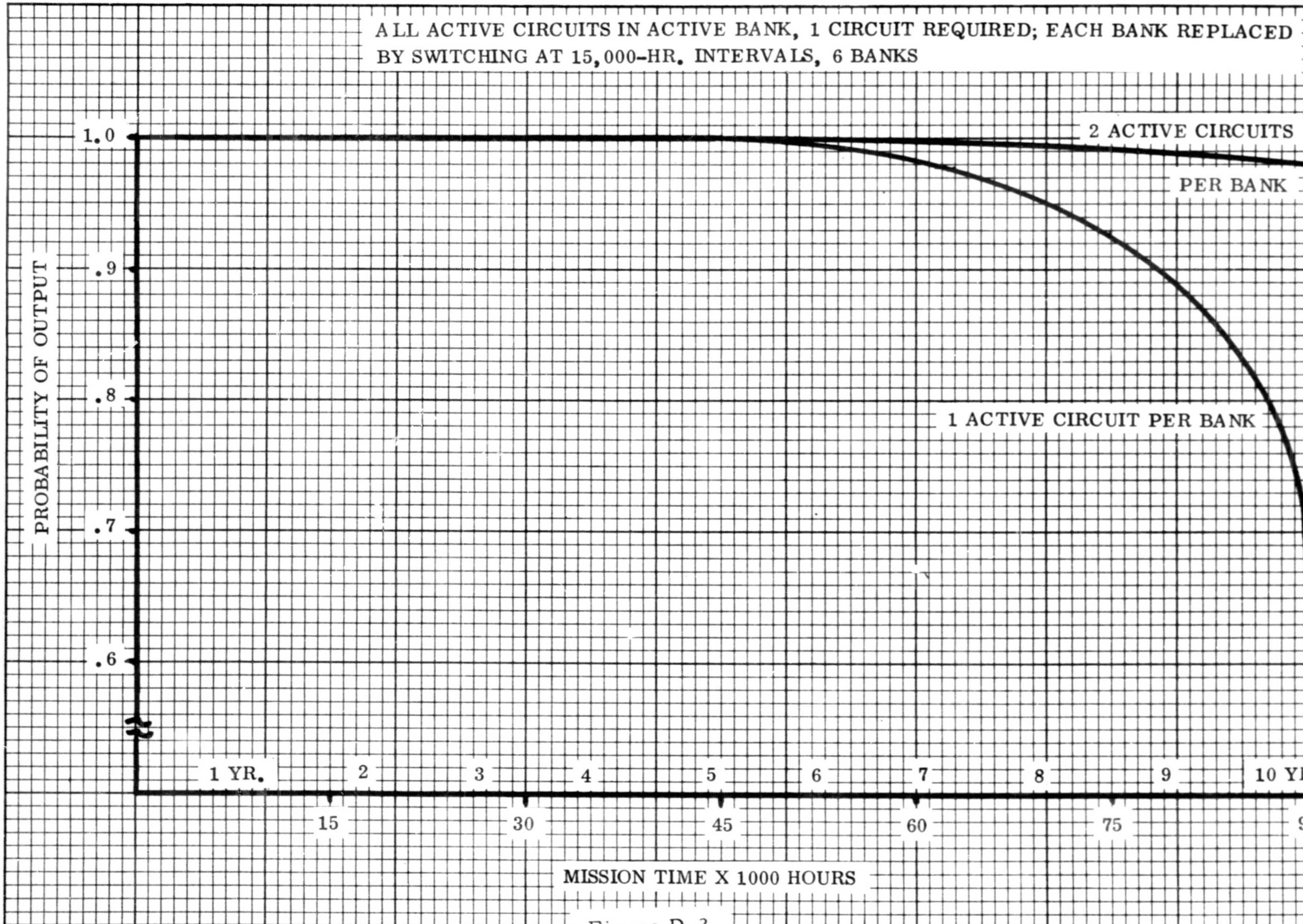
ALL ACTIVE CIRCUITS IN ACTIVE BANK, 1 CIRCUIT REQUIRED; EACH BANK REPLACED BY SWITCHING AT 15,000-HR. INTERVALS, 6 BANKS
2 ACTIVE CIRCUITS PER BANK
1 ACTIVE CIRCUIT PER BANK
PROBABILITY OF OUTPUT
1.0
.9
.8
.7
.6
1 YR.
2
3
4
5
6
7
8
9
10 YRS.
15
30
45
60
75
90
MISSION TIME X 1000 HOURS

Figure D-2.

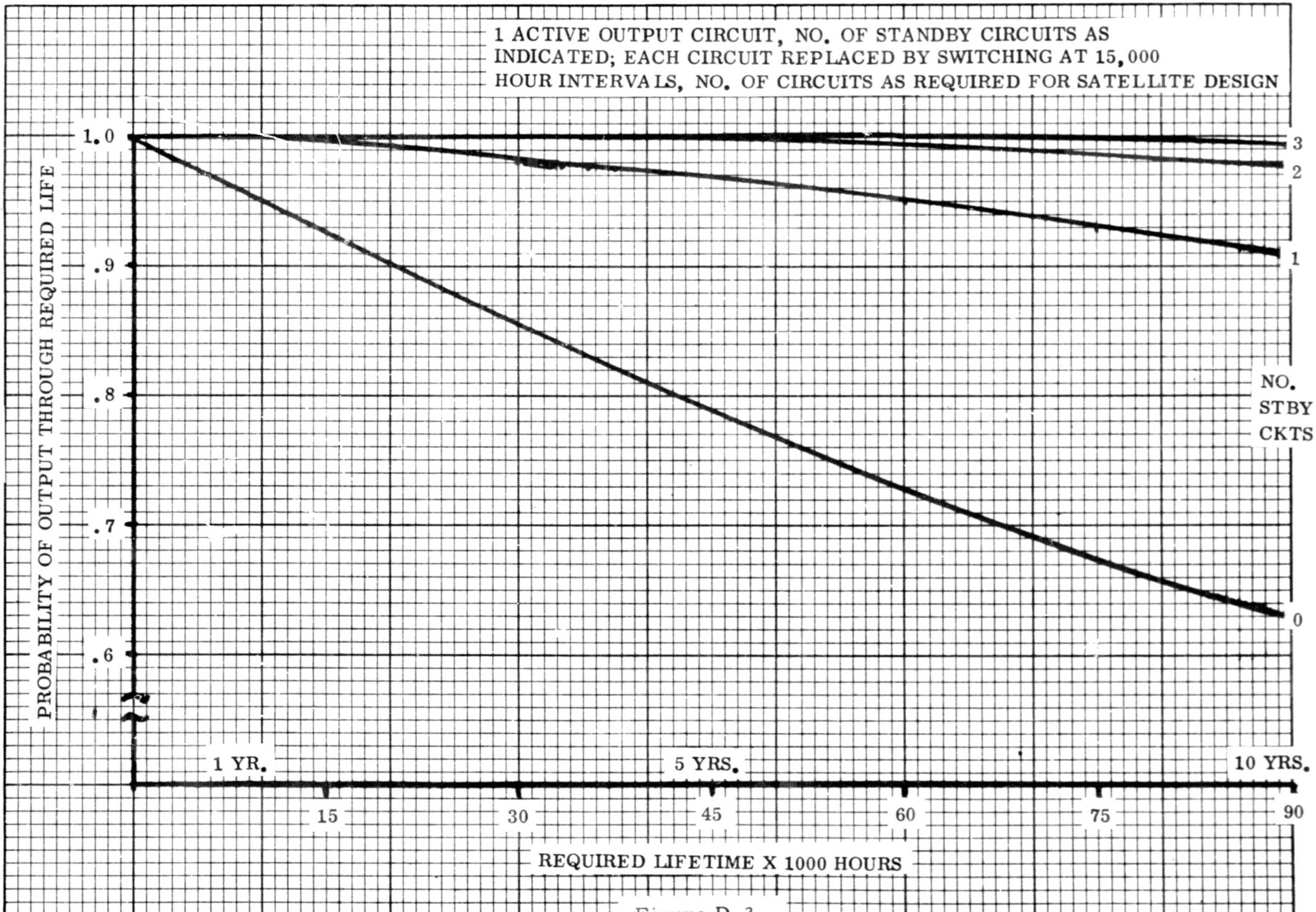
1 ACTIVE OUTPUT CIRCUIT, NO. OF STANDBY CIRCUITS AS INDICATED; EACH CIRCUIT REPLACED BY SWITCHING AT 15,000 HOUR INTERVALS, NO. OF CIRCUITS AS REQUIRED FOR SATELLITE DESIGN
PROBABILITY OF OUTPUT THROUGH REQUIRED LIFE
1.0
.9
.8
.7
.6
3
2
1
0
NO. STBY CKTS
1 YR.
5 YRS.
10 YRS.
15
30
45
60
75
90
REQUIRED LIFETIME X 1000 HOURS

Figure D-3.

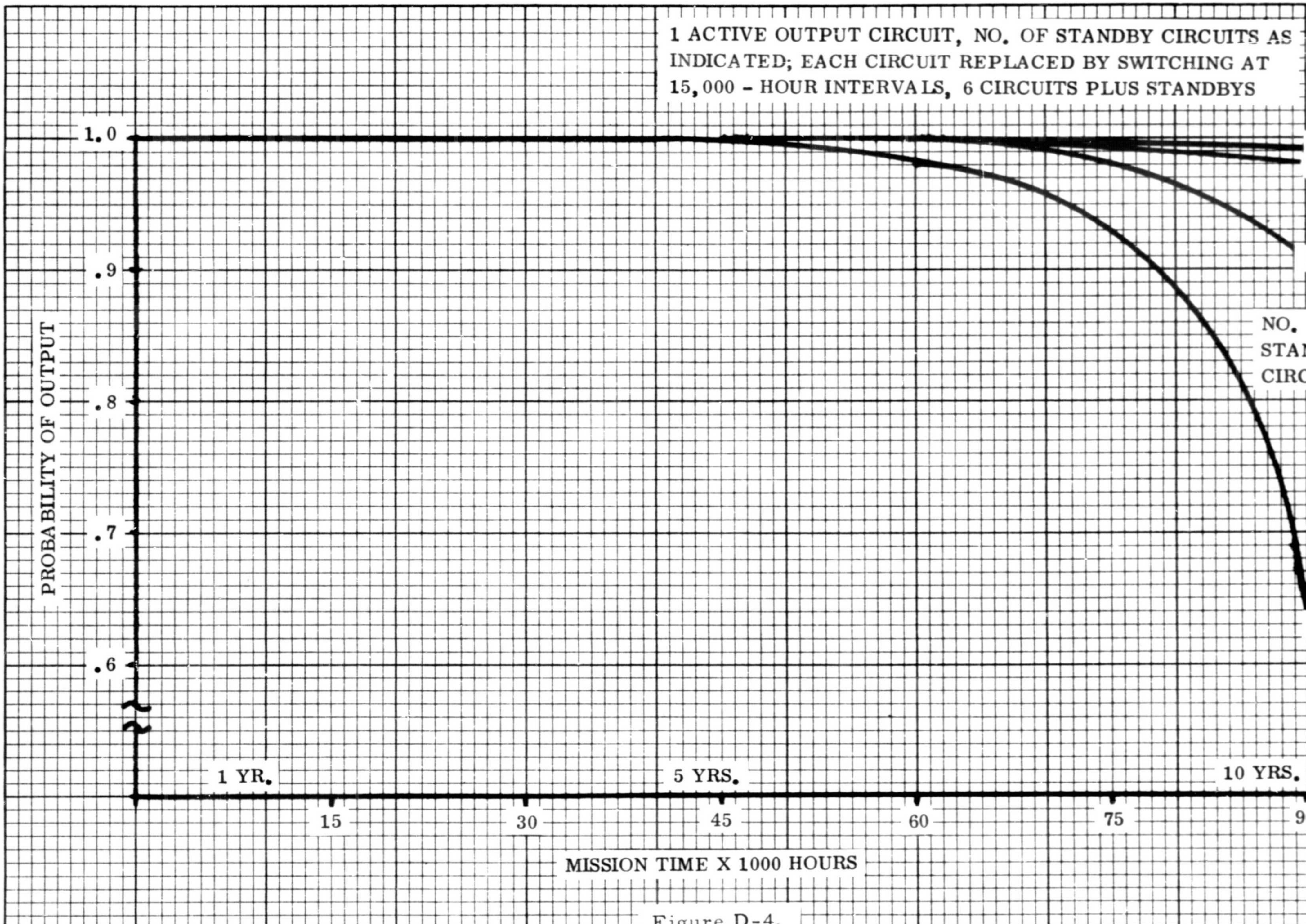
1 ACTIVE OUTPUT CIRCUIT, NO. OF STANDBY CIRCUITS AS INDICATED; EACH CIRCUIT REPLACED BY SWITCHING AT 15,000 - HOUR INTERVALS, 6 CIRCUITS PLUS STANDBYS
PROBABILITY OF OUTPUT
1.0
.9
.8
.7
.6
3
2
1
0
NO. STANDBY CIRCUITS
1 YR.
5 YRS.
10 YRS.
15
30
45
60
75
90
MISSION TIME X 1000 HOURS

Figure D-4.

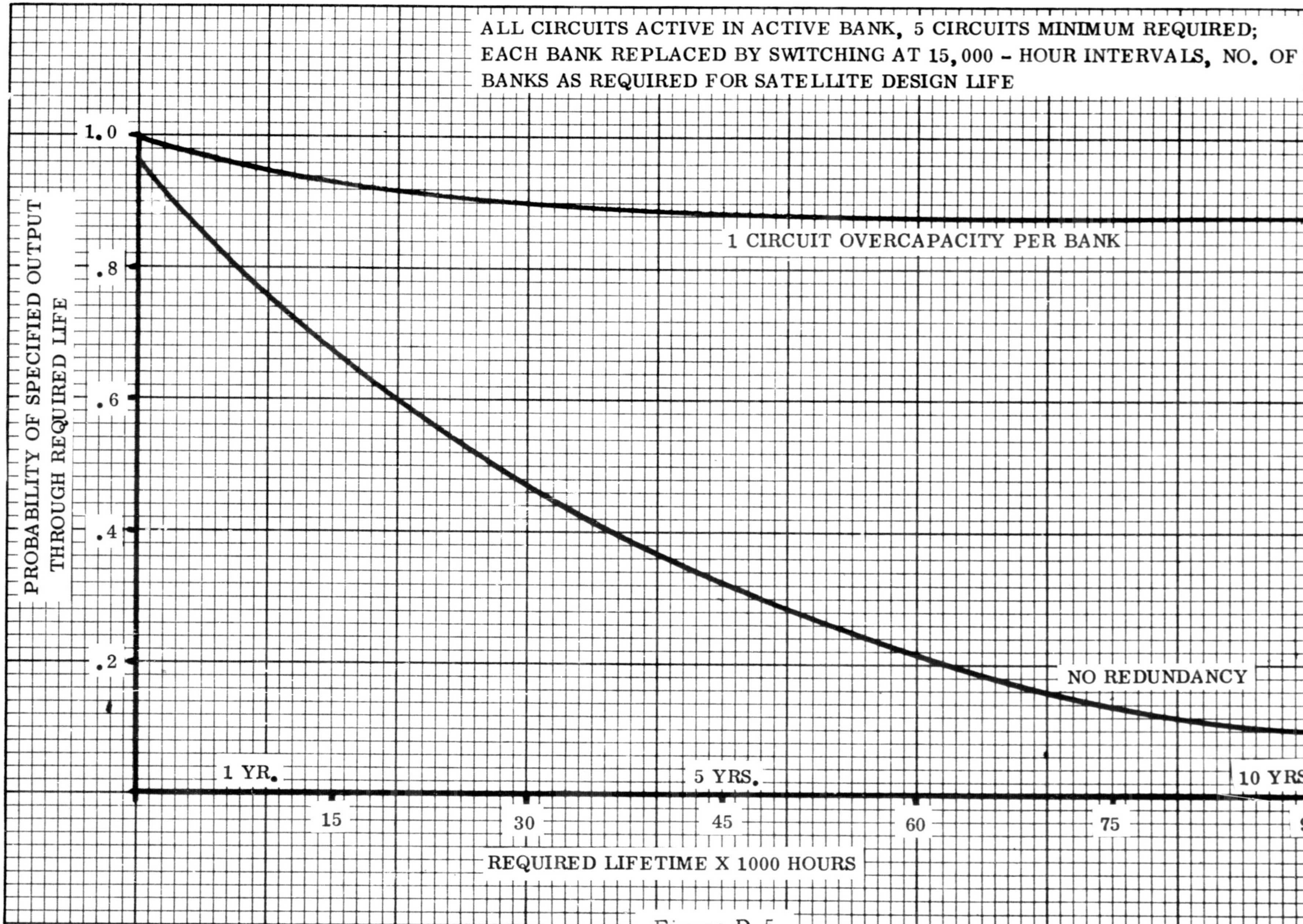
ALL CIRCUITS ACTIVE IN ACTIVE BANK, 5 CIRCUITS MINIMUM REQUIRED; EACH BANK REPLACED BY SWITCHING AT 15,000 - HOUR INTERVALS, NO. OF BANKS AS REQUIRED FOR SATELLITE DESIGN LIFE
PROBABILITY OF SPECIFIED OUTPUT THROUGH REQUIRED LIFE
1.0
.8
.6
.4
.2
1 CIRCUIT OVERCAPACITY PER BANK
NO REDUNDANCY
1 YR.
5 YRS.
10 YRS.
15
30
45
60
75
90
REQUIRED LIFETIME X 1000 HOURS

Figure D-5.

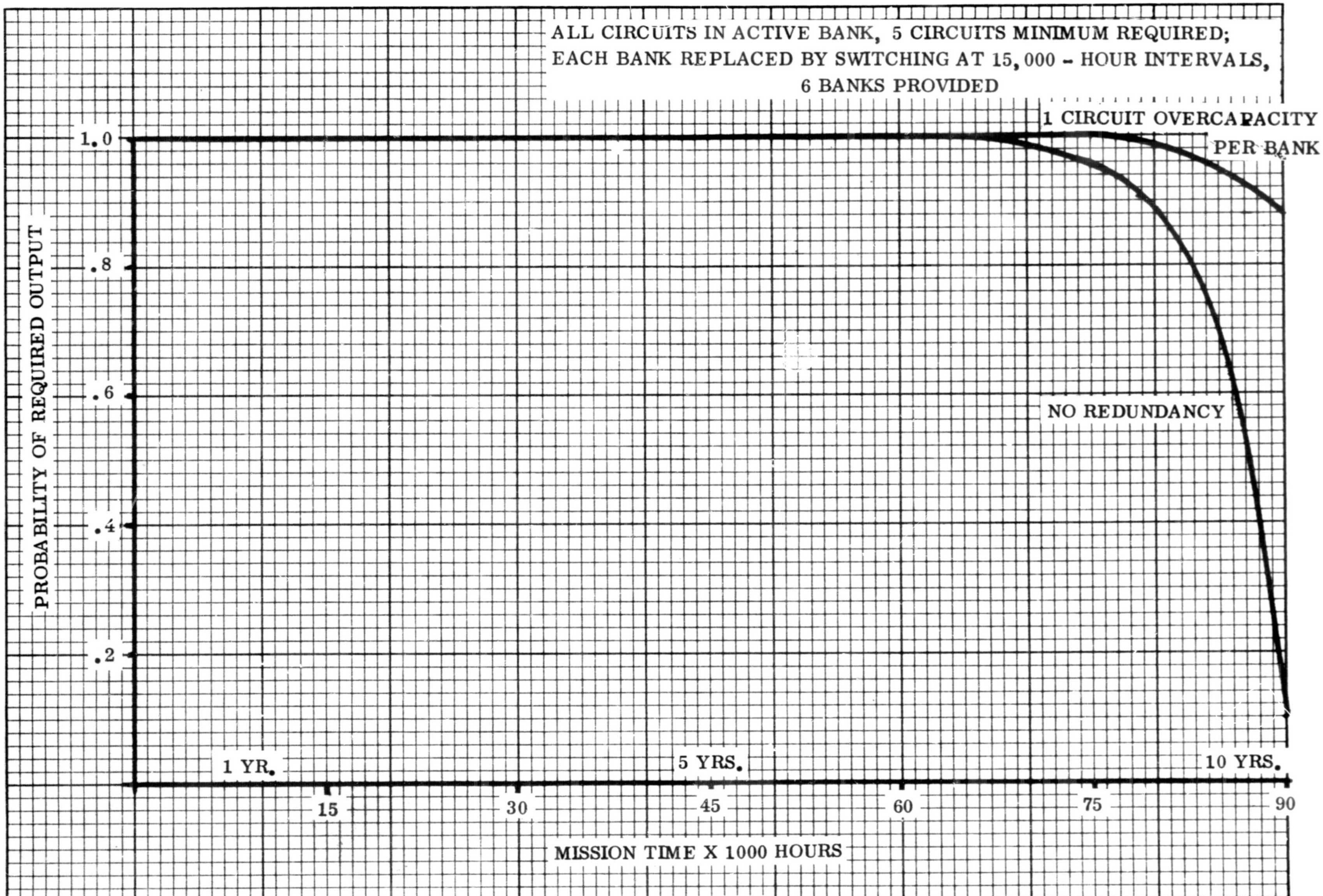
ALL CIRCUITS IN ACTIVE BANK, 5 CIRCUITS MINIMUM REQUIRED;
EACH BANK REPLACED BY SWITCHING AT 15,000 - HOUR INTERVALS,
6 BANKS PROVIDED
1 CIRCUIT OVERCAPACITY PER BANK
NO REDUNDANCY
PROBABILITY OF REQUIRED OUTPUT
1.0
.8
.6
.4
.2
1 YR.
5 YRS.
10 YRS.
15
30
45
60
75
90
MISSION TIME X 1000 HOURS

Figure D-6.

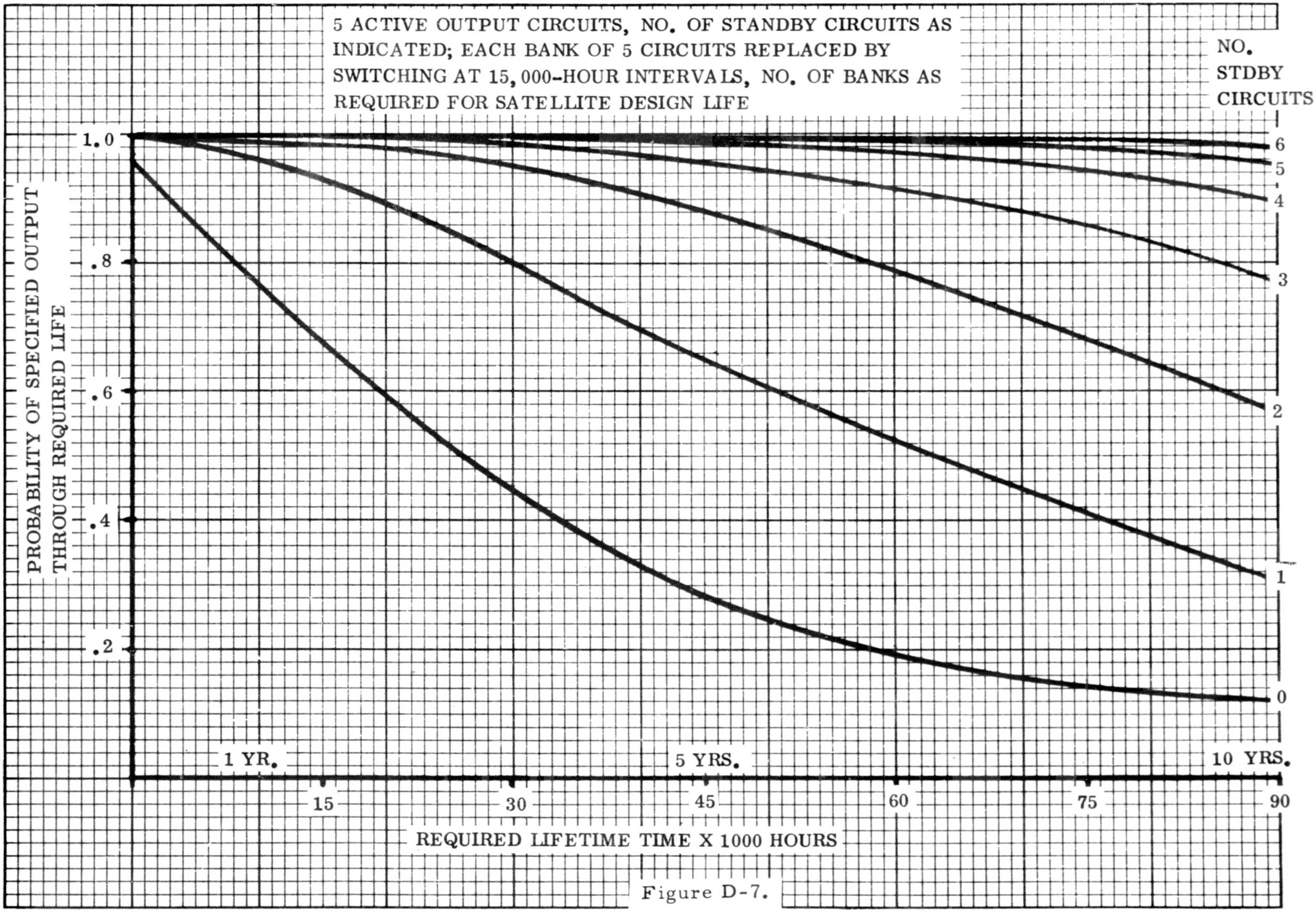
5 ACTIVE OUTPUT CIRCUITS, NO. OF STANDBY CIRCUITS AS INDICATED; EACH BANK OF 5 CIRCUITS REPLACED BY SWITCHING AT 15,000-HOUR INTERVALS, NO. OF BANKS AS REQUIRED FOR SATELLITE DESIGN LIFE
NO. STDBY CIRCUITS
6
5
4
3
2
1
0
1.0
.8
.6
.4
.2
PROBABILITY OF SPECIFIED OUTPUT THROUGH REQUIRED LIFE
1 YR.
5 YRS.
10 YRS.
15
30
45
60
75
90
REQUIRED LIFETIME TIME X 1000 HOURS

Figure D-7.

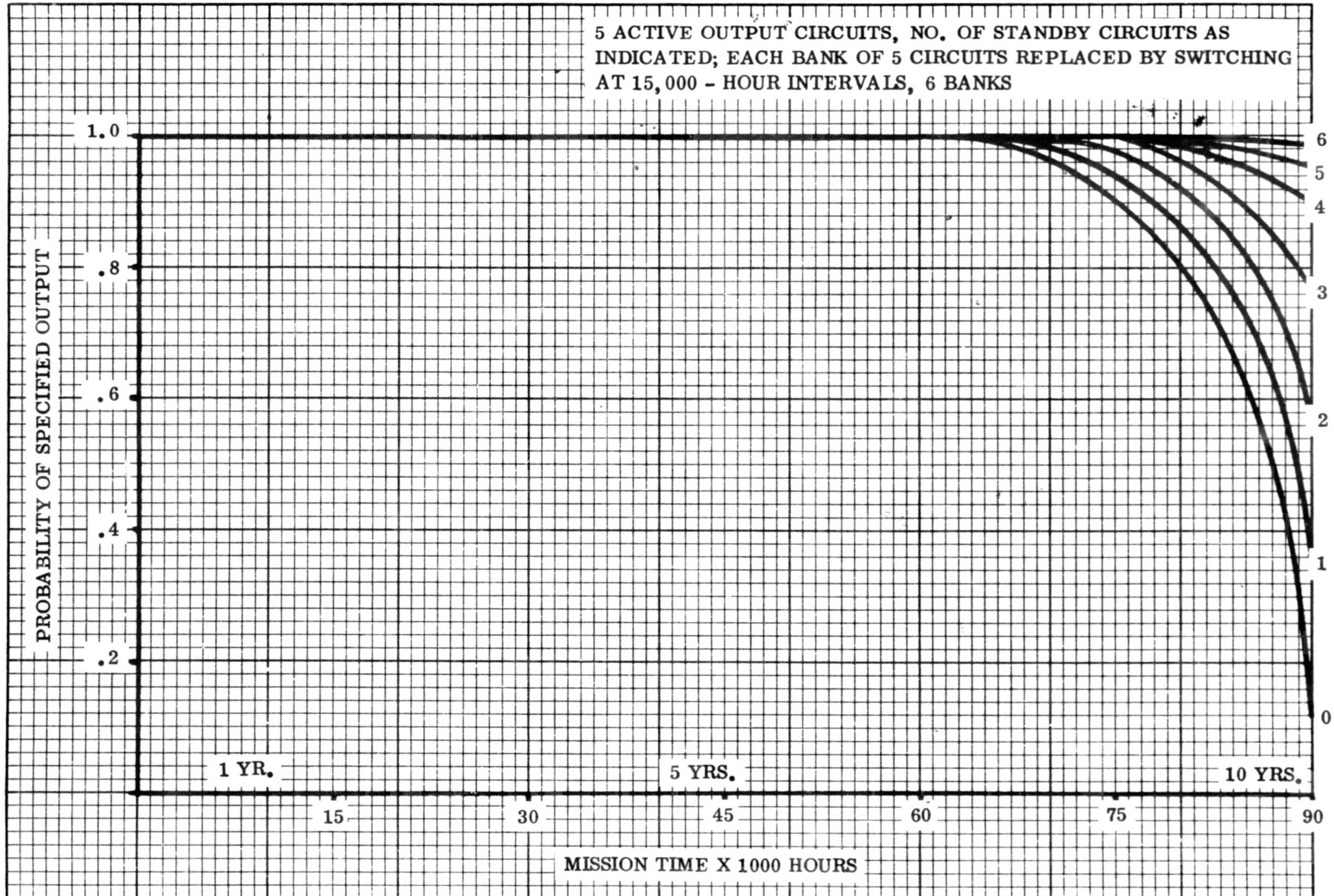
5 ACTIVE OUTPUT CIRCUITS, NO. OF STANDBY CIRCUITS AS INDICATED; EACH BANK OF 5 CIRCUITS REPLACED BY SWITCHING AT 15,000 - HOUR INTERVALS, 6 BANKS
PROBABILITY OF SPECIFIED OUTPUT
1.0
.8
.6
.4
.2
6
5
4
3
2
1
0
1 YR.
5 YRS.
10 YRS.
15
30
45
60
75
90
MISSION TIME X 1000 HOURS

Figure D-8.

Report GDC-DCF 70-002

TELEVISION BROADCAST SATELLITE STUDY

FINAL REPORT - VOLUME IV

TECHNICAL APPENDICES

Contract NAS8-21036

31 December 1970

APPENDIX E

DYNAMIC ANALYSIS

Convair Aerospace Division

GENERAL DYNAMICS

APPENDIX E

DYNAMICS ANALYSIS

1. GENERAL

A subsystem trade study was performe d between the most promising propulsion devices for attitude control and station keeping. Of the approaches considered, the ion-propulsion system seems most appropriate, and the sizing equations were established from the characteristics of this system.

The major source of attitude control perturbation at synchronous orbit is solar pressure. All other steady-state forces are one to two orders of magnitude lower. Trades, therefore, were based on frontal area and offset of center of pressure of the solar arrays.

A back-up system, having higher thrust levels meets the requirements for initial orientation of the satellite, stabilization during docking maneuvers, and stabilization during low orbit assembly and check-out (if required).

2. TVBS DYNAMICS CONSIDERATIONS

REQUIREMENTS
- UP TO FIVE-YEAR LIFETIME
- ANTENNA POINTING TOLERANCE DOWN TO $\pm$ 0.1 DEG.
- COMPLETE NORTH-SOUTH & EAST-WEST STATIONKEEPING
- SUN ORIENTATION OF SOLAR ARRAYS
- POWER REQUIREMENTS UP TO 100 KW

KEY TECHNOLOGIES
- ACTIVE CONTROL SELECTION
- SOLAR ARRAY, ANTENNA, SATELLITE VIBRATIONS
- SOLAR ARRAY ORIENTATION DISTURBANCES
- CSM DOCKING LOADS
- COMPONENT RELIABILITY
- MEASURE SMALL VEHICLE ANGULAR RATES

The requirements listed above have major influence in the design of the attitude control and station keeping subsystem. Five year life time signifies that propellant weight will be significant, and north - south drift which could have been left uncorrected for a shorter mission will be a factor. The antenna pointing accuracy required establishes need for precise attitude sensing and control, a problem complicated by the large sun-oriented solar panels.

3. RELATIVE ACTIVE CONTROL INPULSE (LB.-SEC.)

STATIONKEEPING	ENVIRONMENT	ACS LIMIT CYCLING
NORTH-SOUTH DOMINATES	SOLAR PRESSURE ON ARRAYS DOMINATES	POINTING TOLERANCE & STRUCTURAL VIBRATIONS DOMINATE
LIFETIME, SATELLITE WEIGHT ARE KEYS	$\frac{(AM)}{L_{JET}}$ IS KEY	
	(AM) AREA MOMENT ABOUT CG CP-CG OFFSET 2% L_J - JET ARM JETS MOUNTED ON SATELLITE BODY (USUALLY)	TIGHTER POINTING IS ASSOCIATED WITH LARGER, MORE FLEXIBLE STRUCTURES
ONE SYSTEM FOR STATIONKEEPING (TRANSLATION)	ANOTHER SYSTEM FOR ENVIRONMENT, ACS (ROTATIONAL)	

The relative order of magnitude of control impulse needed to satisfy requirements for a five-year life time satellite are:

1. Station keeping
2. Correction of Environmental distrubances
3. ASC limit cycling

North-south drift control dominates the station keeping impulse requirements. Uncorrected N-S peak drift is 0.8 deg per year. Of the environmental effects, solar torque dominates in the synchronous orbit. Solar panels of 10,000 sq. ft. may be used. Solar torque is estimated by assuming a CG-CP offset for each panel of 2% of the panel's center to satellite CG distance.

ACS limit cycling operation is influenced by pointing tolerance and structural vibration. The larger, more flexible satellites generally require more accurate pointing, which complicates the selection of limit cycling parameters.

4. VEHICLE ORIENTATION

With the factors that affect vehicle orientation; large sun-oriented arrays dominant station keeping impulse requirements, and large satellites with close pointing tolerance, three approaches to attitude control were considered. These are:

Multispin - The satellite has a significant spinning mass, with a despun sun oriented segment (array), and a despun earth oriented segment (antenna). This approach makes station-keeping complicated because of the difficulty of directing the thrust through the C.G. of the vehicle.

Sun Oriented - The main body of the satellite and solar arrays are oriented toward the sun. On this platform, the earth oriented antennas are mounted and controlled. Antenna pointing to the required tolerance is difficult.

Local Vertical - The main body of the satellite, and the antenna is locked to and controlled in yaw about the local vertical. The solar arrays are relatively fixed in space, rotating 360 degrees with respect to the satellite body each day. The power decrease resulting from the solar arrays pointing out of the ecliptic is acceptable.

The selected approach for vehicle system sizing is the orientation to local vertical. This approach greatly simplifies station keeping and makes possible use of low thrust, high duty cycle ion propulsion for station keeping as well as attitude control.

5. TYPICAL SYSTEM

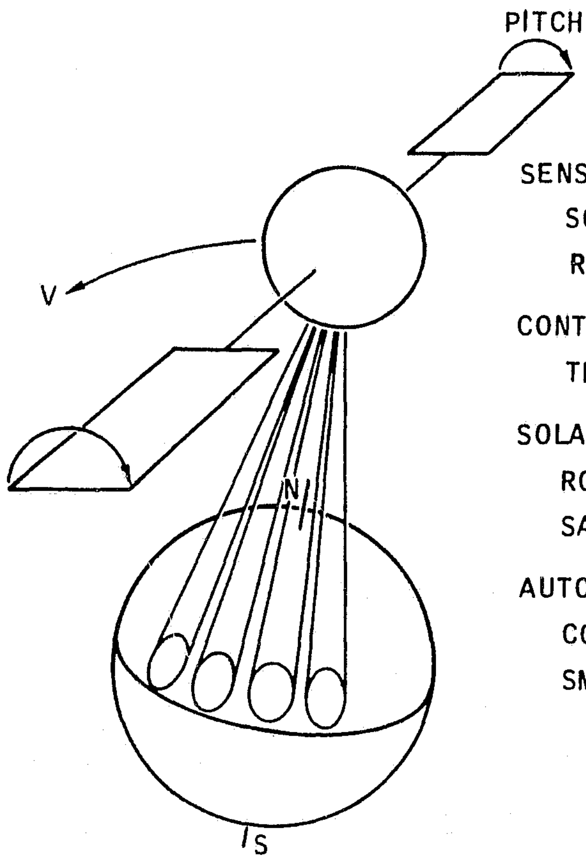

SENSORS

SOLAR & HORIZON SENSORS, RATE GYROS,
RF INTERFEROMETER*, STAR TRACKER*

CONTROL

TRANSLATION & ROTATION THRUSTERS, INERTIA WHEEL(S)*

SOLAR ARRAY ORIENTATION

ROTATION ABOUT PITCH AXIS, BY DIRECT LINEAR CONTROL
SATELLITE YAW ROTATION PROBABLE FOR UNI-BEAM CONCEPTS

AUTOPILOT

COMPENSATION FOR STRUCTURAL VIBRATION, DETERMINE
SMALL ANGULAR RATES OF ORDER $\left(\frac{1}{50}\right)$ EARTH RATE

*OPTIONAL

The typical system has two large solar arrays, rotatable in pitch, mounted on opposite sides of the rim of the large antenna. Sensors include solar and horizon sensors and rate gyros. Determination of antenna orientation using RF interferometers and ground beacons is a likely option for tight control. Use of star trackers is less likely.

Control devices include thrusters for station keeping and for rotation about three axes. Optional are inertia wheels about pitch only or about all three axes.

Solar array orientation is about pitch axis, using a direct linear drive control of the type being studies by Hughes and Westinghouse.

6. ACTIVE CONTROL DEVICES

THRUSTERS	THRUST LEVEL (LB.)	WEIGHT	I_{SP} (SEC.)	POWER (W)	RELIABILITY
COLD GAS	> 0.02	HEAVIEST	60	1	BEST
HYDRAZINE	> 0.001	HEAVY	235	1	
HYDROGEN PEROXIDE	> 0.01	HEAVY	160	1	
RESISTOJET	0.01 – 0.00001	MODERATE	350	20	
WATER ELECTROLYSIS	10 – 0.1	MODERATE	360	20	?
ION PROPULSION	0.01 – 0.000001	HAS HIGH CONSTANT WT.	4,500 - 9,500	1,000	

Thrusters considered are shown above with their characteristics.

Thrust level is to be kept low to minimize vibration excitement. Ion propulsion weight includes that for necessary solar cells and power conditioning. This constant weight is lifetime independent. Propellant volume as well as weight becomes excessive for all but ion propulsion for the heavier satellite, longer lifetime concepts. Power requirement is significant only for ion propulsion. Reliability is best for the heaviest system, the high thrust cold gas, and is questionable for water electrolysis.

Inertia wheels are the indicated momentum exchange device for this large, slowly moving satellite. No weight savings occur, but wheels provide lower variable torques, causing less vibration excitement. A single wheel may be provided for the high disturbance pitch axis or three wheels provided for all axis control.

Five year wheel reliability is a problem. Thrusters sizes for speedy wheel desaturation are larger than desirable for all thruster control. Thruster backup for wheel failure may therefore require an additional ACS thruster set.

7. ACS THRUSTER SELECTION

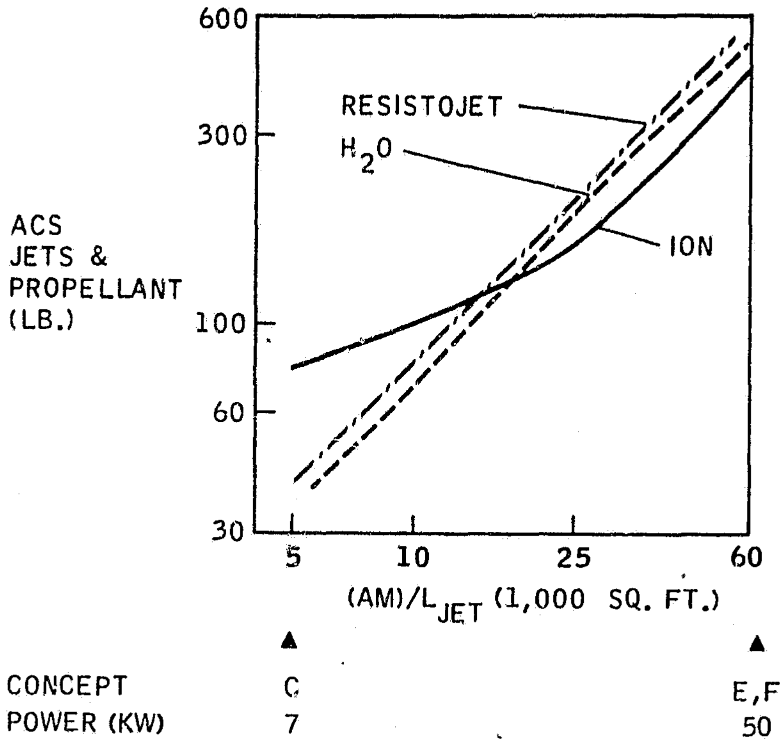

FOR 5 YR. CROSSOVER IS $(AM)/L_{JET} = 1.5 \times 10^4$

SELECT

ION PROPULSION ABOVE, RESISTOJET BELOW CROSSOVER

CROSSOVER POINT DECREASES WITH SHORTER LIFETIMES, BECAUSE MUCH ION PROPULSION WEIGHT IS LIFETIME INDEPENDENT

The selection is made on the basis of weight, power and volume. Power is converted to weight, using solar array and power conditioning characteristics, and is included.

ACS propulsion and propellant subsystem weights are compared for the resistojet, electric hydrolysis, and ion propulsion, for five year lifetime. The area moment to jet arm ratio os the independent variable. Concept C, 7KW, has 0.5×10^4 sq. ft. and concept E and F, each 50 KW, have 6.0×10^4 sq. ft. Above the crossover point of 1.5×10^4 sq. ft. ion propulsion is selected and below the resistojet is used.

The crossover point decreases with shorter lifetimes. Much ion propulsion subsystem weight is for associated solar cells and power conditioning equipment, which is lifetime independent. Ion propulsion power can exceed one KW; typical power values for other control are twenty watts.

Other ACS component weights are not included in the figure. Total ACS weight is dominated by the propulsion and propellant subsystem, which can be nearly 1% of satellite weight. ACS sensors and autopilot are 60 lb. typically.

8. STATION KEEPING THRUSTER SELECTION

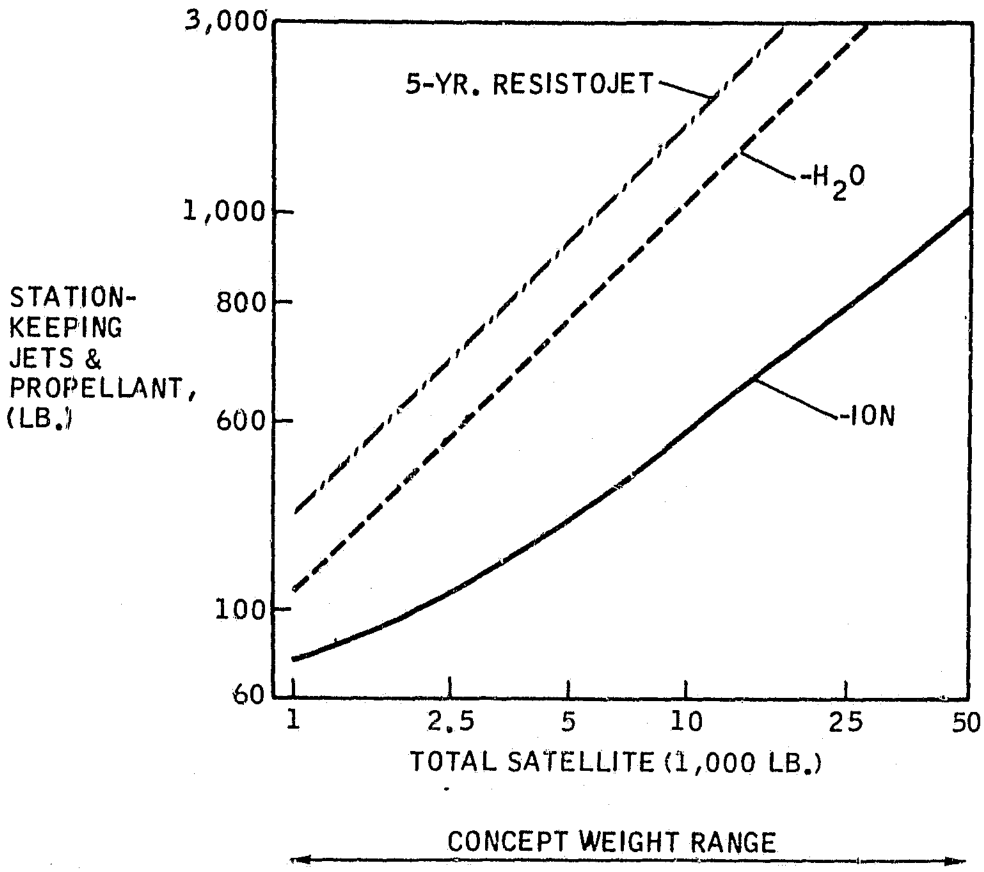

FOR 5-YR. ION PROPULSION CONSIDERABLY LIGHTER ACROSS ALL CONCEPT WEIGHTS

USE ION PROPULSION ABOVE ABOUT TWO YEARS, RESISTOJET BELOW - CROSSOVER IS SATELLITE WEIGHT DEPENDENT

EXCESSIVE PROPELLANT VOLUME OF NH_3, H_2O IS TRADEOFF FACTOR

The selection is made primarily on a weight basis, although the excessive propellant volumes of NH_3 and H_2O are factors.

Station keeping propulsion and propellant subsystem weights are compared for resistojet, electric hydrolysis, and ion propulsion, for five year lifetime. Total satellite weight is the independent variable. Station keeping weights are 2%, 10%, 17%, and 21% of total satellite weight for ion, hydrolysis, resistojet, and hydrazine. Ion propulsion is clearly lighter across the entire range of concepts for five year life.

A crossover occurs for shorter lifetimes due to ion system fixed weights. Resistojet vs hydrolysis weight differences are significant for station keeping, but are small for ACS.

9. OPERATIONAL CONSIDERATIONS

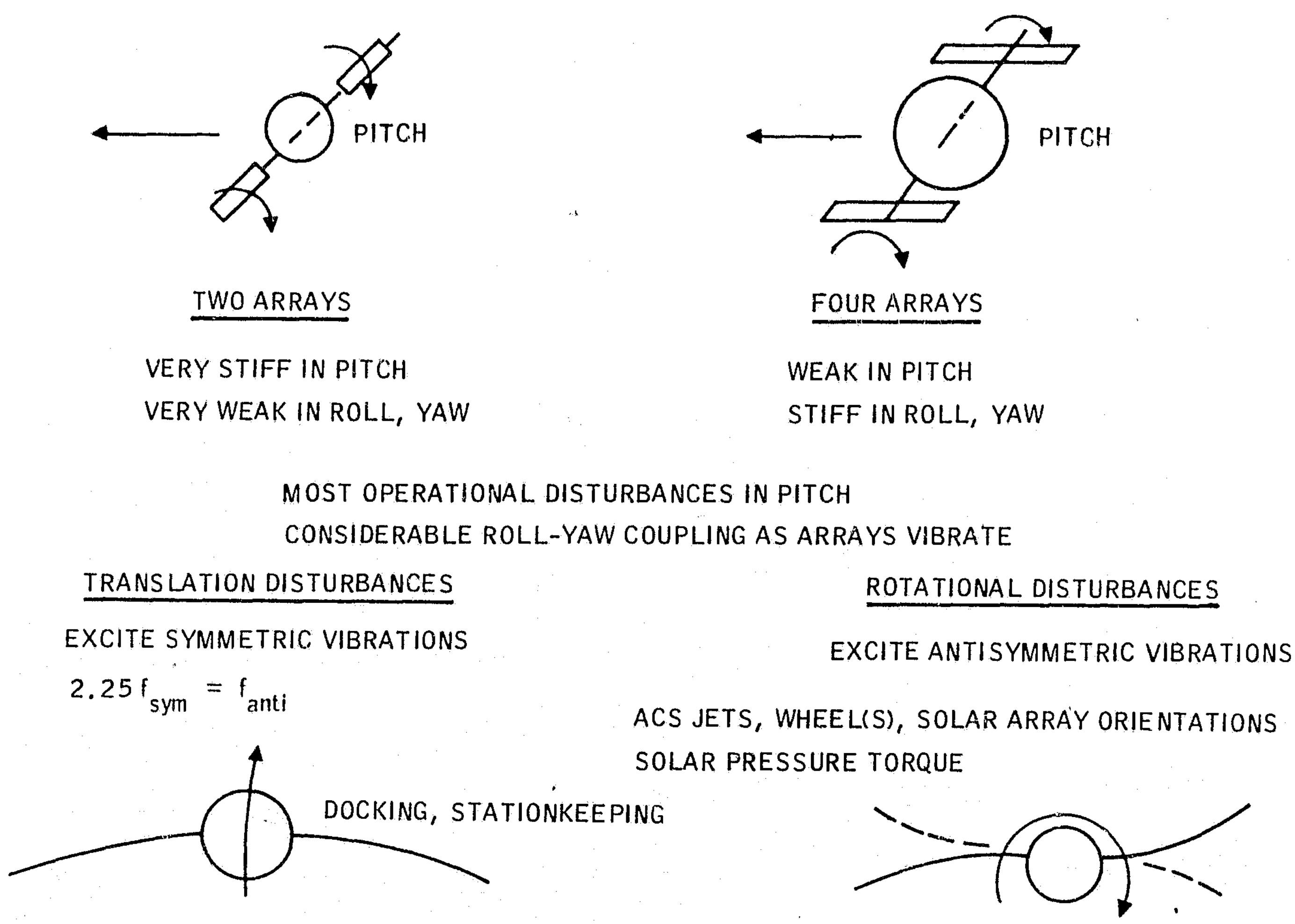

There are two practical vehicle configurations which provide for rotation of the solar arrays about the pitch axis; one has two large arrays with their major axes aligned along the pitch axis, the other has four smaller arrays extending out from the pitch axis as shown above.

The two arrays are very stiff in pitch and very weak in roll and yaw. The four arrays are weak in pitch (but not as weak as two in roll and yaw) and stiff in roll and yaw. Most operational disturbances occur in pitch because of array pitch axis rotations and solar torque characteristics. However, considerable roll-yaw coupling exists for either configuration as the arrays oscillate in bending. Consequently, selection of the best arrangement requires a detailed examination of each approach.

Translational disturbances excite the first symmetric bending mode. Rotaional disturbances excite the first anti-symmetric mode, whose frequency is about 2.25 times the symmetric frequency.

10. TYPICAL ACS CHARACTERISTICS

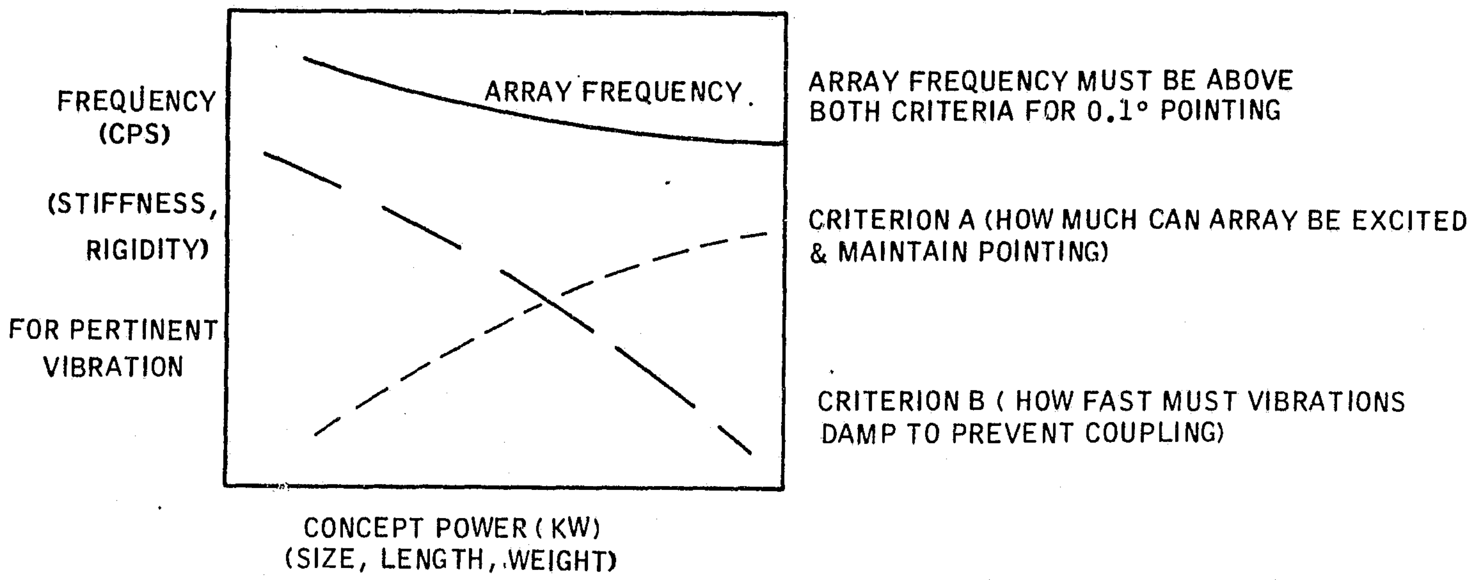

ARRAY FREQUENCY CALCULATIONS ARE ACCURATE

CRITERIA DEPENDENT ON VARIETY OF ASSUMPTIONS & CONCEPT SPECIFICS

- SOLAR ARRAY WEIGHT, ASPECT RATIO, STIFFENING
- SATELLITE INERTIA, THRUSTER LEVEL, POINTING TOLERANCE
- ACS TORQUE, DEADZONE, DRIFT VELOCITY, BURN TIME

Modal frequencies for the pertinent vibration are plotted above vs array power. Frequency is a measure of stiffness or rigidity. Power is related to array size, length, weight, etc.

The solid line is the actual array structural frequency. This must exceed both the criteria used to estimate array vibration effects on antenna beam pointing.

Criteria A considers how much a vibration can be excited without degrading pointing about a specific axis. The ACS rotational impulse is dependent upon maximum solar torque and desired limit-cycle operation, and is fixed for a specific concept sizing. Thus criteria A establishes the minimum frequency necessary to obtain the desired single axis pointing. Smaller satellites experience lower solar torque values and hence lower frequencies for criteria A.

Criteria B examines how quickly a vibration must damp in order to avoid appreciable interchannel coupling. Smaller configurations are rotated faster by the rotational impulses sized for the associated lower solar torque because inertias decrease faster than do the solar torques with decreasing satellite size. Hence, smaller satellites will damp faster and experience higher frequencies for criteria B.

11. FOUR-ARRAY CONFIGURATION - PITCH CONTROL

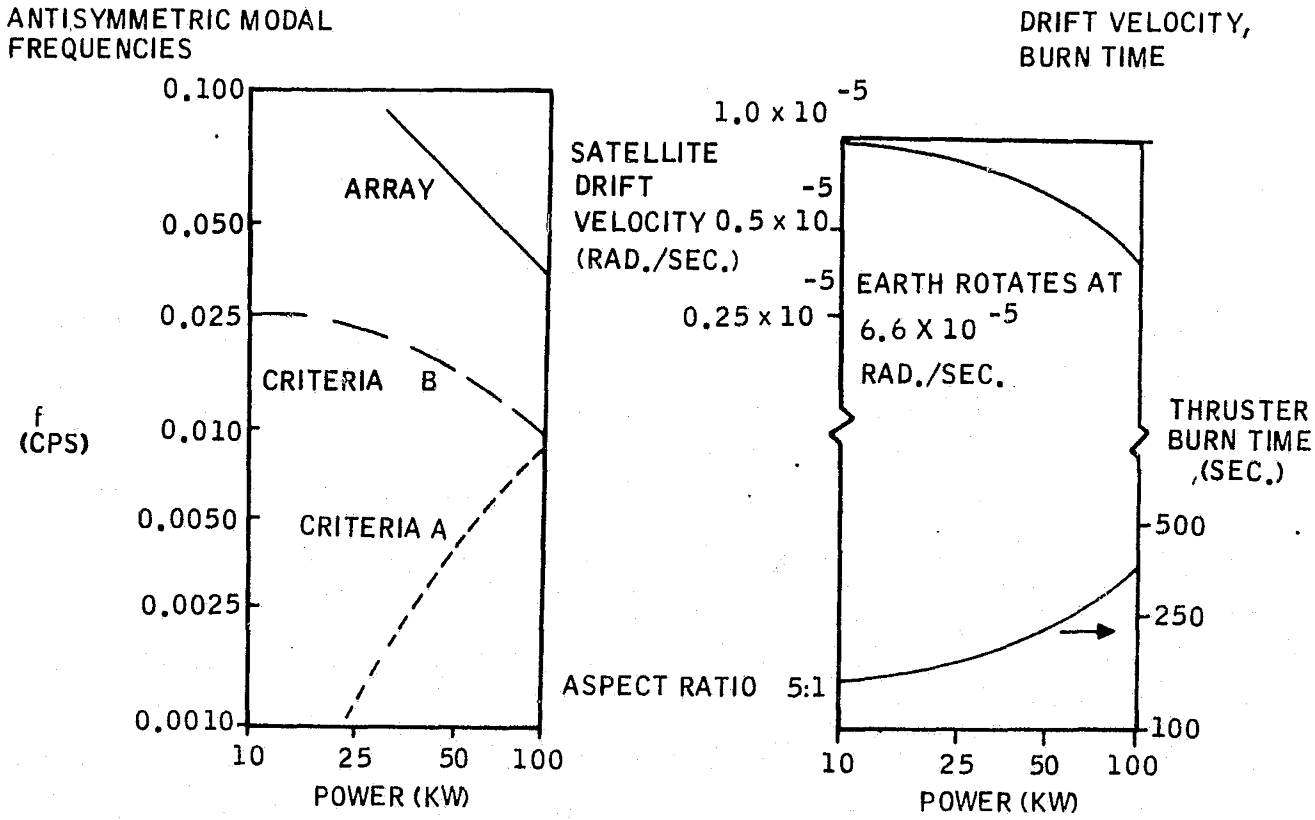

ARRAY FREQUENCY SAFELY ABOVE CRITERIA

SMALL DRIFT VELOCITY, BURN TIME EXCEEDS ARRAY MODAL PERIOD

The pitch channel is the key channel for the four-array configuration. The above data is for a thrust level of 1.2 milli-lbf., generated by either a resistojet or ion propulsion system. The limit cycle characteristics are set by the assumption that maximum angular displacement, $\Delta\theta_B$, is 0.02 deg. during thruster pulse time.

The array frequency is observed to be safely above both criteria. Note that the array length width (aspect) ratio is 5:1.

The satellite drift velocity and thruster burn time are also shown. Since the once per day earth rotation rate is 6.6×10^{-5} radians/second, it is clear that very small vehicle rates must be attained and measured. Accurate rate determination is a potential problem area.

12. TWO-ARRAY CONFIGURATION - YAW CHANNEL

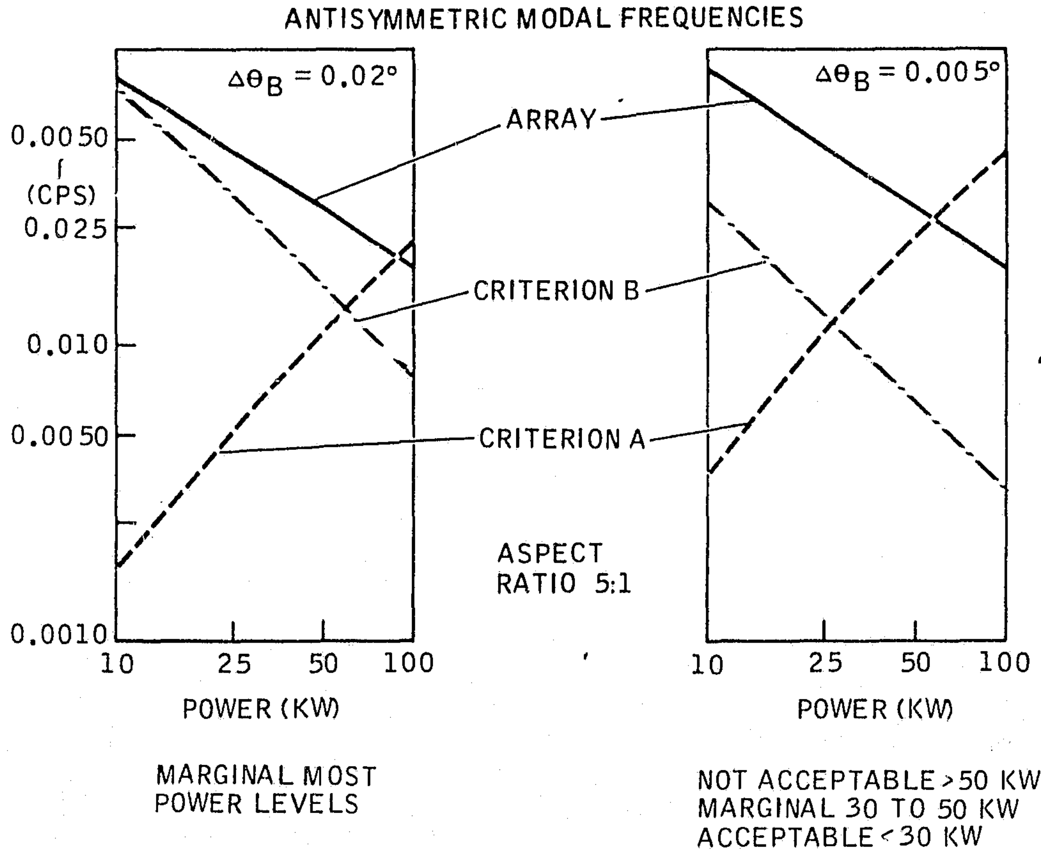

CONCLUSIONS
1. IMPROVED ANALYSIS REQUIRED
2. CONSIDER LOW-TORQUE INERTIA WHEELS
3. DESIGN CHANGES IN ASPECT RATIO, STRUCTURAL MEMBERS INCREASE STIFFNESS
4. FOLDOUTS ACCEPTABLE ALL CONCEPTS WITH DESIGN CHANGES

This data is for the yaw channel of the two-array configuration. Thrust is set at 3.2 milli-lbf. for the yaw channel because the area moment is larger than for the pitch channel discussed previously. Two values are assumed for $\Delta\theta_B$, 0.02 and 0.005 deg. Observe that frequencies for criteria A and B vary with opposing changes in power level, therefore, improvements in concept are not necessarily possible which will lower the criteria frequencies.

Smaller displacement means a smaller rotational impulse and smaller resultant vehicle drift velocities. Tighter restrictions must be placed on rigidity to prevent array vibrations from overpowering this smaller rate. Thus criterium A goes up in frequency. Since the drift rate has been decreased, longer limit-cycle periods results. More time is available for damping, and criterium B goes down.

The 0.02 degree data is marginal at most power levels, since array frequency is only slightly above the criteria. The 0.005 degree data is not acceptable above 50 KW, marginal at 30 to 50 KW, and acceptable below 30 KW.

Improved analysis is required because frequency differences are often smaller than the effects of analysis assumption. Considerations should be given to low torque inertia wheels. Wheels can be commanded to supply that torque currently necessary, while thrusters must be sized by maximum solar torque.

Design changes in array aspect ratio and the individual panel edge member structure can increase over-all stiffness. Data such as is shown next leads to the conclusions that fold out solar arrays are acceptable for all concepts; design improvements are necessary for higher powered two-array configurations.

13. ARRAY ASPECT RATIO AND STIFFENER EFFECTS

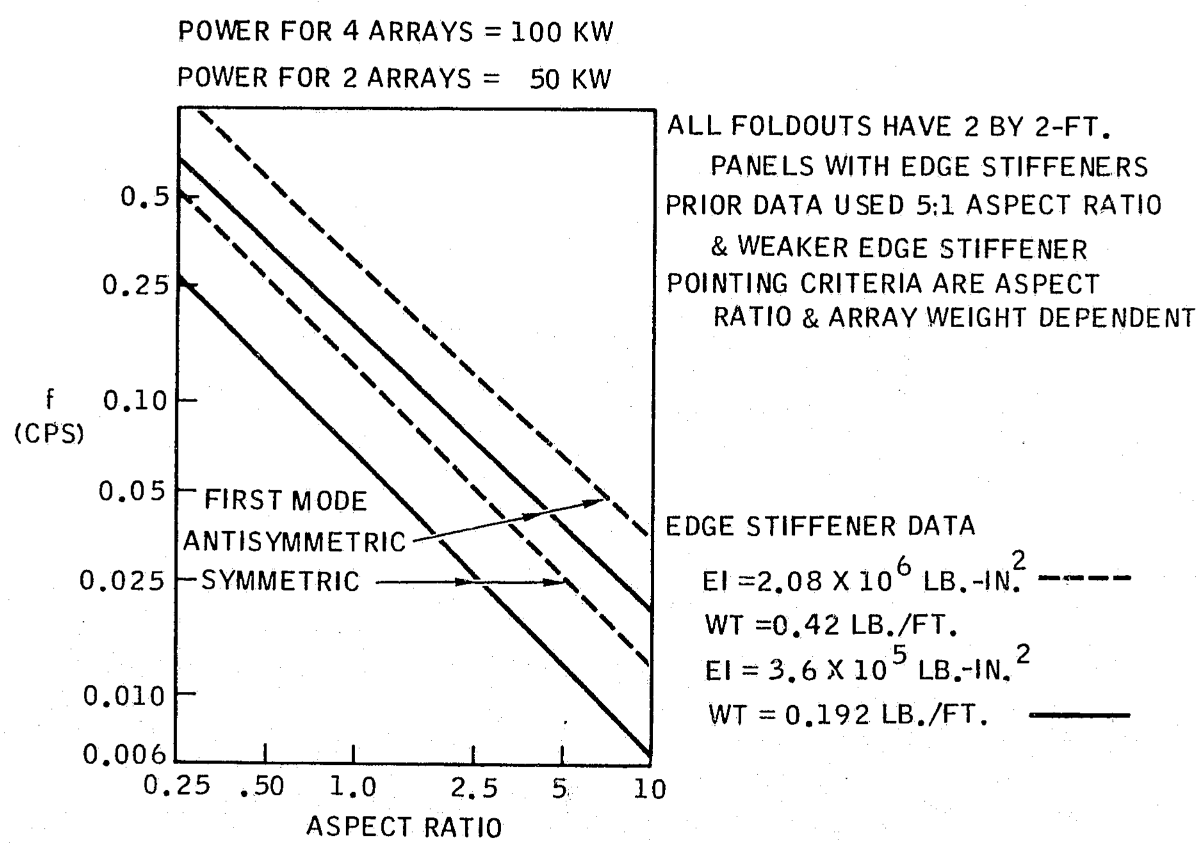

Nominally shaped fold-out arrays have a 5 to 1 aspect ratio. An array comprises a series of panels of two sq. ft. each. Each panel has edge beam stiffeners; nominal EI is 3.6×10^5 lb-inch^2. Frequencies increase with decreasing aspect ratios and increasing stiffness. Weight penalties result from the stiffer edge beams. Design and deployment difficulties increase as the aspect ratio is decreased below 4:1 into the region 3:1 to 2.5:1.

Pointing criteria are sensitive to both aspect ratio and weight.

Data indicates that aspect ratios near 4:1 and moderate edge beam weight increases will allow satisfactory pointing operation up to 100 KW, for the two-array configuration.

14. FOUR-ARRAY ROLL-OUT CONFIGURATION

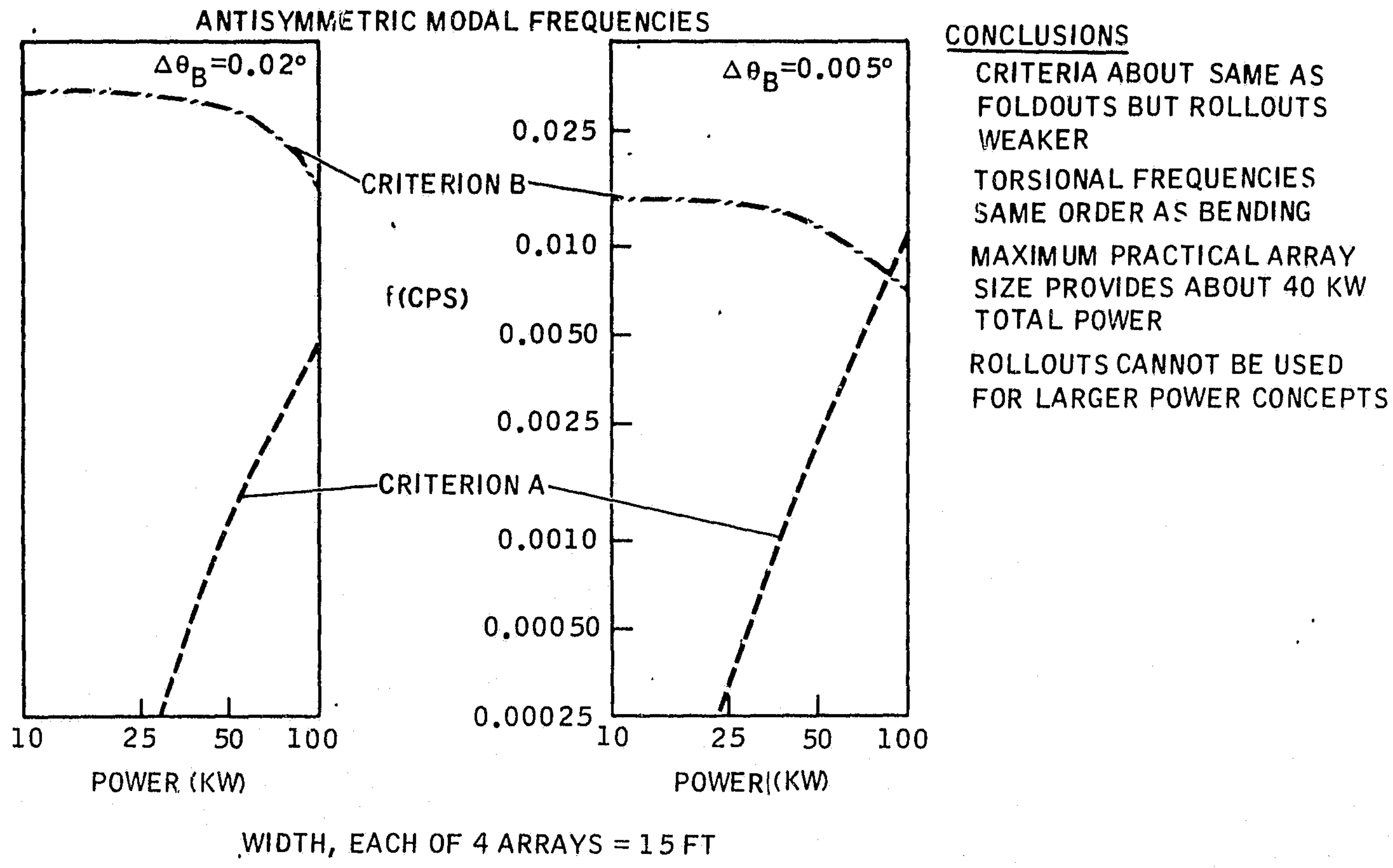

Pitch is again the key channel, and thrust is set at 2.0 milli-lbf.

The launch vehicle dimensions restrict drum length (array width). A 15 ft. width is used for each array, with aspect ratio varying with the length requirement for specific power levels. This results in increased solar torque and corresponding thruster level.

Criteria A and B are shown for two $\Delta\theta_B$ values. The criteria are close to the values of fold-out criteria, but roll-outs are weaker in out-of-plane bending. Further roll-out torsional frequencies can be the same order of magnitude as bending frequencies.

Design changes in array stiffener beams (actually tubes) have been examined. There are practical limits on the size and weight increases.

Maximum practical roll out array size provides about 40 KW total power with four and substantially less with two arrays. Roll outs can not be used for the larger power concepts.

15. ARRAY ROOT BENDING MOMENTS

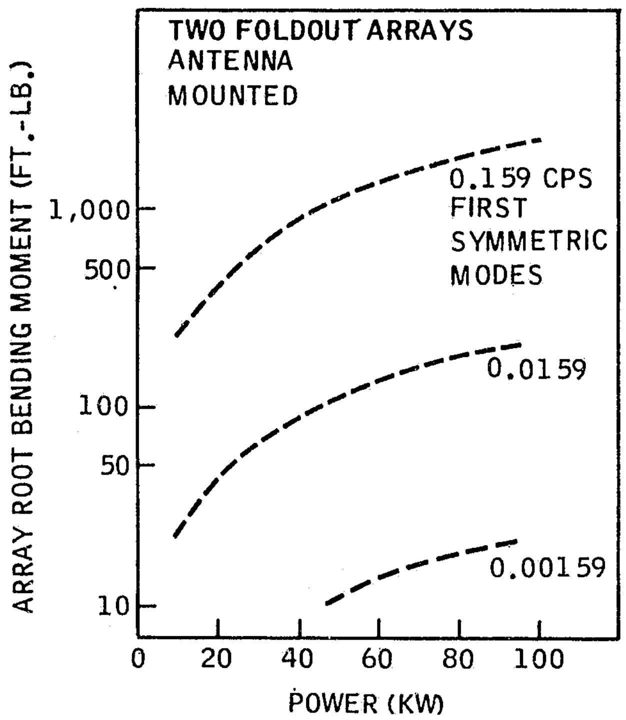

The dominant array bending moment occurs at the root due to CSM docking. Data is shown for four fold out arrays mounted on the antenna rim. Likely closure velocities are 0.15 fps, with satellite weight (less arrays) of 32,000 lb. Maximum loads are several thousands ft-lbs. This requires strengthening the rotation tube at the array root. The diameter necessary to handle bending moments could reach six inches. No significant vehicle weight change results because the tubes are relatively short. Consequently, docking loads on the fold-outs are acceptable.

However, some satellite concepts have arrays mounted on long supporting members to clear the antenna. These loads are not likely to be acceptable for the larger-antenna, higher-power configurations.

Roll outs are assumed to be retracted prior to CSM docking.

Station keeping loads are minimal. A one-lb. thruster would cause only 20 ft-lb. of moment. For the planned thruster levels, there is no possible structural damage for any concept in any configuration.

16. DYNAMICS TECHNOLOGY SUMMARY

Attitude control system and station keeping functions are affected by the recommended local-vertical orientation and the solar panel arrays' single-degree-of-freedom rotation about the vehicle pitch axis. Selected ACS thrusters are ion propulsion for larger configurations and longer lifetime concepts; others use resistojets. Station keeping thrusters selected are ion propulsion for satellite lifetime above two years and resistojets below. The crossover point is satellite weight dependent. Inertia wheel(s) are optional; no weight savings accrue but control generated disturbances are smaller. Sensors most likly will be horizon and solar scanners, and rate gyros. A probable option is an RF interferometer, and a star tracker is a less likely option.

Control-structural vibration interaction studies concerned the solar arrays effects with respect to 0.1 degree pointing, emphasizing configurations with larger power. Both fold-out and roll-out arrays are below stress level in the launch environment. Fold-outs can be used to the maximum desired power levels; but some array design changes may be necessary for two-array configurations. Roll-outs are limited to about 40 KW total power. CSM docking loads are acceptable on antenna-mounted fold-outs after simple local stiffening. Satellite body mounting is unacceptable for the larger-antenna, higher-power concepts. Roll-outs are assumed to be retracted for docking.

Other key technologies areas are 1) achieving satisfactory component reliability for five year lifetime and 2) measurement of small vehicle angular rates.

Report GDC-DCF 70-002

TELEVISION BROADCAST SATELLITE STUDY

FINAL REPORT - VOLUME IV

TECHNICAL APPENDICES

Contract NAS8-21036

31 December 1970

APPENDIX F

STRUCTURAL VIBRATION - POINTING CONTROL INTERACTIONS

Convair Aerospace Division

GENERAL DYNAMICS

APPENDIX F

STRUCTURAL VIBRATION - POINTING CONTROL INTERACTIONS

It is found that attainment of ± 0.1 degree TV beam pointing is compatible with sun-oriented solar arrays, with limited design improvements for the fold-out type and with the roll-out type utilization being restricted in maximum power.

This ability to meet pointing requirements under the complication of large highly flexible continually sun oriented solar arrays is achievable because of five factors. These are:

1. The permissive environment at synchronous altitudes.
2. Utilization of low level thrusters
3. Absence of any vehicle maneuvering requirements
4. Accurate pointing orientation measurements, and
5. Direct linear drive controlling solar panel orientations.

The initial operational phases of ejection, insertion into orbit at desired longitude, attitude acquisition and antenna and array deployment are feasible. Examination of these phases is not necessary for this systems study.

Included in this section is an examination of possible damage to the solar arrays by CSM docking.

1 ATTITUDE CONTROL SYSTEM PERFORMANCE

1.1 RIGID BODY LIMIT CYCLE OPERATION

Solar panel vibration effects on TV beam pointing are investigated by considering limit cycle operation. Idealized rigid body limit cycle operation is shown on the phase plane plot of Figure F-1. The vehicle remains within the desired pointing tolerance, $\pm\Delta\theta_{E_k}$. Actual TV yaw tolerance is looser than for roll or pitch, being very broad for a uni-beam. Roll and pitch tolerances will be nearly identical for most beams. Phase plane trajectory is a parabola during thruster operation. The vehicle moves through the angle $\Delta\theta_{B_k}$ in the first half of the burn, and retreats $\Delta\theta_{B_k}$ in the second half. Subsequent to burn, the vehicle drifts through the angle $2\Delta\theta_{D_k}$ at angular rate $\dot{\theta}_{D_k}$.

The angular acceleration during burn is:

$$\ddot{\theta}_{B_k} = \tau_{JET_k} / (I_{R_k} + I_{SB_k})$$

Burn time is determined from:

$$\Delta\theta_{B_k} = \tfrac{1}{2}\,\ddot{\theta}_{B_k}\,(t_{B_k})^2 \quad \text{, with}$$

$$t_{B_k} = \sqrt[2]{2\Delta\theta_{B_k} / \ddot{\theta}_{B_k}}$$

The angle change during burn, $\Delta\theta_{B_k}$, will be established as a fraction of pointing tolerance, $\Delta\theta_{E_k}$, depending on the error budget.

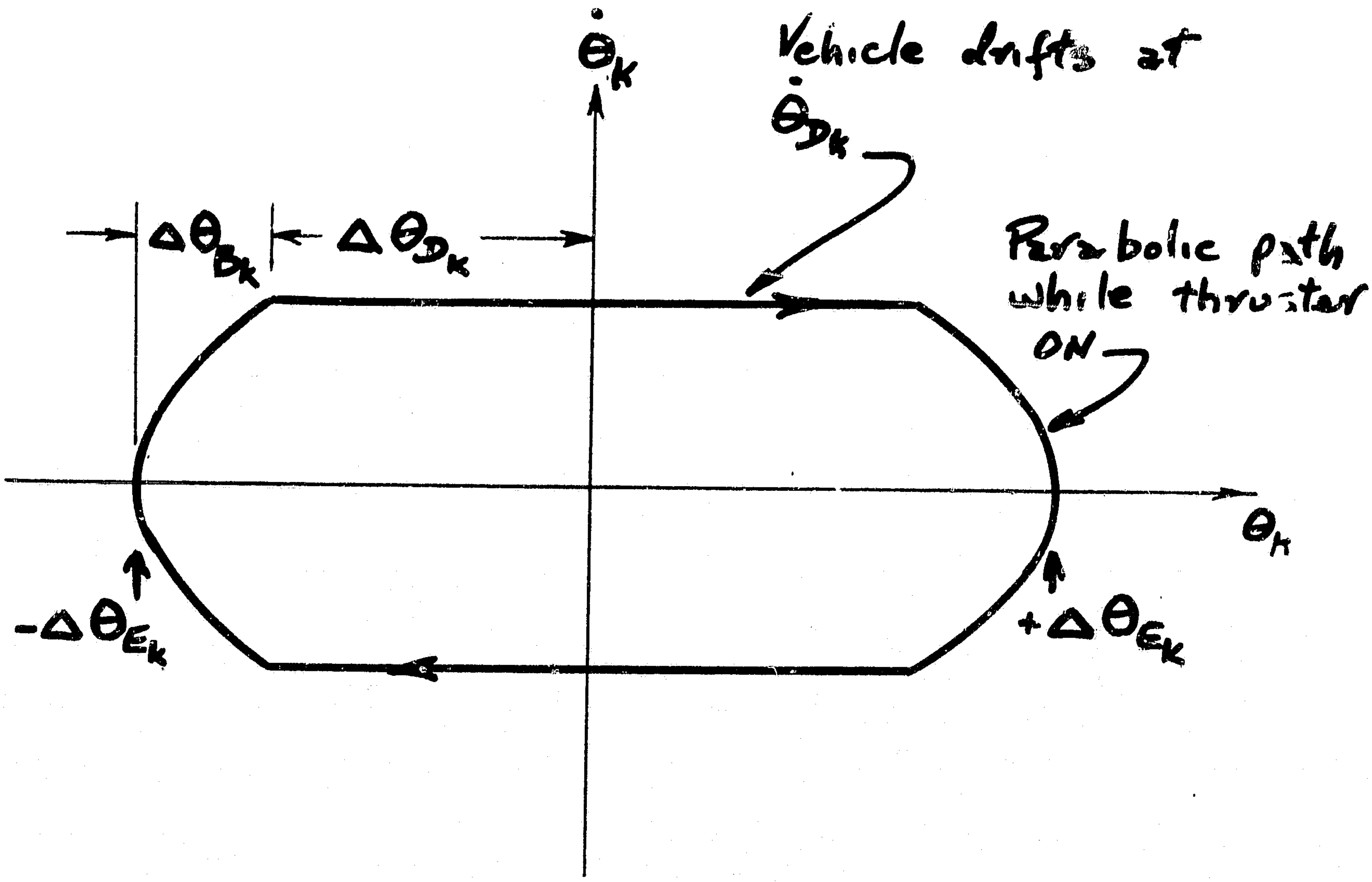

$$\Delta\theta_{B_K} \le \Delta\theta_{E_K}$$

$$\Delta\theta_{D_K} \le \Delta\theta_{E_K}$$

$$\Delta\theta_{B_K} + \Delta\theta_{D_K} = \Delta\theta_{E_K}$$

Figure F-1. Idealized rigid body limit cycle operation, k th axis

The drift rate is:

$$\dot{\theta}_{D_k} = \ddot{\theta}_{B_k} \left(t_{B_k} / 2 \right)$$

The drift time is:

$$T_{D_k} = 2 \left(\Delta\theta_{E_k} - \Delta\theta_{B_k} \right) \Big/ \dot{\theta}_{D_k} .$$

Smaller drift rates and burn times result in pointing errors within the pointing tolerance; larger drift rates and/or burn times cause pointing errors to exceed the tolerance. Analysis examines the situation in which errors are equal to the tolerances $\Delta\theta_{B_k}$ and $\Delta\theta_{E_k}$.

30

1.2 SOLAR PANEL VIBRATION DISTURBANCE OF LIMIT CYCLE OPERATION

Analysis model obtains the array angular momentum with respect to vehicle coordinates due to vibration. Only the first antisymmetric mode is examined, and the half mode shape is assumed parabolic. Thus the angular moment of each of the two or four individual arrays is given by:

$$J_{K_1}(t) = J_{K_1 MAX} \sin\left(\omega_{iA_1} t + \theta_{iA_1}\right) e^{-\xi_{iA_1} \omega_{iA_1} t}$$

t being zero at burn termination.

It is also assumed that the inertia and angular momentum of each individual array with respect to a specific vehicle axis are identical. This follows from symmetery for each concept. Thus the total solar panel array angular momentum is:

$$J_K(t) = N_P J_{K_1}(t)$$

and

$$J_{K MAX} = N_P J_{K_1 MAX}$$

N_P being number of individual arrays.

An expression is developed for $J_{K_1 MAX}$, under the assumption that thruster burn time is longer than modal period. Vibratory angular momentum is thus due to a constant acceleration.

This expression is not valid for the two array configuration pitch channel, because those individual arrays are on both sides of pitch axis. Since this flexibility is extremely strong, little need is foreseen for the valid formula.

The single axis situation is shown in Figure F-2.

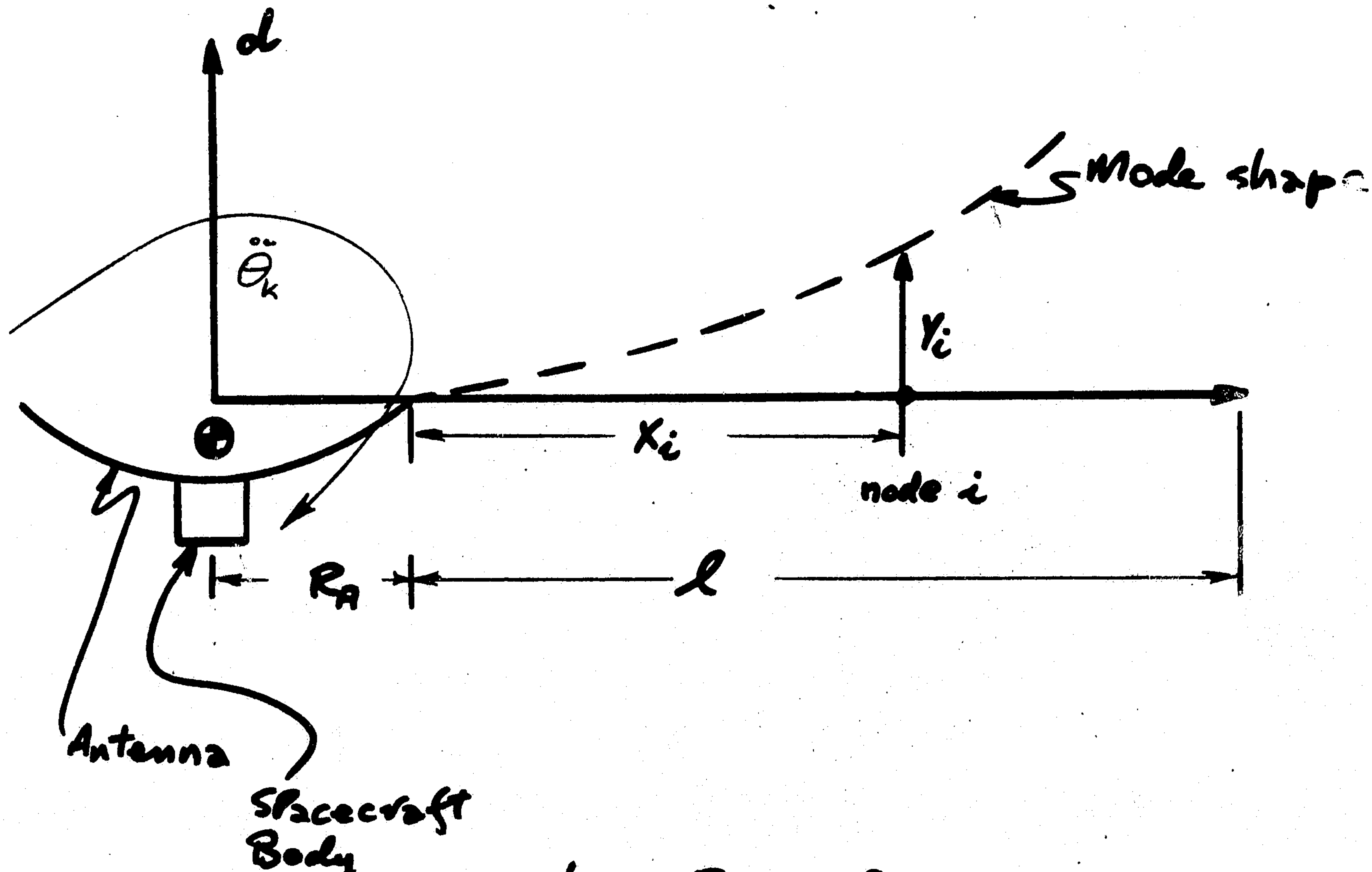

$$\ell' = R_A + \ell$$

$$Y_i\,(X_i = \ell) = 1$$

k ≡ pitch for two arrays

Plane of figure is perpendicular to k axis.

Mode of interest is first anti-symmetric mode of panels cantilevered off opposite sides of spacecraft antenna.

Figure F-2. Solar panel flexibility angular momentum

The generalized force at node i for mode j_{A_1} is;

$$Q_{j_{A_1},i} = \mathcal{F} \, Y_{j_{A_1},i}$$
$$= m_i * (X_i + R_A)\ddot{\theta} \; Y_{j_{A_1},i}$$

and

$$Q_{j_{A_1}} = \ddot{\theta} \sum_{i=1}^{N_i} m_i * (X_i + R_A) \, Y_{j_{A_1},i}$$

omitting the axis index k.

Assuming half of mode shape of a uniform density beam is represented by a parabla normalized to one at tip,

$$Y_{j_{A_1},i} = (X_i/\ell)^2$$

Converting expression for $Q_{j_{A_1}}$ to a continuous model, the generalized force for the beam is

$$Q_{j_{A_1}} = \ddot{\theta} \int_0^{\ell} \lambda * (x + R_A)(x/\ell)^2 dx$$
$$= \ddot{\theta} \lambda \ell \left[\frac{\ell}{4} + \frac{R_A}{3}\right] = \ddot{\theta} \frac{M_{P_1}}{4}\left(\ell + \frac{4R_A}{3}\right) \text{ since}$$

$$M_{P_1} = \lambda \ell$$

The approximation form

$$Q_{j_{A_1}} = \frac{\ddot{\theta} M_{P_1}}{5} \ell'$$

$$\ell' = \ell + R_A$$

was used for the midterm calculations.

The generalized mass is

$$m_{j_{A_1}} = \sum_{i=1}^{N_i} m_i \left(Y_{j_{A_1},i}\right)^2$$

For the uniform density beam with parabolic mode shape

$$m_{jA_1} = \int_0^{\ell} \lambda \left[\left(x/\ell \right)^2 \right]^2 dx = \frac{\lambda \ell}{5} = \frac{M_{P_1}}{5}$$

The maximum deflection of node i (ie at X_i) is

$$d_{MAX_i} = \frac{Y_i \, 2 Q_{jA_1}}{(\omega_{jA_1})^2 m_{jA_1}}$$

$$= \frac{Y_i \, 2 \ddot{\theta} M_{P_1} \left[\ell + 4R_A/3 \right]}{(\omega_{jA_1})^2 m_{jA_1} \, 4}$$

and the maximum velocity of node i is

$$\dot{d}_{MAX_i} = \omega_{jA_1} d_{MAX_i}$$

$$= \frac{Y_i \, 2 \ddot{\theta} M_{P_1} \left[\ell + 4R_A/3 \right]}{\omega_{jA_1} m_{jA_1} \, 4}$$

The angular momentum due to mode jA_1 is assumed to approximate the total, and

$$J_{k1_{MAX}} \gtrsim J_{kjA_{1_{MAX}}} = \int_0^{\ell} \dot{d}_{MAX}(x) \lambda * (X + R_A) \, dX$$

$$= \frac{\lambda \, 2 \ddot{\theta} M_{P_1} \left[\ell + 4R_A/3 \right]}{4 \omega_{jA_1} m_{jA_1}} \int_0^{\ell} \frac{X^2}{\ell^2} (X + R_A) \, dx$$

again assuming parabolic modal shape. Thus

$$J_{K_{jA_{1\,max}}} = \frac{2\ddot{\theta} M_{P_1} 2\ell}{\omega_{jA_1} m_{jA_1}} \left[\frac{\ell}{4} + \frac{R_A}{3}\right]^2$$

$$= \frac{2\ddot{\theta} (M_{P_1})^2}{\omega_{jA_1} m_{jA_1}} \frac{[\ell + 4R_A/3]^2}{4^2}$$

noting that $m_{jA_1} = M_{P_1}/5$

$$J_{k_{jA_{1\,max}}} = \frac{25\ddot{\theta} m_{jA_1}}{8\omega_{jA_1}} \left[\ell + 4R_A/3\right]^2$$

$k \doteq$ pitch for two arrays.

The approximate forms

$$Q_{jA_1} = \ddot{\theta} M_{P_1} \ell'/5$$ and

$$J_{k_{jA_{1\,max}}} = 2\ddot{\theta} m_{jA_1} (\ell')^2/\omega_{jA_1}$$, with

$$\ell' = \ell + R_A$$

were utilized for the midterm calculations. These were derived by an approximate model which considered all the mass to be represented by generalized mass being at tip. The more accurate expressions result in higher criteria A values (stiffer arrays required).

Checking units, J should be ft.lb.sec. Since $\ddot{\theta}$ is rad/sec^2, m slugs, ℓ and R_A ft. and ω rad/sec, we have

$$\frac{(\text{rad.}/\text{sec.}^2)}{\text{rad.}/\text{sec.}} \times \text{slug} \times \text{ft.}^2 = \frac{\text{slug ft.}^2}{\text{sec.}}$$

Noting slugs are lb sec^2/ft, one obtains

$$\left(\frac{\text{lb. sec.}^2}{\text{ft.}}\right) \frac{\text{ft}^2}{\text{sec.}} = \text{lb. ft. sec.}$$

1.3 THRUSTER LEVEL

The low level ACS thrusters are sized by the maximum solar torque. These are resistojet, ion propulsion, and water hydrolysis. Higher level thrusters are sized near their practical minimum. Hydrazine is assigned 0.010 lbs.

An assumed CG-GP offset of 2% is used.

$$\tau_{SOL_{MAX}} = (AM) \times 0.02 \times 2 P_{SOL} \quad \text{, where}$$

$$P_{SOL} = 9.85 \times 10^{-8} \ lb./ft.^2$$

$$\tau_{SOL} = 4.00 \times 10^{-9} (AM) \quad ft.\ lb.$$

ACS propellant sizing calculations used a more conservative approach, multiplying τ_{SOL} by $(1 + 1/\sqrt{2})$. There the maximum torque is 6.83×10^{-9} (AM) and thrusters are sized by $T = 1.70 \times 10^{-8} (AM/L_{JET})$.

Here

$$2\, T_{JET} L_{JET} DC_{ACS} = \tau_{SOL}$$

With typical value of 0.2 for DC_{ACS}

$$T_{JET} = 1.00 \times 10^{-8} \left(\frac{AM}{L_{JET}}\right)$$

Checking units, the 1.00×10^{-8} carries the units of P_{SOL}. Hence T_{JET} has the units of $(lb/ft.^2) \times ft.^3/ft$, which are lbs, as desired.

1.4 VEHICLE DRIFT VELOCITY WITH SOLAR ARRAY VIBRATION

This simple analysis asssumed antennas to be rigid and solidly attached to satellite body. Antenna vibrations should be examined, particularly for the antenna supports of concept D.

Therefore the antenna beam orientation drift velocity is

$$\dot{\varphi}_{D_k}(t) = \dot{\theta}_{D_k} + \dot{\gamma}_{D,P_k}(t)$$

where $\dot{\gamma}_{D,P_k}(t)$ is the antenna angular rate due to solar array oscillations.

The antenna angular momentum due to array vibration must equal corresponding array momentum, except for a phase shift, yielding

$$\dot{\gamma}_{D,P_k}(t) = \frac{N_P}{I_{S_K}}\left[J_{k_{jA_1\,MAX}}\right] \sin\left(\omega_{jA_1} t + \theta_{jA_1}\right) e^{-\zeta_{jA_1}\omega_{jA_1} t}$$

and finally

$$\dot{\varphi}_{D_K}(t) = \dot{\theta}_{D_K} + \frac{N_P}{I_{S_K}}\left[J_{k_{jA_1\,MAX}}\right] \sin\left(\omega_{jA_1} t + \theta_{jA_1}\right) e^{-\zeta_{jA_1}\omega_{jA_1} t}$$

1.5 TWO CRITERIA ON VIBRATIONS

It is necessary to develop criteria on allowable vibratory response and it is convenient to express them in terms of minimum frequency for the solar array first antisymmetric mode. Criterion A establishes conditions for satisfactory pointing in the k channel, whose thrusters excited the vibrations. Criterion B establishes conditions for prevention of coupling the vibratory errors into other channels and/or coupling with subsequent k channel thruster operation.

Criteria A is a restriction on ratio between rigid body rate and vibration caused maximum rate:

$$F_A \left(\frac{N_P J_k}{I_{SB_k}} \right) \leq \dot{\theta}_{D_k}$$

where the modal index j_{A_1}, denoting first anti symmetric mode has been dropped, and F_A is a factor selected by intuition. Nominal F_A values is $\sqrt{2}$.

Criteria B is a requirement that vibration magnitude damp to a fraction of its original value while satellite drifts between successive thruster firings:

$$e^{-\zeta \omega t_D} \leq F_B$$

Nominal F_B value is taken to be $1/(3\sqrt{2})$.

These expressions are next to be manipulated into relationships for minimum modal frequency. Noting that J_k includes ω in its denominator, criteria A becomes

$$F_A \frac{N_P}{I_{SB_k}} \frac{[\omega J_k]}{\omega} \leq \dot{\theta}_{D_k} \text{ , \& using}$$

$$\dot{\theta}_{D_k} = \left(t_B/2 \right) \ddot{\theta}_{B_k}$$

$$\omega \geq \frac{F_A N_P [\omega J_k]}{I_{SB_k} \left(t_B/2 \right) \ddot{\theta}_{B_k}}$$

where $[\omega J_k]$ is frequency independent.

Algebraic simplifications can be introduced to simplify the formula and the calculations.

The ω expression for the approximate model is, for example

$$\omega \geqslant \frac{(4/5)\, F_A\, N_P\, M_{P_1}\, (\ell')^2}{I_{SB_k}\, (t_B/2)}$$

Computations of the individual steps yields values for various physical parameters, providing insight into the physical situation, and is therefore recommended.

Criteria B becomes

$$\omega \geqslant \frac{1}{\zeta\, t_D}\, \ln_e \left(1/F_B\right)$$

Damping ratio ζ must be estimated and it is representative of solar array damping in a zero g field. Such damping is not precisely known; estimates are in the range 0.005 to 0.02. Nominal value was taken to be 0.02, which is not particularly conservative.

1.6 SAMPLE NUMERICAL CALCULATION

Data is shown for a 100 KW four fold out solar array antenna mounted pitch axis. Basic configuration data is in Table F-1.

TABLE F-1.

SAMPLE CASE, 4 ARRAY FOLD-OUT CONFIGURATION DATA, Pitch

area moment	$(AM/L_{JET})_{roll}$		1.24×10^5 ft.^{2}
area moment	$(AM/L)_{pitch}$		1.12×10^5 ft.^{2}
thruster jet arm	L_{JET}		5.0 ft.
satellite less array inertia	$I_{SB_{pitch}}$		2.16×10^5 slug ft.^{2}
solar array inertia (all)	$I_{P_{pitch}}$		1.30×10^6 slug ft.^{2}
no. of arrays	N_P		4
pointing tolerance	$\Delta\theta_E$	.001745 radians	(0.1 deg)
burn drift	$\Delta\theta_B$	.000349	(.02 deg)
mass of one array	M_{P_1}	77.7 slugs	(2500 lbs)
CG to array base	R_A		0* ft.
total array power			100 KW
individual array length,	ℓ		112 ft.
width, pitch	ω		22.4 ft.
duty cycle	DC_{ACS}		0.2
array CP-CG offset			2%
criteria factors	F_A, F_B		$\sqrt{2}$, $1/[(3)\sqrt{2}]$
damping factor	ζ		.02

* array base is approximately at pitch axis on four array configuration

Thruster levels are sized by the maximum solar torque among all three channels. Roll channel is the largest here;

$$\tau_{SOL_{MAX}} = \left[(1.24 \times 10^5) \times 5\right] \times 4.00 \times 10^{-9} = 2.48 \times 10^{-3} \text{ ft. lb.}$$

$$T_{JET} = 1.00 \times 10^{-8} \times 1.24 \times 10^5 = 1.24 \times 10^{-3} \text{ lb.}$$

$$\ddot{\theta}_{B_k} = \frac{1.24 \times 10^{-3} \times 2 \times 5}{(1.30 + 0.22) \times 10^6} = 8.16 \times 10^{-9} \text{ rad./sec.}^2$$

$$t_{B_k} = 2\sqrt{\frac{2 \times 0.000349}{8.16 \times 10^{-9}}} = 585 \text{ sec.}$$

$$\dot{\theta}_{D_k} = 8.16 \times 10^{-9}\left(\frac{585}{2}\right) = 2.39 \times 10^{-6} \text{ rad./sec.}$$

This is very small. Earth rate (once/24 hr) for example, is 6.6 X 10^{-5} rad/sec.

$$t_{D_k} = \frac{2(0.001745 - 0.000349)}{2.39 \times 10^{-6}} = 1{,}167 \text{ sec.}$$

Note that the duty cycle under this condition is 585/1167 = 50.1%, while 20% was assumed at beginning.

The maximum angular momentum due to any one of the four panels is, by the approximate expression,

$$J_{kA_{1MAX}} = 2 \times 8.16 \times 10^{-9} \times \left(\frac{77.7}{5}\right)(112 + \text{zero})^2 / \omega_{jA_1}$$

$$= 3.46 \times 10^{-3} / \omega_{jA_1} \text{ ft. lb. sec.}$$

and by the more exact expression,

$$J_{kA_{1MAX}} = \left(\frac{25}{8}\right) 8.16 \times 10^{-9} \left(\frac{77.7}{5}\right)(112 + \text{zero})^2 / \omega_{jA_1}$$

$$= 5.41 \times 10^{-3} / \omega_{jA_1} \text{ ft. lb. sec.}$$

The corresponding maximum vehicle (antenna under analysis assumptions) rates are

$$\left(\frac{4}{2.16 \times 10^5}\right) \frac{3.46 \times 10^{-3}}{\omega_{jA_1}} = \frac{6.40 \times 10^{-8}}{\omega_{jA_1}} \text{ rad./sec.}$$

and

$$\left(\frac{4}{2.16 \times 10^5}\right) \frac{5.41 \times 10^{-3}}{\omega_{jA_1}} = \frac{1.00 \times 10^{-7}}{\omega_{jA_1}} \text{ rad./sec.}$$

Criteria A is then

$$\omega \gtrsim \frac{(\sqrt{2})\, 4 \times 13.46 \times 10^{-3}}{2.16 \times 10^5 \times \left(\frac{585}{2}\right) \times 8.14 \times 10^{-9}}$$

$\omega \gtrsim .0377$ rad/sec, $\qquad f \gtrsim .00600$ cps

using the approximate expression, and

$\omega \gtrsim .0593$ rad/sec, $f \gtrsim .00945$ cps using the more exact expression.

Criteria B is then

$$\omega \gtrsim \frac{1}{0.02 \times 1167} \left(\ln_e 3\sqrt{2}\right) = 0.0619 \text{ rad./sec.}$$

$$f \gtrsim 0.00986 \text{ cps.}$$

The first antisymmetric modal frequency for this solar panel array configuration is .0349 cps, and therefore rigidity exceeds both criteria.

1.7 SOLAR TORQUE DISTORTION OF IDEALIZED LIMIT CYCLE

Solar pressure on the solar arrays alters drift time, affecting Criteria B.

Drift velocity is not constant, as assumed in the idealized rigid body limit cycle, because solar torque accelerates or decelerates the satellite. Acceleration decreases drift time, allowing less time for damping the ACS thruster vibration excitement and criteria B requires higher modal frequencies (stiffer arrays).

The maximum solar torque acceleration, $\ddot{\theta}_{ST_{MAX}}$, for a channel, is

$$\ddot{\theta}_{ST_{MAX}} = \frac{\tau_{SOL}}{I_{SB} + I_P}$$

and a previous result is

$$\tau_{SOL} = 4 \times 10^9 \ (AM)$$

Acceleration value used, $\ddot{\theta}_{ST}$, is a fraction, F_{ST}, of maximum,

$$\ddot{\theta}_{ST} = F_{ST} \, \ddot{\theta}_{ST_{MAX}} \quad , \quad F_{ST} \leq 1$$

nominally F_{ST} is $\sqrt{2}/2$.

Drift time is obtained from

$$\frac{1}{2} \ddot{\theta}_{ST} (t_D)^2 + \dot{\theta}_D t_D - 2\left[\Delta\theta_E - \Delta\theta_B\right] = 0$$

as

$$t_D = \frac{-\dot{\theta}_D + \sqrt{(\dot{\theta}_D)^2 + 4\,\ddot{\theta}_{ST}\left(\Delta\theta_E - \Delta\theta_B\right)}}{\ddot{\theta}_{ST}}$$

For cases in which solar torque alteration of the limit cycle is small, the square root value approaches $\dot{\theta}_D$. Then significance is lost in the subtraction. A satisfactory expression is obtained using the binomial expansion.

$$t_D = \frac{2(\Delta\theta_E - \Delta\theta_B)}{\dot{\theta}_D} - \frac{2\,\ddot{\theta}_{ST}}{(\dot{\theta}_D)^3}\left(\Delta\theta_E - \Delta\theta_B\right)^2$$

for $\ddot{\theta}_{ST}$ small.

Numerical results, using the previous example and $F_{ST} = .707$, are now given.

$$\ddot{\theta}_{ST} = F_{ST}\,\ddot{\theta}_{ST_{MAX}} = \frac{F_{ST}\,\tau_{SOL}}{I_{SB} + I_P}$$

$$= \frac{F_{ST} \times 4.00 \times 10^{-9}}{I_{SB} + I_P}(4m) = \frac{0.707 \times 4 \times 10^{-9} \times 5.60 \times 10^{-5}}{1.52 \times 10^{6}}$$

$$= 1.04 \times 10^{-9}\ \text{rad./sec.}^2$$

This $\ddot{\theta}_{ST}$ is not small. The accurate formula gives

$$t_D = \frac{1}{1.04 \times 10^{-9}}\left[-2.39 \times 10^{-6} + \sqrt{(2.39 \times 10^{-6})^2 + 4 \times 1.04 \times 10^{-9} \times 1.396 \times 10^{-3}}\right]$$

$$= 948\ \text{sec.}$$

The drift time was 1167 seconds using the idealized limit cycle. It is seen that solar torque caused acceleration during drift significantly changes drift time, and hence criteria B, for this example.

Recalling that Criteria B is

$$\omega \geq \frac{1}{\xi t_D} \ln_e \left(1/F_B \right)$$

the minimum frequency is increased by 1167/948 = 1.232 times. This is from .00986 to .01217 cps.

Utilization of the approximate drift time formula yields an erroroneous number because $\ddot{\Theta}_{ST}$ is not small.

$$t_D = \frac{2 \times 1.396 \times 10^{-3}}{2.39 \times 10^{-6}} - \frac{2 \times 1.04 \times 10^{-9} \times (1.396 \times 10^{-3})^2}{(2.39 \times 10^{-6})^3}$$

$$= 1167 - 297 = 870 \text{ sec.}$$

which is too low a value.

2 SOLAR ARRAY ORIENTATION DISTURBANCES

The effects on pointing accuracy due to a solar array orientation were estimated for a mechanism utilizing direct shaft torquing and continuous linear control. These effects are insignificant except for the largest arrays considered, being of the same order as the limit cycle criteria at 100 KW.

2.1 ARRAY ORIENTATION MECHANISM

The solar arrays are oriented towards the sun by rotating them about the vehicle pitch axis at earth rate. This is a major ACS disturbance despite the low angular velocity because the arrays have large inertias.

A recent study of solar array orientation for earth-oriented satellites by Hughes has examined the mechanism technology (Reference 2). Continuous linear control was chosen as being most compatible with the flexible arrays in avoiding repetitive modal frequency excitation. The specified mechanism is gearless, using direct shaft torqueing.

2.2 MODEL OF MOMENTUM TRANSFER

A reaction torque is exerted on the satellite as the mechanism rotates the solar arrays. This reaction disturbance is to be prevented from reducing pointing accuracy by the ACS torquers. These torquers may be either thrusters or momentum devices. Momentum devices will more effectively reduce the reaction torque disturbances.

Mechanism operation excites array vibrations, and these vibrations disturb the limit cycle as has been previously discussed. Momentum devices are potentially capable of reducing the effects of array vibrations on pointing. The potential exists because the devices are directly controlled and respond much faster than the arrays oscillate. The analysis does not explore this potential, taking the conservative approach of requiring antenna motions due to array orientation disturbances to be well within mission pointing tolerances.

All angular momentum due to array vibration is assigned to the first anti symmetric mode by the model. The solar array rotation velocity

$\omega_{SOL}(t)$, following mechanism operation, is

$$\omega_{SOL}(t) = \omega_e + O_V \omega_e (\cos \omega_{SM} t)\, e^{-\xi_{SM} \omega_{SM} t}$$

where ω_e is earth rate, O_V is fractional maximum error ω_{SM} and ξ_{SM} are the solar orientation mechanism control frequency and damping ratio. Nominal value for O_V is taken to be .05.

The mechanism will be reasonably well damped and the ω_{SOL} variation for the impulse calculation can be approximated by

$$\omega_{SOL}(t) = \omega_e + O_V \omega_e \cos \omega_{SM} t ; \quad 0 \le t \le \frac{T_{SM}}{2}$$
$$= \omega_e ; \quad t > \frac{T_{SM}}{2}$$

The solar mechanism torque, τ_{SM}, is

$$\tau_{SM} = \frac{d J_{SM}}{dt} = \frac{d}{dt}\left(I_p\, \omega_{SOL}(t) \right)$$
$$= I_p O_V \omega_e (-\omega_{SM} \sin \omega_{SM} t); \quad 0 \le t \le \frac{T_{SM}}{2}$$
$$= 0, \quad t > \frac{T_{SM}}{2}$$

The momentum change applied to the arrays, J_{ap}, is

$$J_{ap} = \int_0^{\frac{T_{SM}}{2}} \tau_{SM}\, dt = I_p O_V \omega_e \int_0^{\frac{T_{SM}}{2}} -\omega_{SM} \sin \omega_{SM} t$$

$$= 2 I_p O_V \omega_e$$

Since the control is much faster than the array first anti-symmetric mode ($\omega_{SM} \gg \omega_{P_{jA_1}}$), the momentum transfer occurs as an impulse.

2.3 MODEL FOR FREQUENCY CRITERIA

Next analysis step is to relate the momentum transfer to the solar arrays with the mission pointing tolerance. The relationship can not be in termsof drift velocity, $\dot{\theta}_D$, as was done for limit cycle operation. This is because solar orientations occur randomly with respect to the ACS torquer operation which establishes the limit cycle.

The angular momentum transferred to the arrays is manifested by array motion at maximum vibration velocity and by perturbed satellite motion when vibration velocity is zero (maximum vibration deflection). Thus

$$I_{SB}\,\dot{\theta}_{SB_{SM\,MAX}} = I_P\,\dot{\theta}_{P_{SM\,MAX}} = J_{OP}$$

so

$$\dot{\theta}_{SB_{SM\,MAX}} = \frac{I_P}{I_{SB}}\, 2 \times O_v\, \omega_c$$

then

$$\theta_{SB_{SM\,MAX}} = \frac{1}{\omega_{P_{jA_1}}}\, \frac{I_P}{I_{SB}}\, 2 \times O_v\, \omega_c$$

The frequency criteria is

$$\omega_{P_{jA_1}} \geqslant \frac{I_P}{I_{SB}}\, 2 \times O_v\, \omega_c \left(\frac{1}{\theta_{SB_{SM\,MAX}}} \right)$$

with $\theta_{SB_{SM\,MAX}}$ being determined by mission requirements.

Only pitch frequencies are subject to this criteria, because the only array orientation is in pitch. Only the four solar array configuration is of interest, because array inertia about pitch axis for the two array configuration is low. Note that pitch is the axis of weakest array structure for the four array configuration, and that limit cycle criteria on structural rigidity are obtained for that axis.

2.4 TYPICAL RESULTS

A sample calculation is illustrated using the data of Table F-1. and .05 for O_V and .03 deg. (5.23×10^{-4} radians) for $\Theta_{SB_{SM\,MAX}}$.

$$\omega \geq \frac{1.30 \times 10^{6} \times 2 \times 0.05 \times 6.6 \times 10^{-5}}{2.16 \times 10^{5} \times 5.23 \times 10^{-4}} = 0.0760 \text{ rad./sec.}$$

Corresponding results across the configuration power range are shown in Table F-2. The frequency minimum sharply decreases with decreasing power because array moment of inertia sharply decreases.

Limit cycle derived minimums for 100 KW were found to be .00600 cps for Criteria A and .00986 cps for Criteria B. Since criteria B rises with lower power, array orientation is concluded to effect rigidity requirements only at the highest power levels. A more detailed examination is recommended at those higher power levels, because of gross approximations in this analysis.

TABLE F-2.

FREQUENCY MINIMUM CRITERIA DUE TO ARRAY ORIENTATION
4 array configuration, pitch channel

$O_V = 0.05$; $\Theta_{SB_{SM\,MAX}} = 0.03$ deg.

Power KW	Frequency Minimum rad/sec	cps
100	.076	.012
50	.019	.0030
25	.0047	.00075
10	.00076	.00012

3.0 CSM DOCKING LOADS FOR SOLAR ARRAYS

Both manned and unmanned TV satellite concepts are being investigated. The solar arrays are the weakest vehicle structure and therefore most susceptible to structural damage caused by the CSM docking impact.

Roll out type arrays are readily retractable. It is assumed that they will be retracted prior to docking. The more rigid fold out arrays are not retractable as currently designed and this feature could be implemented only with considerable difficulty. Therefore it is assumed that fold out arrays will be fully deployed during docking operations.

The two array is more susceptible to damage than the four array configuration because the array segments are larger and more flexible. Damage susceptibility is maximum when the docking impact is perpendicular to the plane of the solar arrays, exciting the lateral out of plane bending modes. Since the array plane rotates in pitch once each day, array flexibility along the docking impact direction varies. Thus the impact can but not necessarily will occur at a time of maximum damage susceptibility.

The analysis is conducted for a two fold out type array configuration with impact perpendicular to array plane.

Docking impact excites the symmetric modes of the solar array-vehicle-antenna structure. These modes have lower frequencies than the antisymmetric modes excited by ACS operation.

Bending moment due to impact is obtained as a function of maximum array tip deflection. Two models are used to predict tip deflection, one based on an energy model and one based on an impulse model. Root bending moment is then computed from tip deflection.

Two assumptions are basic to the tip deflection models. Both are valid in this situation. 1) The modal periods are taken to be long with respect to the docking impact time duration. 2) Tip deflection must be a reasonable displacement for the array size. The model is subject to unacceptable errors for deflection greater than array half length.

3.1 ENERGY MODAL APPROACH: ARRAY TIP DEFLECTION CALCULATION

Prior to docking, the CSM at mass M_1 has a velocity V_1, relative to the satellite vehicle less solar arrays, of mass M_2. Conserving linear momentum,

$$M_1 V_1 = (M_1 + M_2) V_2$$

with the array mass being neglected with respect to satellite vehicle mass. Following the approach of Reference 3, the docking energy loss which must be dissipated in the docked structures is

$$\Delta E_D = -\frac{1}{2} M_1 V_1^2 \left[\frac{M_2}{M_1 + M_2} \right]$$

The energy going into array vibration, ΔE_{SOL}, is thus bounded,

$$|\Delta E_{SOL}| \leq |\Delta E_D|$$

The approximate model of the array segments is that the first mode shape is parabolic and that the vibration can be represented by a damped harmonic oscillator of mass equal to the first mode general mass, $m_{j=1}$, located at array tip.

The first mode kinetic energy is

$$KE_{j=1} = N_P \, d_{tip} \, \frac{1}{2} \left(\omega_{j=1} \right)^2 m_{j=1}$$

where d_{tip} is maximum tip deflection, feet and the general mass for a parabolic shape is one fifth the structure mass. Since most vibration energy will be in the first mode, an approximate relationship is obtained by considering all energy to be in first mode. Then

$$\frac{\Delta E_{SOL}}{N_P} = d_{tip} \frac{1}{2} (\omega_{j=1})^2 m_{j=1}$$

and

$$d_{tip} = \frac{1}{\omega_{j=1}} \sqrt{\frac{2 (\Delta E_{SOL}/N_P)}{m_{j=1}}}$$

3.2 IMPULSE MODEL APPROACH: ARRAY TIP DEFLECTION CALCULATION

The impulse model applicability is based on the docking impact time duration being short with respect to period of the significant modes. The impulse applied is

$$M_2 V_2 = \frac{M_1 M_2 V_1}{(M_1 + M_2)} = \int f(t)\, dt = \dot{d}_{tip} m_{j=1}$$

The maximum tip deflection is

$$d_{tip} = \frac{2 \int Q_{j=1}\, dt}{\omega_{j=1}\, m_{j=1}}$$

where the generalized force, $Q_{j=1}$, for the parabolic mode shape, is

$$Q_{j=1} = \frac{F(t)}{3}$$

Since $$\int F(t)\,dt = M_2 V_2$$

$$d_{tip} = \frac{(2/3)\, M_2 V_2}{\omega_{j=1}\ m_{j=1}}$$

3.3 CALCULATION OF ARRAY TIP DEFLECTION

A docking velocity of 0.15 fps is representative. M_1 is 700 slugs, M_2 is taken to be 32,200 lbs (1000 slugs).

Then

$$V_2 = \frac{700}{1000 + 700} \times 0.15 = 0.0617 \text{ FPS.}$$

$$M_2 V_2 = 1000 \times 0.0617 = 61.7 \text{ ft. lb. sec.}$$

and

$$\Delta E_D = -\frac{1}{2}\, 700 \times (0.15)^2 \left[\frac{1000}{1700}\right]$$

$$= -4.63 \text{ ft. lb.}$$

The energy going into array vibration is bounded by 4.63 ft. lbs., and is assumed to be 4 ft. lbs.

$$\Delta E_{SOL} \equiv 4 \text{ ft. lb.}$$

Each of the two arrays weighs 5000 lbs. (154 slugs) for 100 KW, and has a first mode general mass of 31.1 slugs.

The energy model predicts maximum tip deflection of

$$d_{tip} = \frac{1}{\omega_{j=1}} \sqrt{\frac{2(4.00/2)}{31.1}} = \frac{0.359}{\omega_{j=1}} \text{ ft.}$$

The impulse model predicts maximum tip deflection of

$$d_{tip} = \frac{1}{\omega_{j=1}} \frac{(2/3)\,61.7}{31.1} = \frac{1.32}{\omega_{j=1}} \text{ ft.}$$

Both models are conservative. Actual solar array tip deflection will be smaller than that predicted for either model. The energy model yields smaller maximums across the conceptual range of power requirements and vehicle weights as well as for these results for maximum power and weight. Therefore the energy model is used.

Tip deflection data vs power for specific modal frequencies are shown in Figure F-2. Array frequency has been computed to be .116 rad/second at 100 KW, increasing to .438 rad/second at 10KW for the two array configuration. Thus tip deflections are well below the array half length bound, Y_{tip} is 3.09 ft. at 100 KW, eg.

Figure F-2. Maximum array tip deflection due to CSM docking vs power

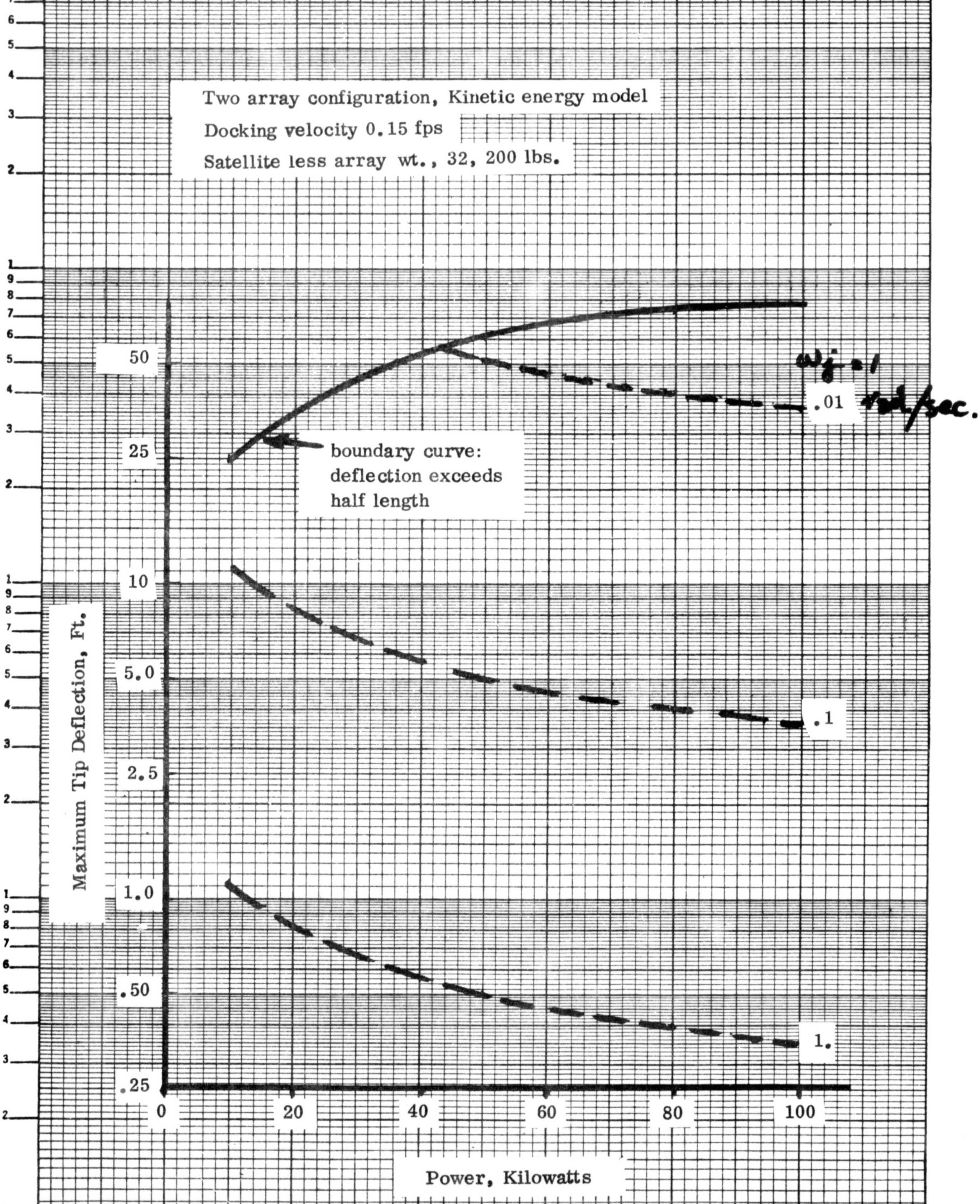

3.4 ROOT BENDING MOMENT MODEL

An expression is derived for the root bending moment of an array, as a function of tip deflection, array segment length, and first symmetric mode frequency.

The previous assumptions apply. The moment is assumed to be due to the first mode and the first mode shape of an array segment is assumed to be parabolic.

Thus the tip normalized mode shape is

$$Y(x) = x^2/\ell^2$$

The force due to acceleration of an array length element is

$$df = m(x)\ddot{Y}(x)\,dX = m(x)\,\omega_{j=1}^2\,Y(x)\,dX$$

$$= \lambda\,\omega_{j=1}^2\left(x^2/\ell^2\right)dx$$

$$\lambda = m(x)$$

and the moment about the array root is

$$d\,BM_r = X\,df = \lambda\,\omega_{j=1}^2\,X\left(X^2/\ell^2\right)dX$$

when the tip deflection is one foot.

$$BM_r = d_{tip}\int_0^\ell d\,BM_r\,dx$$

$$= d_{tip}\,\omega_{j=1}^2\,\lambda\int_0^\ell\left(X^3/\ell^2\right)dX$$

$$= d_{tip}\,\lambda\,\omega_{j=1}^2\,\frac{\ell^2}{4}\quad ft.\,lb.$$

3.5 ROOT BENDING CALCULATION

The two array configuration has each array weighing 5000 lbs. and being 158.5 ft. long for 100 KW of power, noting the nominal 5:1 aspect ratio. Then

$$\lambda = \frac{5000/32.2}{158.5} = 0.98 \text{ slug/ft.}$$

For $\omega/\omega_1 = 1.0$, $d_{tip} = .36$ ft. from Figure F-2, and

$$BM_r = (0.36)(0.98)(1)^2 \times (158.5)^2/4$$
$$= 2{,}220 \text{ ft. lb.}$$

which is one point on the docking bending moment curves.

For the anticipated .116 rad/sec. at 100 KW, d_{tip} is 3.09 ft. and

$$BM_r = 3.09 \times 0.98 \times (0.116)^2 \times \frac{(158.5)^2}{4} = 233 \text{ ft. lb.}$$

These bending moment values are not likely to cause appreciable difficulties for antenna rim solar array mountings. Local stiffening would be required for bending moments of the order of a few thousand ft. lbs.

Necessary size for the tube attaching array to antenna rim is examined for a moment of 25,000 inch lbs. The stress level, σ, is given by $\sigma = \frac{BM * r}{AI}$, noting σ is PSI, BM units are inch lbs, tube radius r is in inches, and the area inertia is inches^4. Since

$$AI = \frac{(2\pi r t)r^2}{2} = \pi t r^3$$

t being tube wall thickness, inch,

$$r^2 t > BM/(\pi \sigma_{MAX})$$

or tube will break. Noting that σ_{max} is 10^4 psi for aluminium,

$r^2t > .796$ inch^3.

For $r = 4$ inch, $t \geq .05$ inch,

for $r = 2$ inch, $t \geq .20$ inch, which are reasonable numbers. Since the tube is short, weight increases are low.

A detailed calculation of internal array stresses due to CSM docking impact bending moments is advisable. Local stiffening of the array itself might be required.

Bending moments will be higher for concepts which mount the solar arrays directly to the main satellite structure with the long tube necessary to avoid array shadowing by the antenna. Appreciable weight increases could result from the required stiffening. Fortunately the satellite mounted array concepts are usually low powered and therefore have relatively small bending moments.

4 NOMENCLATURE

AI	area inertia, $inch^4$
AM	solar array total area moment, total area times distance vehicle GG to CP of array portion on one side of axis of interest, ft^3
BM	bending moment, inch lbs.
BM_r	bending moment about array root, ft. lbs.
CG	center of gravity
CP	center of pressure
d	beam deflection, ft.
DC	duty cycle fraction
ΔE_D	energy dissipated in docking, ft. lbs.
ΔE_{SOL}	docking energy dissipated in solar arrays, ft. lbs.
f	frequency, cps
f	inertia reaction force, lbs.
F(t)	docking force, lbs.
F_A, F_B	factors used in criteria A, B.
F_{ST}	factor in solar torque alteration of limit cycle, $F_{ST} \leq 1$.
I_{P_k}	complete solar panel array inertia about vehicle k axis, slug $ft.^2$
I_{SB_k}	vehicle inertia (complete satellite less solar arrays) about vehicle k axis, slug $ft.^2$
J	solar array angular momentum, ft. lb. sec.
J_{a_P}	angular momentum transferred to soalr arrays by solar orientation mechanism, ft. lb. sec.
ℓ	individual array length, ft.
ℓ'	CG to array tip distance, ft.
ln_e	log to base e
L_{JET}	thruster moment arm, ft.
M	mass, slugs
M_1	CSM mass, slugs.

M_2 satellite less solar array mass, slugs.

M_{P_1} individual array mass, slugs.

$\mathfrak{m}$ generalized mass of mode j, slugs.

N_i number of nodes

N_P number of individual arrays in a configuration, nominally two or four

O_V fractional maximum error (maximum error expressed as a fraction of steady state value)

P_{SOL} solar pressure at earth orbit, lbs. per ft.^{2}, nominally 9.85×10^{-8}.

Q generalized force, nominally lbs.

r tube radius, inch

R_A CG to array base distance perpendicular to k axis, ft.

t time, seconds

t tube wall thickness, inch

T thrust, lbs.

T period, seconds

V_1 CSM velocity before docking, fps

V_2 CSM and satellite velocity after docking, fps

w individual array width, ft.

X longitudinal distance along beam, ft.

Y mode shape, normalized to one at maximum

$\gamma, \dot{\gamma}$ antenna orientation, rate due to vibration; radians, rad/sec.

ζ structural damping

$\theta_k, \dot{\theta}_k, \ddot{\theta}_k$ rigid body angle, rate, and acceleration about vehicle k axis; radians, rad/sec, rad/sec^2

$\Delta\theta_B$ Allowable vehicle angle change during ACS thruster burn, radians

$\Delta\theta_E$ mission pointing requirement tolerance, radians

λ beam running density, slug/ft.

σ	stress, Psi
τ	torque, ft. lbs.
τ_{JET_K}	thruster torque about k axis, ft. lbs.
$\phi, \dot{\phi}$	phase angle, radians
$\psi_K, \dot{\psi}_k$	antenna orientation angle, rate; radians, rad/sec.
ω	frequency, radians/sec.
ω_e	earth rate, 6.6×10^{-5} radians/sec.
$m(X)$	linear density at X, slugs/ft
m_i	lumped mass at node i, slugs

SUBSCRIPTS

A	antenna
ACS	attitude control system
B	thruster burn portion of limit cycle
D	vehicle drift portion of limit cycle
E_k	pointing error tolerance for k axis
i	index for lumped parameter node
j	index for mode
j_{A_1}	first anti symmetric mode
j_{S_1}	first symmetric mode
k	index for vehicle axes; 1 denotes roll, 2 pitch, 3 yaw
k_1	one individual solar array
m	maximum
P	solar array
SB	satellite body
SM	solar orientation mechanism
SOL	solar
ST	solar torque
tip	array tip

REFERENCES, APPENDIX F

1. "Television Broadcast Satellite Study Midterm Presentation" contract NAS 8-21036, GD/ Convair, 29 June 1969.

2. Hughes, Space Systems Division, El Segundo, "OLSCA, Orientation Linkage for a Solar Cell Array," Hughes Report No. SSD 8022 1R, July, 1968, AD No. 836 663.

3. Hayden Mitchell, "Docking and Separation", section 4.5.3, Final Report, 'Large Space Structure Experiments for AAP, Vol V, Parabolic Antenna," GD/Convair Report No. GDC-DCL 67-009, 20 November, 1967.